Observational and numerical modeling constraints on the global ocean biological carbon pump

Scott C. Doney[1], Kayla Alexis Mitchell[1], Stephanie Anne Henson[2], Emma L Cavan[3], Timothy DeVries[4], Nicolas Gruber[5], Judith Hauck[6], Colleen B. Mouw[7], Jens Daniel Müller[5], and Francois W. Primeau[8]

[1]University of Virginia
[2]National Oceanography Centre
[3]University of Tasmania
[4]University of California Santa Barbara
[5]ETH Zürich
[6]Alfred Wegener Institute Helmholtz Centre for Polar and Marine Research
[7]University of Rhode Island
[8]University of California, Irvine

April 05, 2024

Abstract

This study characterized ocean biological carbon pump metrics in the second iteration of the REgional Carbon Cycle Assessment and Processes (RECCAP2) project, a coordinated, international effort to constrain contemporary ocean carbon air-sea fluxes and interior carbon storage trends using a combination of observation-based estimates, inverse models, and global ocean biogeochemical models. The analysis here focused on comparisons of global and biome-scale regional patterns in particulate organic carbon production and sinking flux from the RECCAP2 model ensemble against observational products derived from satellite remote sensing, sediment traps, and geochemical methods. There was generally encouraging model-data agreement in large-scale spatial patterns, though with substantial spread across the model ensemble and observational products. The global-integrated, model ensemble-mean export production, taken as the sinking particulate organic carbon flux at 100 m (6.41 ± 1.52 Pg C yr–1), and export ratio defined as sinking flux divided by net primary production (0.154 ± 0.026) both fell at the lower end of observational estimates. Comparison with observational constraints also suggested that the model ensemble may have underestimated regional biological CO2 drawdown and air-sea CO2 flux in high productivity regions. Reasonable model-data agreement was found for global-integrated, ensemble-mean sinking particulate organic carbon flux into the deep ocean at 1000 m (0.95 ± 0.64 Pg C yr–1) and the transfer efficiency defined as flux at 1000m divided by flux at 100m (0.121 ± 0.035), with both variables exhibiting considerable regional variability. Future modeling studies are needed to improve system-level simulation of interaction between model ocean physics and biogeochemical response.

Observational and numerical modeling constraints on the global ocean biological carbon pump

Scott C. Doney[1], Kayla A. Mitchell[1,2], Stephanie A. Henson[3], Emma Cavan[4], Tim DeVries[5], Nicolas Gruber[6], Judith Hauck[7], Colleen B. Mouw[8], Jens D. Müller[6], and Francois W. Primeau[2]

Submitted, March 4th, 2024

[1] Department of Environmental Sciences, University of Virginia, Charlottesville, VA, USA,

[2] Department of Earth System Science, University of California, Irvine, Irvine, CA, USA,

[3] National Oceanography Centre, Southampton, UK,

[4] Department of Life Sciences, Silwood Park Campus, Imperial College London, Berkshire, UK,

[5] Earth Research Institute and Department of Geography, University of California, Santa Barbara, Santa Barbara, CA, USA,

[6] Environmental Physics, Institute of Biogeochemistry and Pollutant Dynamics, ETH Zurich, Zürich, Switzerland

[7] Alfred-Wegener-Institut, Helmholtz-Zentrum für Polar- und Meeresforschung, Bremerhaven, Germany

[8] Graduate School of Oceanography, University of Rhode Island, Narragansett, RI, USA.

Corresponding author: Scott Doney (sdoney@virginia.edu) ORCID: 0000-0002-3683-2437

Key Points:

- Global-scale, ocean biogeochemical simulations are compared with observation-based estimates of the marine biological carbon pump.
- A multi-model ensemble exhibits relatively good agreement with observation-based metrics for carbon export flux and transfer efficiency.
- Based on identified model-observation and inter-model differences, we provide guidance for future model evaluations and development.

Abstract

This study characterized ocean biological carbon pump metrics in the second iteration of the REgional Carbon Cycle Assessment and Processes (RECCAP2) project, a coordinated, international effort to constrain contemporary ocean carbon air-sea fluxes and interior carbon storage trends using a combination of observation-based estimates, inverse models, and global ocean biogeochemical models. The analysis here focused on comparisons of global and biome-scale regional patterns in particulate organic carbon production and sinking flux from the RECCAP2 model ensemble against observational products derived from satellite remote sensing, sediment traps, and geochemical methods. There was generally encouraging model-data agreement in large-scale spatial patterns, though with substantial spread across the model ensemble and observational products. The global-integrated, model ensemble-mean export production, taken as the sinking particulate organic carbon flux at 100 m (6.41 ± 1.52 Pg C yr^{-1}), and export ratio defined as sinking flux divided by net primary production (0.154 ± 0.026) both fell at the lower end of observational estimates. Comparison with observational constraints also suggested that the model ensemble may have underestimated regional biological CO_2 drawdown and air-sea CO_2 flux in high productivity regions. Reasonable model-data agreement was found for global-integrated, ensemble-mean sinking particulate organic carbon flux into the deep ocean at 1000 m (0.95 ± 0.64 Pg C yr^{-1}) and the transfer efficiency defined as flux at 1000m divided by flux at 100m (0.121 ± 0.035), with both variables exhibiting considerable regional variability. Future modeling studies are needed to improve system-level simulation of interaction between model ocean physics and biogeochemical response.

Plain Language Summary

Phytoplankton in the surface ocean create each year an amount of organic carbon approximately equivalent to all the annual photosynthesis by plants on land. A small fraction of this newly formed organic carbon is exported below the surface layer, and an even smaller amount makes it all the way to the deep ocean. The transport of organic carbon to the sub-surface ocean, called the biological carbon pump, influences the global-scale distributions of ocean nutrients, oxygen, and inorganic carbon as well as the amount of carbon dioxide in the atmosphere. The global rates and geographic patterns of photosynthesis and carbon flux out of the surface ocean have previously been constructed from ship measurements and satellite remote sensing. Here, we compare these observation-based estimates to a suite of three-dimensional, numerical ocean models and find broadly similar results. The model simulations also capture aspects of the biological carbon pump deeper in the water column, where there are fewer direct constraints from field observations. Our comparison of observations and simulations identifies some deficiencies in the models that should be corrected in order to better simulate climate change impacts on the biological carbon pump.

1 Introduction

Marine biogeochemical processes play a central role in the global Earth System, modulating the distribution of inorganic carbon, oxygen, and nutrients within the ocean and the partitioning of carbon between ocean and atmosphere reservoirs (Broecker and Peng, 1982; Sarmiento and Gruber, 2002; Devries, 2022; Iversen, 2023; Siegel et al., 2023). Because of the

strong oceanic influence on atmospheric CO_2 concentration and thus planetary climate, there is considerable scientific focus on quantifying both the baseline and trends in ocean carbon storage and fluxes arising from the uptake of anthropogenic CO_2 and climate change impacts on marine biogeochemical and physical dynamics (Henson et al., 2016; DeVries et al., 2019; Hauck et al., 2020; Canadell et al., 2021; Crisp et al., 2022; Wilson et al., 2022; Gruber et al., 2023). The REgional Carbon Cycle Assessment and Processes (RECCAP) project is a coordinated, international effort to constrain contemporary ocean carbon air-sea fluxes and interior storage trends using a combination of observation-based estimates, inverse models, and global ocean biogeochemical models (GOBMs) (Wanninkhof et al., 2013; Khatiwala et al., 2013). The second phase, RECCAP2, extends the original synthesis using additional years of ocean observations and updated methodology and numerical results (DeVries et al., 2023; Hauck et al., 2023) as well as expanding the scope of the analysis, in this case into biological carbon pump magnitude and efficiency.

In a simple 1-D form, the marine biological carbon pump can be viewed as the net production of particulate organic carbon (POC) and inorganic carbon (PIC) in the surface ocean, downward vertical transport of particulate carbon into the thermocline and deep sea, and subsequent respiration and remineralization of particulate carbon back into dissolved inorganic carbon (DIC) (Volk and Hoffert, 1985). The downward organic carbon transport, or export flux, drives subsurface marine biogeochemistry, fuels deep-ocean ecosystems, and influences ocean carbon storage and atmospheric CO_2. The biological pump accentuates the vertical gradient in DIC already established from CO_2 system thermal solubility and temperature gradients, and deep-ocean carbon storage reflects a net balance between the biological carbon pump source and physical ocean circulation processes that return elevated deep-ocean DIC waters back to the surface ocean via upwelling and vertical mixing (Sarmiento and Gruber, 2006). The relationship between ocean carbon storage and the strength of the biological pump is not necessarily straightforward because of physical-biological interactions; for example, stronger overturning circulation can enhance both biological export through increased nutrient supply and the physical return of high-DIC deep-ocean waters to the surface (Doney et al., 2006). The vertical structure of the biological carbon pump is also important. Sinking POC fluxes decline rapidly in the thermocline (0 to ~1000 m depth), with only a fraction of surface export flux reaching the deep ocean below 1000 m (Martin et al., 1987; Lutz et al., 2007; Lima et al., 2014; Dinauer et al., 2022). Deeper remineralization depths, that is the transport of a greater fraction of POC into the lower thermocline or deep ocean prior to respiration, enhances ocean carbon storage because of generally reduced physical return rates to the surface ocean for deeper waters, and therefore longer retention times for the remineralized DIC, although with substantial regional variations associated with circulation pathways and rates (Kwon et al., 2009; Siegel et al., 2021).

Net primary production (NPP) by surface ocean phytoplankton generates POC and dissolved organic carbon (DOC), and most marine NPP is converted rapidly back to DIC through zooplankton grazing of living biomass and detritus or through the microbial loop involving consumption of POC and DOC pools. Export fluxes require an excess of community production of organic carbon over respiration that in turn must be supported by an external supply of new nutrients over sufficient time and space scales (Ducklow and Doney, 2013). The fraction of NPP that is exported (export ratio = export flux/NPP), is modulated by the magnitude and seasonality of NPP, environmental conditions, and phytoplankton and zooplankton community composition (Laufkötter et al., 2016). Export flux from the euphotic zone occurs through multiple pathways including gravitational sinking of POC (e.g., living and dead cells; fecal pellets; marine snow),

physical subduction and mixing of POC and DOC below the surface layer, and active biological transport by vertically migrating organisms (Siegel et al., 2016). Contemporary models capture, with varying levels of sophistication and skill, biological processes involved in NPP and export flux from the upper ocean (Fennel et al., 2022), though models tend to focus on gravitational particle sinking and many do not incorporate all of the relevant export pathways (Boyd et al., 2019; Henson et al., 2022) or dynamics governing vertical carbon fluxes from the surface to the deep sea (Burd, 2024). Here we focus on simulated export via gravitational particle sinking, which is incorporated in virtually all global ocean biogeochemical models in some form. Observation-based estimates of the global export flux have a large range (~5-12 Pg C yr^{-1}; Siegel et al., 2016), which is almost identical to the range in export estimates for the modern-day era simulated by coupled climate models (4.5-12 Pg C yr^{-1}; Henson et al., 2022), i.e. the observations-based estimates of export flux provide a poor constraint for biogeochemical models. Because of differences in model climate responses and parameterizations of the ocean biological carbon pump, substantial uncertainties also plague projections of future changes in export flux in response to climate change. For example, Henson et al. (2022) found a large inter-model spread in projected changes in export flux by 2100 of between +0.16 and -1.98 Pg C yr^{-1} (+1.8 to -41%) under the high-emission SSP5-8.5 scenario.

Much of the export flux of organic carbon from the euphotic zone, taken here as the downward flux through 100m (F_{100}), is consumed by respiration in the mesopelagic zone (100 – 1000 m). The diverse mechanisms for vertical transport and remineralization of organic matter in the mesopelagic are only partially captured in models (Fennel et al., 2022). A steep decline with depth in the gravitational sinking flux of particles is well documented from mid-depth sediment traps (e.g., Lutz et al., 2007; Lima et al., 2014; Dinauer et al., 2022), but the exact processes involved are less well quantified and may include physical and biological particle fragmentation (Briggs et al., 2020) as well as particle consumption and repackaging by zooplankton (Stukel et al., 2019). Particle fluxes and the depth-scale of remineralization are affected by particle composition, size, density, and sinking speeds. Particles can vary widely from small, slowly sinking dead cells and detrital material, to large marine snow aggregates with enhanced sinking speeds from captured ballast material, to large rapidly sinking fecal pellets (Lam et al., 2011; Omand et al., 2020). Vertical migrators transport organic carbon downward from the euphotic zone into the mesopelagic, respiring CO_2 and releasing fecal pellets at depth (Archibald et al., 2019). Sinking particle fluxes and mesopelagic biological processes typically are not modeled in great mechanistic detail in contemporary global ocean biogeochemical models, and often relatively simplistic empirical relationships such as variants of the Martin power-law flux curve (Martin et al., 1987) are used in place of explicit representation of the processes controlling mesopelagic flux attenuation.

The proportion of sinking exported POC that survives remineralization in the mesopelagic zone to reach depths > 1000 meters is referred to as the transfer efficiency, given here as the ratio of sinking fluxes at 100 and 1000 meters ($E_{1000/100}$). POC reaching 1000m depth is remineralized below the main thermocline and is likely sequestered on timescales of >100 years, thus contributing to the long-term ocean carbon sink (Siegel et al., 2021). There is currently little consensus on the global magnitude or spatial patterns of transfer efficiency, with some approaches suggesting that $E_{1000/100}$ is high at high latitudes and low at low latitudes (Marsay et al., 2015; Weber et al., 2016; DeVries and Weber, 2017), whilst others imply the opposite pattern (Lam et al., 2011; Henson et al., 2012; Guidi et al., 2015; Mouw et al., 2016b; Dinauer et al. 2022). A variety of approaches have been used to generate these estimates, including paired in situ

observations of ^{234}Th-derived export flux and deep sediment trap flux (Henson et al. 2012), vertical profiles of flux from drifting sediment traps (Marsay et al., 2015) or inverting the observed nutrient and/or oxygen distributions using an inverse model (Weber et al., 2016; Devries and Weber, 2017; Cram et al., 2018). The differing approaches, and differing time and space scales that they integrate over, are likely a significant source of the uncertainty in global $E_{1000/100}$ patterns. In CMIP6 models, there are substantial differences in both the preindustrial mean $E_{1000/100}$ (varying from 3% to 25% across models) and its response to 21st century climate change, with projections showing both increases and decreases in $E_{1000/100}$ over time (Wilson et al., 2022).

Early model skill assessments relied heavily on model-data comparisons to transient tracers, ocean physics, and sub-surface nutrient and oxygen fields that reflect the imprint of biological pump fluxes and ocean circulation (e.g., Matsumoto et al., 2004; Doney et al. 2004; Najjar et al. 2007). However, observational constraints on the ocean biological carbon pump have advanced considerably since the early global 3-D ocean biogeochemical modelling efforts (e.g., Bacastow and Maier-Reimer, 1990; Maier-Reimer, 1993). Global-scale data compilations of primary production, surface export and mesopelagic sinking carbon fluxes are now available based on a wealth of satellite remote sensing, sediment traps, and geochemical methods (e.g., Henson et al. 2012; Mouw et al., 2016a). Past model-data skill assessments using multi-model ensembles have highlighted differences in simulated ocean biological carbon pump patterns, magnitudes, and mechanisms and identified model biases relative to admittedly imperfect observational estimates (Laufkötter et al., 2015; Laufkötter et al., 2016). This study expands on these past assessment efforts of the ocean biological carbon pump to include the current generation of global ocean biogeochemical models compiled for RECCAP2 (DeVries et al., 2023).

The objective of this study is to characterize the global-scale biological carbon pump from RECCAP2 models and compare the simulation results with observation-based metrics. The focus is on the spatial patterns and global-integrated rates from the multi-model ensemble mean taking into consideration inter-model spread. Key metrics include export of sinking POC from the surface euphotic zone and the efficiency of POC transfer through the mesopelagic ocean, both of which are central to ocean carbon storage. Based on identified model-observation and inter-model differences, we also provide guidance for future global ocean biogeochemical model evaluations and development that could include targeted, more detailed analyses of dynamics and biases within individual RECCAP models.

2 Methods and Data

2.1 RECCAP2 model simulations and observational data products

This study leveraged a collection of ocean simulation and observational data sets, outlined in Table 1, assembled for RECCAP2 following standardized protocols and data reporting for numerical and observation-based pCO_2 products (RECCAP2 Ocean Science Team, 2022; DeVries et al., 2023; Müller, 2023). The RECCAP2 ocean data sets included monthly surface and annual ocean interior output for the contemporary period from more than a dozen global ocean biogeochemical model hindcast simulations, including both forward and data-assimilated models, along with observation-based surface ocean pCO_2 interpolation products. Many of the models included in the RECCAP2 suite have been used in the Global Carbon Project to assess the ocean carbon sink (Hauck et al., 2020; Friedlingstein et al., 2022). Here, we present model results for

1985 to 2018 from RECCAP2 simulation A, which was forced with historical atmospheric reanalysis data and increasing atmospheric CO_2, and hence represents both steady-state and variable climate processes and both natural, pre-industrial carbon fluxes and anthropogenic carbon fluxes caused by rising atmospheric CO_2 (DeVries et al., 2023).

Table 1. Description of RECCAP2 global ocean biogeochemical hindcast models, global data-assimilated models, and observation-based products used in this study. For more details see Tables S1 and S2 in DeVries et al. (2023). The World Ocean Atlas (WOA) data set was also used in the model-data evaluation.

Global hindcast models	**Data range**	**References**
CCSM-WHOI	1958-2017	Doney et al. (2009)
CESM-ETHZ	1980-2018	Lindsay et al. (2014); Yang and Gruber (2016)
CNRM-ESM2 -1	1980-2018	Séférian et al. (2019; 2020); Berthet et al. (2019)
EC-Earth3	1980-2018	Döscher et al. (2021)
FESOM-REcoM-LR	1980-2018	Hauck et al. (2020)
MPIOM-HAMOCC	1980-2018	Ilyina et al. (2013); Mauritsen et al. (2019)
MOM6-Princeton	1980-2018	Liao et al. (2020); Stock et al. (2020)
MRI-ESM2-1	1980-2018	Urakawa et al. (2020); Tsujino et al. (2017)
NorESM-OC1.2	1980-2018	Schwinger et al. (2016)
NEMO-PlankTOM12.1	1980-2018	Le Quéré et al. (2016); Wright et al. (2021)
ORCA1-LIM3-PISCES	1980-2018	Aumont et al. (2015)
Data-assimilated models		
ECCO-Darwin	1995-2018	Carroll et al. (2020; 2022)
SIMPLE-TRIM	Climatology	DeVries and Weber (2017)
pCO_2 interpolation products		
CMEMS-LSCE-FFNN	1985-2018	Chau et al. (2022)
JenaMLS	1985-2018	Rödenbeck et al. (2013); Rödenbeck et al. (2022)
MPI-SOMFFN	1982-2018	Landschützer et al. (2016)
NIES-ML3	1980-2020	Zeng et al. (2022)
OceanSODA-ETHZ	1985-2018	Gregor and Gruber (2021)
LDEO_HPD	1985-2018	Gloege et al. (2022)
UOEX_Wat20	1985-2019	Watson et al. (2020)
World Ocean Atlas		
Oxygen and AOU	Climatology	Garcia et al. (2019)
Biological carbon pump metrics		
net primary production, export production, and sinking POC flux	Climatology	Mouw et al. (2016a; 2016b)

Spatial 2D model output and pCO_2 interpolation products were provided to RECCAP2 with 1° x 1° resolution at monthly time steps, and 3D model output was resolved at annual time

steps. All estimates derived in this study were computed on the 1° x 1° grid. Global multi-model ensembles, spatial integrals and averages were computed as needed from the gridded results. For the aggregation to sub-basin ocean regions, ocean biomes based on Fay and McKinley (2014) were used in most instances to facilitate consistent regional intercomparison across RECCAP2 studies (e.g., Hauck et al., 2023). Longhurst provinces (Supplement Figure S1; Reygondeau et al., 2013) were additionally used in some of the biological pump model-observational comparisons to be consistent with one of the key observational data synthesis products (Mouw et al., 2016a). The notation and units for the biological, chemical and physical variables used in this study are described in Table 2. More details on the RECCAP2 ocean data sets can be found in DeVries et al. (2023).

We also used an observational compilation of surface ocean export production and sinking POC flux combined with satellite ocean color data products for primary production synthesized in Mouw et al. (2016a) and as aggregated to Longhurst regional provinces in Mouw et al. (2016b). The full dataset includes over 15000 individual sediment trap and ^{234}Th POC flux measurements at 673 locations, combined with satellite-derived estimates of NPP. Chlorophyll measurements collected from the SeaWiFS sensor on the OrbView-2 ocean color satellite, spanning from August 1997 to December 2010, were used to derive NPP using the vertically generalized production model (VGPM) (Behrenfeld and Falkowski, 1997) on an equal-area grid with 9-km resolution. The climatology in Mouw et al. (2016a) used an interpolation approach to combine the satellite timeseries and short-deployment (<30 days trap cup intervals) sediment trap POC flux measurements at overlapping locations. Over 43% of the POC flux measurements were collected after 1997, overlapping with the satellite record. For each POC flux location, median monthly values are computed and binned into biogeochemical Longhurst provinces for the climatology. The POC flux climatology also has a depth dimension, with depth bins centered at 20 m for a near-surface layer, in 50 m intervals in the upper thermocline, and in 200 m intervals from 500 m to 5000 m.

Table 2. Glossary and description of modeled, observed, and derived variables including notation and units.

Variable Name	Units	Output frequency	Description
2D or surface ocean properties			
pCO_2	µatm	monthly	Surface ocean pCO_2
NPP	mol C m^{-2} yr^{-1}	monthly	Vertically-integrated net primary production of organic carbon
F_{100}	mol C m^{-2} yr^{-1}	monthly	POC sinking flux at 100 m
F_{1000}	mol C m^{-2} yr^{-1}	monthly	POC sinking flux at 1000 m
3D or Interior Ocean Properties			
T	°C	annual	Seawater potential temperature
S	-	annual	Salinity (PSS-78)
F_{3D}	mol C m^{-2} yr^{-1}	annual	3D field of POC sinking flux

O_2	mol O_2 m^{-3}	annual	Dissolved oxygen concentration
Derived Variables			
$E_{100/NPP} = F_{100}/NPP$	-	monthly	Surface Export Ratio
$E_{1000/100} = F_{1000}/F_{100}$	-	monthly	Mesopelagic Transfer Efficiency
$E_{1000/NPP} = F_{1000}/NPP$	-	monthly	Surface to Deep-sea Export Efficiency
AOU	μmol kg^{-1}	monthly	Apparent oxygen utilization

2.2 Ocean biological pump and biogeochemical metrics

Our analysis utilized biogeochemical model estimates of vertically integrated NPP and export fluxes of sinking POC flux across a shallow surface at the approximate base of the euphotic zone (100 m, F_{100}) and at the base of the main thermocline (1000 m, F_{1000}). Note that the 1000 m fluxes were not provided for all models (see Figure 2c), and therefore the ensemble means for F_{100} and F_{1000} were constructed from different subsets of RECCAP2 simulations. The export ratio, $E_{100/NPP}$, was computed as the ratio of POC sinking flux at 100 m divided by net integrated primary production:

$$E_{100/NPP} = \frac{F_{100}}{\mathrm{NPP}} \quad (1)$$

The transfer efficiency across the 1000 m depth horizon, $E_{1000/100}$, was similarly computed as the ratio of sinking POC fluxes at 100 m and 1000 m:

$$E_{1000/100} = \frac{F_{1000}}{F_{100}} \quad (2)$$

A depth of 1000 m is taken as an approximate boundary between the main thermocline with ventilation timescales of years to decades and the deep ocean with time-scales of a century and longer (Siegel et al., 2021).

The relationship between the biological pump and the inorganic CO_2 system was examined by partitioning the seasonal variability in surface seawater pCO_2 into thermal and non-thermal components following Takahashi et al. (2002). We refer readers interested in a thorough analysis of RECCAP2 CO_2 system seasonality to Rodgers et al. (2023). The temperature effect on pCO_2 was calculated for isochemical seawater using the approximation $\frac{\partial(\ln(pCO_2))}{\partial T} = 0.0423$ (°C^{-1}) from the experimental value from Takahashi et al. (1993). The seasonal cycle in monthly surface temperature anomalies relative to the annual mean surface temperature generated a corresponding seasonal variation in the thermal (temperature-dependent) pCO_2 component about the pCO_2 annual mean:

$$pCO_2^{thermal} = (pCO_2)_{mean} \times exp\left[0.0423\left(T_{monthly} - T_{mean}\right)\right] \quad (3)$$

Ocean hindcast simulations typically capture quite well the seasonal cycle of sea surface temperature because the ocean models are forced by atmospheric reanalysis products and heat flux boundary conditions that effectively contain information on the observed temperature record (Doney et al., 2007); the same model-data agreement transfers to the thermal pCO_2 seasonal component. The non-thermal pCO_2 component was computed by subtracting the thermal component from the monthly pCO_2 values, and the seasonal amplitude $\Delta pCO_{2,\text{non-thermal}}$ was calculated as the seasonal peak-to-trough difference. The non-thermal pCO_2 component reflects seasonal variations in DIC and alkalinity from biological organic and inorganic carbon production and remineralization, air-sea CO_2 gas exchange, and physical transport and mixing. Note that the seasonal phasing of the non-thermal pCO_2 component can be distinct from the phasing of the total pCO_2 cycle. This is especially the case in the low latitudes, where the thermal component dominates the seasonal cycle (Takahashi et al., 1993; Landschützer et al., 2018; Rodgers et al., 2023).

We also computed apparent oxygen utilization (AOU) using modeled dissolved oxygen, salinity, and potential temperature fields. Modeled average AOU at 100 m (AOU_{100}) and 1000 m depth (AOU_{1000}) were found using nearest depth bins in model products (bins centered within 50 m of depths). The simulated AOU fields are compared against the World Ocean Atlas (WOA) data product (Garcia et al., 2019).

3 Results

3.1 Simulated ocean biological carbon pump metrics

Global spatial fields of present-day biological carbon pump variables are displayed in Figure 1 for the RECCAP2 model ensemble mean with the corresponding ensemble standard deviation in Figure S1. Biome-scale ensemble-mean averages and within-ensemble standard deviation values for the biological pump metrics are reported in Table 3 using the standard RECCAP2 biomes by ocean basin (Figure S2; Fay and McKinley, 2014).

The magnitude and spatial patterns of simulated annual mean NPP and export flux from sinking POC (F_{100}) (Figure 1a and 1b) are broadly similar to observational estimates (Section 3.2). Simulated upper-ocean biological pump variables showed large geographic variations with annual-mean NPP ranging on biome scales (Table 3) from 8 to 21 mol C m^{-2} yr^{-1} and F_{100} ranging from 1.1 to 2.9 mol C m^{-2} yr^{-1}. The simulated spatial patterns reflect euphotic zone temperature, nutrient supply, and grazing and loss rates that govern phytoplankton standing stock in the models (Falkowski et al., 1998; Laufkötter et al., 2015; Laufkötter et al., 2016). The imprint of nutrient supply was particularly evident in the elevated NPP and export fluxes found in equatorial and coastal upwelling regions, western boundary currents, and mid-latitude bands of deep seasonal mixing. Within-ensemble standard deviations (σ) of NPP and F_{100} were elevated in the equatorial band, and high σ_{NPP} values were found also in the Southern Ocean indicating substantial model disagreement within the ensemble (Figure S1a and S1b). Biome-scale σ_{NPP} values ranged from 2.1 to 6.6 mol C m^{-2} yr^{-1} (from as low as 0.22 to nearly 0.72 times the ensemble mean in parts of the Southern Ocean); biome-scale σ_{F100} values varied from 0.4 to >1.0 mol C m^{-2} yr^{-1} with the largest absolute and fractional within-ensemble variation of >0.7 times the ensemble mean occurring in the western equatorial Pacific.

359 The local POC sinking flux at the base of the mesopelagic (F_{1000}) ranged at biome scale
360 from 0.09 to 0.54 mol C m^{-2} yr^{-1} with broadly similar patterns to F_{100}, though with some notable
361 exceptions such as the high F_{1000} values in tropical low-oxygen zones in the eastern tropical Pacific
362 and Arabian Sea (Figure 1c). Note the roughly half to full order of magnitude decline in scale in
363 Figure 1 from NPP to F_{100} and then F_{100} to F_{1000}. This indicates first that the bulk of simulated
364 NPP is recycled within the euphotic zone above 100 m, rather than exported as sinking POC flux,
365 and second that most of the sinking POC flux at 100 m is remineralized in the mesopelagic, rather
366 than reaching the deep ocean below 1000 m. As for NPP and F_{100}, some correspondence was found
367 for the spatial patterns of ensemble-mean F_{1000} and σ_{F1000}. Highest biome-scale σ_{F1000} values of
368 0.26 to 0.29 mol C m^{-2} yr^{-1} occurred in the North Pacific and eastern equatorial Pacific, equal to
369 0.85 and 0.53 times the ensemble-mean F_{1000} for those biomes; biome-scale σ_{F1000} values of ~0.5
370 or more of the ensemble-mean were common, with even higher fractional values locally such is in
371 the eastern subtropical North Pacific (Figure S1c; Table 3).

372 The fraction of NPP exported across 100 m, or export ratio ($E_{100/NPP}$, Figure 1d; Table 3)
373 varies at the biome scale in the ensemble mean from 0.12 to 0.21 with elevated values in high
374 latitudes. The spatial patterns for within-ensemble $E_{100/NPP}$ standard deviation (Figure S1d) mirror
375 that of the mean $E_{100/NPP}$ with biome-mean standard deviations of 0.035 to 0.050 in most biomes
376 and up to 0.091 in the sub-polar Southern Ocean biome where there is more within-ensemble
377 model spread.
378
379
380

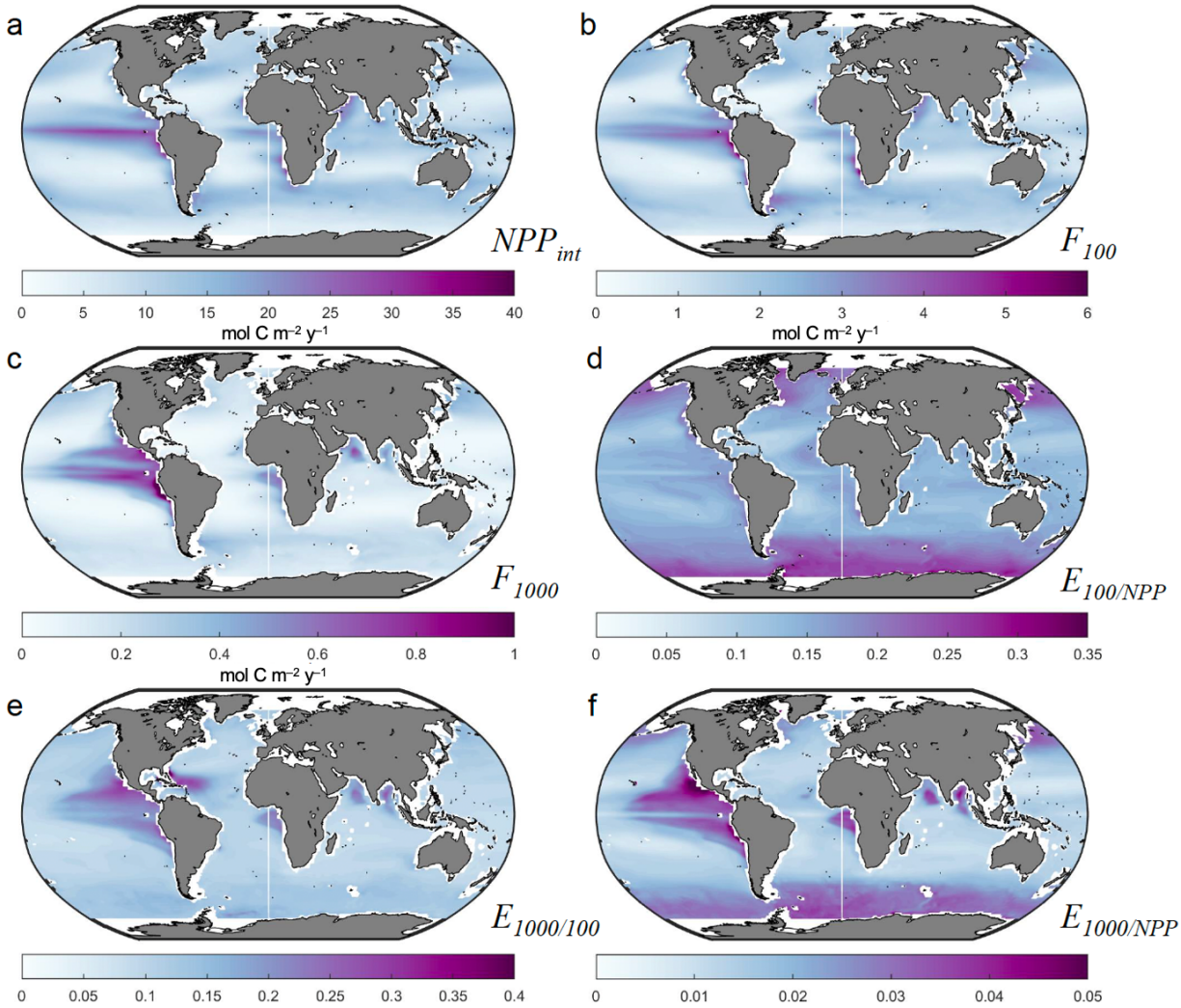

Figure 1. Multi-model ensemble averages of biological pump parameters from 1985 to 2018 across all RECCAP2 model simulations (simulation A). Maps of annual mean (a) integrated net primary productivity NPP, (b) particulate organic carbon export fluxes at 100 m F_{100}, and (c) 1000 m depth F_{1000}, all in mol C m^{-2} yr^{-1}. Ensemble mean (d) surface export efficiency ratio $E_{100/NPP} = F_{100}/NPP$ (Eq. 1), (e) mesopelagic transfer efficiency at 1000 m $E_{1000/100} = F_{1000}/F_{100}$ (Eq. 2), and (f) export efficiency to the deep ocean $E_{1000/NPP} = F_{1000}/NPP$, all ratios unitless.

The ensemble-mean transfer efficiency through the mesopelagic, $E_{1000/100}$ (Figure 1e; Table 3), exhibited background levels at the biome-scale of 0.09-0.14 for most biomes and ranging as high as 0.18 in the eastern equatorial Pacific biome; sub-biome regional values up to 0.3 occurred in the eastern tropical Pacific, western and eastern tropical Atlantic, and Arabian Sea and Bay of Bengal. Some ocean biogeochemical models reduce sub-surface POC remineralization in low-oxygen zones, using a parameterization based on local oxygen concentrations, driving higher $E_{1000/100}$ values in low-oxygen regions such as the eastern tropical Pacific, Arabian Sea and Bay of Bengal. Furthermore, POC flux mineral ballasting from Saharan dust deposition, prescribed as an

external forcing, is likely an important contributor in at least some models (CCSM-WHOI and CESM-ETHZ) to high $E_{1000/100}$ in the western tropical Atlantic (Lima et al., 2014). The ensemble $E_{1000/100}$ standard deviation (Figure S1e) generally followed $E_{1000/100}$ with particularly large $\sigma E_{1000/100}$ values up to 0.3 in the western tropical Atlantic reflecting differences across models in the parameterization of POC sinking in the presence of desert dust. The metric $E_{1000/NPP}$ (Figure 1f), combining surface export and mesopelagic transfer efficiencies, had generally similar spatial patterns to $E_{1000/100}$ but with lower values, reflecting the small fraction of NPP that sinks below 1000 m and is sequestered in the deep ocean. More than a factor of two variation was found for metric $E_{1000/NPP}$ across biomes (0.012 to 0.027) with large within-ensemble variation for some biomes where the standard deviation approached or exceeded the ensemble mean.

Table 3. Model ensemble averages and standard deviations of biological pump parameters by RECCAP2 regional biomes (Figure S2) (see also Figure 1) grouped as Sub-Polar Seasonally Stratified (SPSS), Sub-Tropical Seasonally Stratified (STSS), Sub-Tropical Permanently Stratified (STPS), Equatorial (EQU), and Mediterranean (MED). Table includes annual means and standard deviations for vertically integrated net primary productivity NPP, particulate organic carbon export fluxes at 100 m F_{100}, and 1000 m depth F_{1000}, all in mol C m^{-2} yr^{-1}, and average surface export efficiency ratio $E_{100/NPP} = F_{100}/NPP$, mesopelagic transfer efficiency at 1000 m $E_{1000/100} = F_{1000}/F_{100}$, and export efficiency to the deep ocean $E_{1000/NPP} = F_{1000}/NPP$, all ratios unitless. Ensemble were not computed for the small, high-latitude polar ice biomes due to noisy and/or missing data across the full ensemble.

	NPP	F_{100}	F_{1000}	$E_{100/NPP}$	$E_{1000/100}$	$E_{1000/NPP}$
SPSS						
N. PACIFIC	11.89±4.81	2.21±0.65	0.307±0.263	0.206±0.076	0.124±0.071	0.018±0.012
N. ATLANTIC	9.30±3.00	1.77±0.65	0.177±0.156	0.211±0.075	0.116±0.060	0.014±0.009
SOUTHERN	9.24±6.64	1.59±0.60	0.197±0.119	0.213±0.091	0.132±0.071	0.023±0.025
STSS						
N. PACIFIC	13.53±3.68	2.04±0.70	0.206±0.117	0.161±0.040	0.114±0.049	0.014±0.006
N. ATLANTIC	12.98±3.28	1.93±0.54	0.165±0.069	0.162±0.049	0.099±0.036	0.014±0.006
SOUTHERN	13.91±5.02	2.12±0.39	0.222±0.087	0.173±0.053	0.109±0.040	0.016±0.009
STPS						
N. PACIFIC	8.92±3.24	1.18±0.61	0.177±0.102	0.131±0.047	0.132±0.049	0.017±0.010
N. ATLANTIC	7.70±2.37	0.97±0.44	0.092±0.057	0.121±0.051	0.140±0.097	0.013±0.008
S. ATLANTIC	9.78±2.16	1.33±0.41	0.138±0.090	0.130±0.043	0.104±0.040	0.012±0.008
INDIAN	16.67±4.75	2.25±0.85	0.284±0.162	0.143±0.035	0.130±0.063	0.016±0.008
EQU						
W. PACIFIC	11.03±5.31	1.44±1.06	0.10±0.078	0.134±0.059	0.089±0.050	0.013±0.011
E. PACIFIC	21.16±5.16	2.91±0.74	0.542±0.288	0.151±0.043	0.178±0.086	0.027±0.015
ATLANTIC	14.33±4.71	1.94±0.65	0.272±0.137	0.145±0.039	0.140±0.043	0.019±0.010
MED	9.21±3.71	1.34±0.79	0.074±0.062	0.141±0.060	0.119± 0.107	0.011± 0.008

420

421 To illustrate differences among the models making up the RECCAP2 multi-model
422 ensemble, global integrals of the annual average biological pump metrics are displayed in Figure
423 2. A box-whisker plot is shown for each model ensemble member quantifying the interannual
424 variability for each model for the RECCAP2 reporting period (1985-2018). Note that some
425 RECCAP2 models did not report F_{1000}, resulting in missing estimates for $E_{1000/100}$ and $E_{1000/NPP}$.
426 Some models stood out as either anomalously low (e.g. FESOM-REcoM-LR for NPP) or high
427 (e.g. NEMO-PlankTOM12.1 for F_{100}) relative to the other RECCAP2 ensemble members, though
428 inter-model agreement alone was not necessarily a robust indicator of model skill (see Section
429 3.2). For global $E_{100/NPP}$, the models were roughly split into low (0.10-0.12) and high (0.16-0.19)
430 groups (Figure 2d). Global F_{1000}, $E_{1000/100}$, and $E_{1000/NPP}$ varied widely for the smaller number of
431 available models (Figure 2c, 2e, and 2f).
432

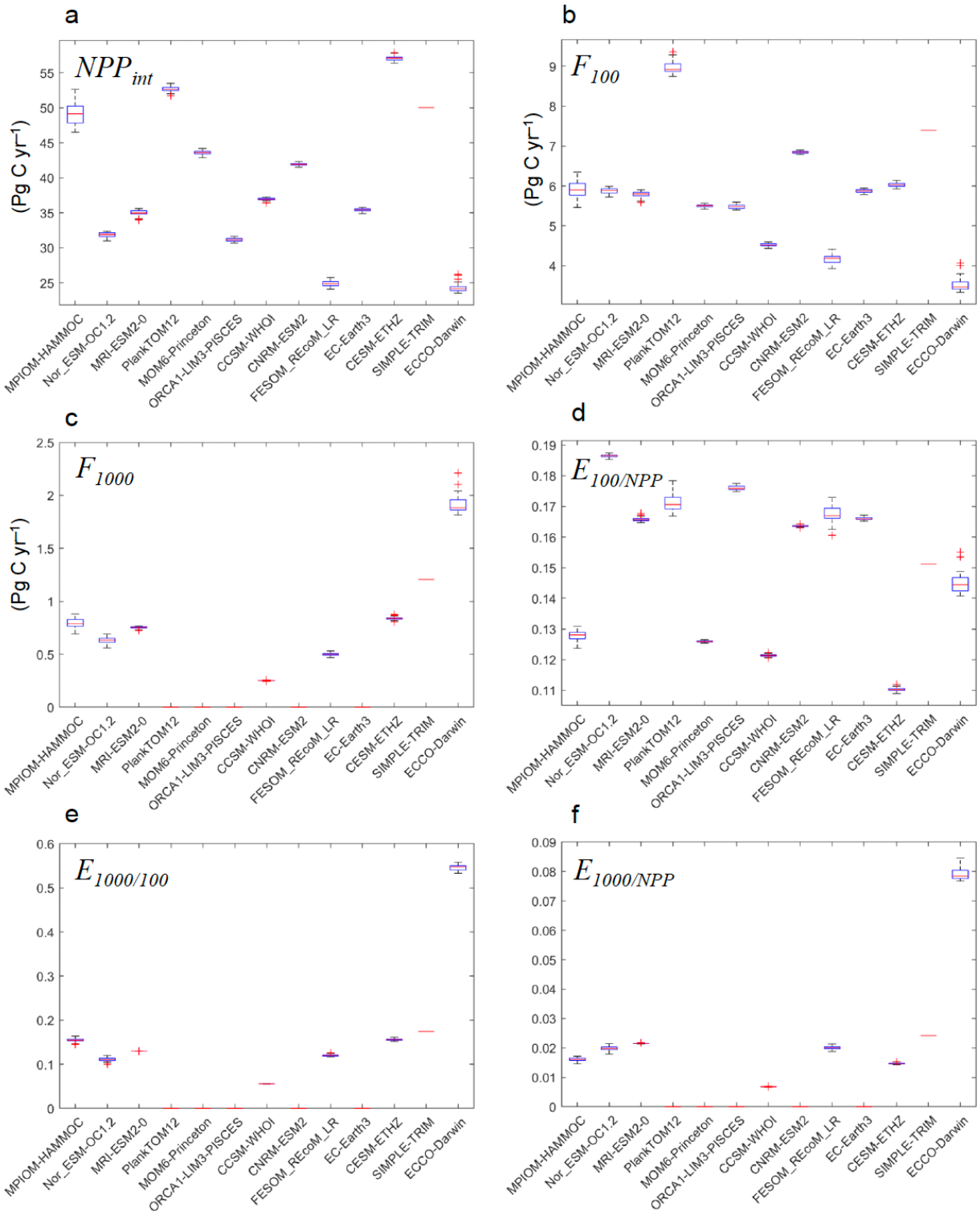

Figure 2. Boxplots showing median values (1985-2018), interannual interquartile ranges, and outliers of biological pump metrics across model products in RECCAP2 ensemble (simulation A). Globally integrated, annual (a) net primary productivity NPP, (b) particulate organic carbon export fluxes at 100 m F_{100}, and (c) 1000 m depth F_{1000} , all in Pg C y^{-1}. Global and annual average (d)

surface export efficiency ratio $E_{100/NPP} = F_{100}/NPP$ (Eq. 1), (e) mesopelagic transfer efficiency at 1000 m $E_{1000/100} = F_{1000}/F_{100}$ (Eq. 2), and (f) export efficiency to the deep ocean $E_{1000/NPP} = F_{1000}/NPP$, all ratios unitless. CCSM-WHOI output does not include the year 2018 and SIMPLE-TRIM does not simulate interannual variability. Efficiency ratios are not given in panels d, e, and f for models lacking the corresponding *NPP*, F_{100}, or F_{1000}.

3.2 Model-observational comparisons

The global ocean biological carbon pump metrics from the RECCAP2 multi-model ensemble were compared against corresponding literature values in Table 4 and Figure 3. The RECCAP2 multi-model ensemble global-integrated NPP value, 42.7 ± 10.9 Pg C yr^{-1}, was at the lower end of literature estimates (43.5-68 Pg C yr^{-1}), and the inter-quartiles have limited overlap. Similarly, global-integrated F_{100} from the multi-model ensemble of 6.41 ± 1.52 Pg C yr^{-1} was lower than the mean of the literature estimates of sinking POC flux (~8 Pg C yr^{-1}, range 4-13 Pg C yr^{-1}), though the inter-quartiles overlapped substantially because of the large range in observation-based estimates. The global-integrated model ensemble F_{1000} value of 0.95 ± 0.64 Pg C yr^{-1} fell between one low estimate of 0.66 Pg C yr^{-1} (Henson et al., 2012) and two other literature estimates of 1.1 Pg C yr^{-1}. The global multi-model ensemble-mean export and transfer efficiencies, $E_{100/NPP}$ (0.15 ± 0.03) and $E_{1000/100}$ (0.12 ± 0.04), were within the range of literature values after removing the high E_{100} values (0.3 and 0.38) from Laws et al. (2000) and acknowledging one low outlier model for global $E_{1000/100}$ (~0.05; CCSM-WHOI; Figure 2e).

The wide range of literature estimates reflects differences in measurement methodologies, biases, and uncertainties in the datasets used for biological carbon pump metric estimation, as well as uncertainties introduced by data sampling biases, aggregation, time/space interpolation and modeling approaches. At global scales, in situ observational sampling for some variables remains sparse and regionally patchy, and satellites, empirical relationships, and numerical models have been used to gap-fill for global-scale product generation. For example, even with field data sets available for ocean NPP based on ^{14}C uptake incubation studies, satellite remote sensing has been required to create uniform global NPP products, which have been calibrated/validated against ^{14}C NPP field data. A variety of in situ methods have been used to estimate surface ocean export flux estimates (~F_{100}) – drifting sediment traps, ^{234}Th deficit, etc. To derive global-scale fields of export, extrapolation from the limited in situ data is required which generates uncertainties in the derived estimates due to the underlying data sparsity (Henson et al., 2024). Typically, satellite data is used to build an empirical relationship between flux and readily derived variables, such as sea surface temperature or chlorophyll concentration. Other approaches include merging satellite data with food-web models (e.g., Siegel et al., 2014). Observation-based global F_{1000} estimates have been generated from sediment trap data (Mouw et al., 2016a), and estimates of both global F_{100} and F_{1000} have been derived from inverse and data-assimilation ocean models (e.g., Devries and Weber, 2017; Nowicki et al., 2022).

478 **Table 4**. Comparison of literature-based, global observation-based ocean biological carbon pump
479 metrics with the RECCAP2 model ensemble means and within-ensemble standard deviations.
480 Note that SIMPLE-TRIM data assimilation results from Devries and Weber (2017) are also
481 included in the RECCAP-2 model ensemble.

482

Net Primary Production *NPP* (Pg C yr^{-1})	**References**
43.5	VGPM Behrenfeld & Falkowski (1997)
52	CAFÉ Silsbe et al. 2016
68	Carr (2002) & Carr et al. 2006
49	Marra et al. (2003)
52	CbPM2 Behrenfeld et al. 2005
42.7 ± 10.9	**RECCAP2 model ensemble mean and STD**
POC Export ~F_{100} (Pg C yr^{-1})	
4	Henson et al. (2012)
9.6	Dunne et al. (2007)
11.1-12.9	Laws et al. (2000)
5.7	Siegel et al. (2014)
9.6	Schlitzer (2000); inversion
9-13	Laws et al. (2011)
8.8 (7.3 at 100 m)	DeVries & Weber (2017); data assimilating
7.3 (6.4 at 100 m)	Nowicki et al. (2022)
6.41 ± 1.52	**RECCAP2 model ensemble-mean and STD**
POC Flux 1000 m F_{1000} (Pg C yr^{-1})	
0.66	Henson et al. (2012)
1.1	DeVries & Weber (2017)
1.1	Nowicki et al. (2022)
0.95 ± 0.64	**RECCAP2 model ensemble mean and STD**
Export Ratio ~$E_{100/NPP}$	
0.1	Henson et al. (2012)
0.19	Dunne et al. (2007)
0.3	Laws et al. (2000); food web
0.38	Laws et al. (2000); empirical
0.103	Siegel et al. (2014)
0.17	Devries & Weber (2017)

0.13 (for POC only) 0.18 (for POC + DOC + vertical migration)	Nowicki et al. (2022)
0.154 ± 0.026	**RECCAP2 model ensemble mean and STD**
Transfer Flux Efficiency $E_{1000/100}$	
0.19	Henson et al. (2012)
0.13	DeVries & Weber (2017)
0.15	Nowicki et al. (2022)
0.121 ± 0.035	**RECCAP2 model ensemble mean**

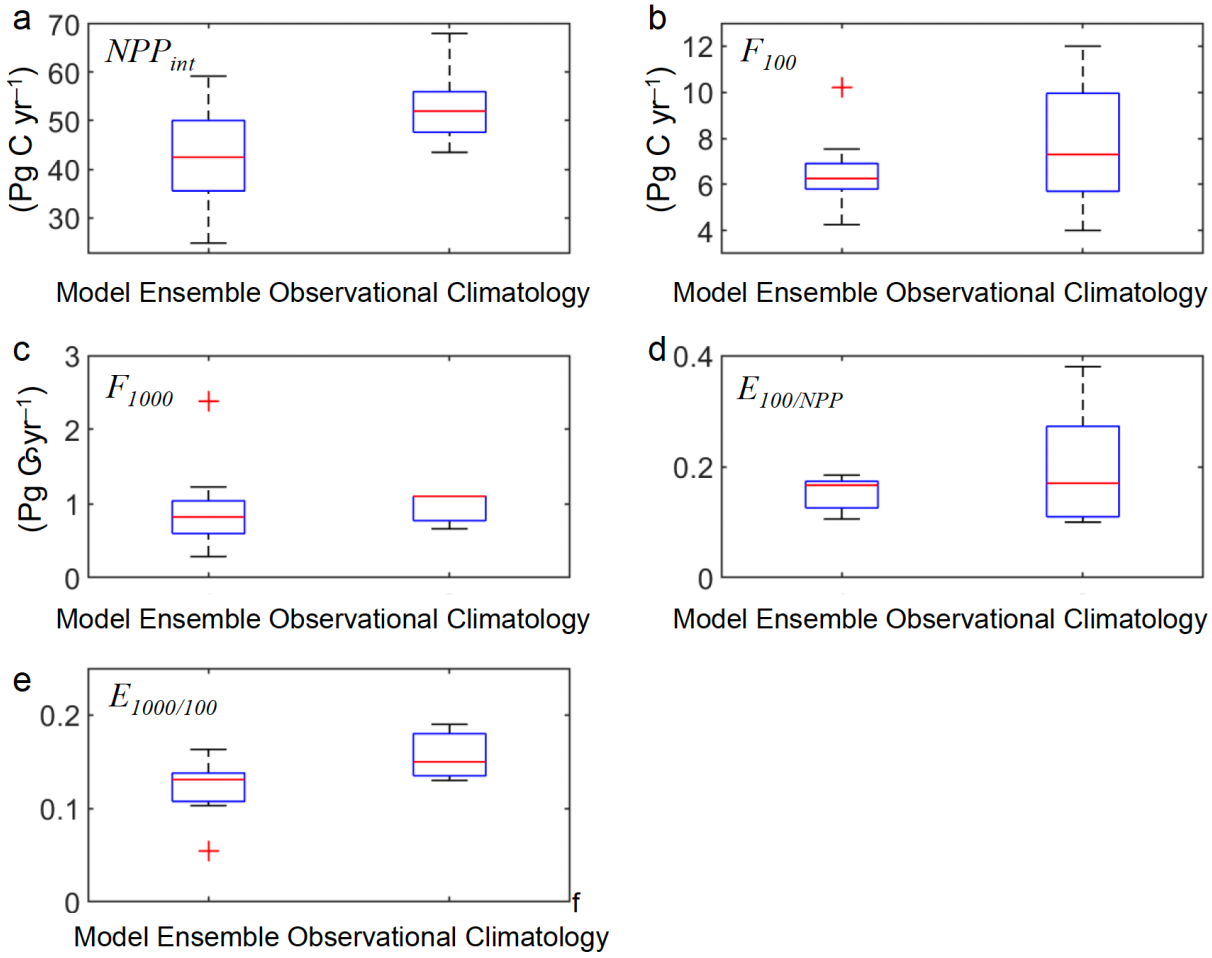

Figure 3. Box-whisker plots showing median values and interquartile ranges of biological pump parameters from 1985-2018 averaged across model products in RECCAP2 ensemble (simulation A). Global integrated, annual (a) net primary productivity *NPP*, (b) particulate organic carbon export fluxes at 100 m F_{100}, and (c) 1000 m depth F_{1000} , all in Pg C yr^{-1} (note that the median line for F_{1000} is also the upper interquartile because two of the three observational estimates match).

491 Global and annual average surface export efficiency ratio (d) $E_{100/NPP} = F_{100}/NPP$ (Eq. 1), and (e)
492 mesopelagic transfer efficiency at 1000 m $E_{1000/100} = F_{1000}/F_{100}$ (Eq. 2), all ratios unitless.

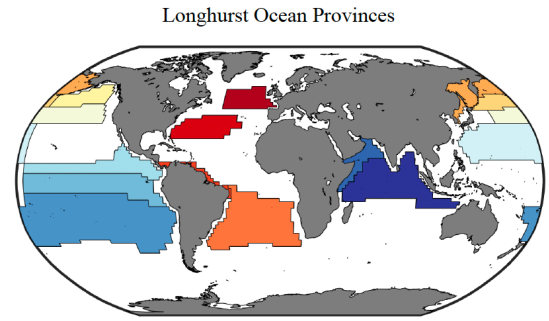

Province Number	Province Code	Province Description
1	NADR	Westerlies - N. Atlantic Drift Province
2	NASW	Westerlies - N. Atlantic Subtropical Gyral Province (West)
3	GUIA	Coastal - Guianas Coastal Province
4	SATL	Trades - South Atlantic Gyral Province (SATG)
5	BERS	Polar - N. Pacific Epicontinental Province
6	PSAW	Westerlies - Pacific Subarctic Gyres Province (West)
7	PSAE	Westerlies - Pacific Subarctic Gyres Province (East)
8	NPPF	Westerlies - N. Pacific Polar Front Province
9	NPSW	Westerlies - N. Pacific Subtropical Gyre Province (West)
10	PNEC	Trades - N. Pacific Equatorial Countercurrent Province
11	PEQD	Trades - Pacific Equatorial Divergence Province
12	SPSG	Westerlies - S. Pacific Subtropical Gyre Province
13	ARAB	Coastal - NW Arabian Upwelling Province
14	MONS	Trades - Indian Monsoon Gyres Province

Figure 4. Map of Longhurst provinces (Reygondeau et al., 2013) used in analysis of biological pump field observations and model results (Mouw et al., 2016a).

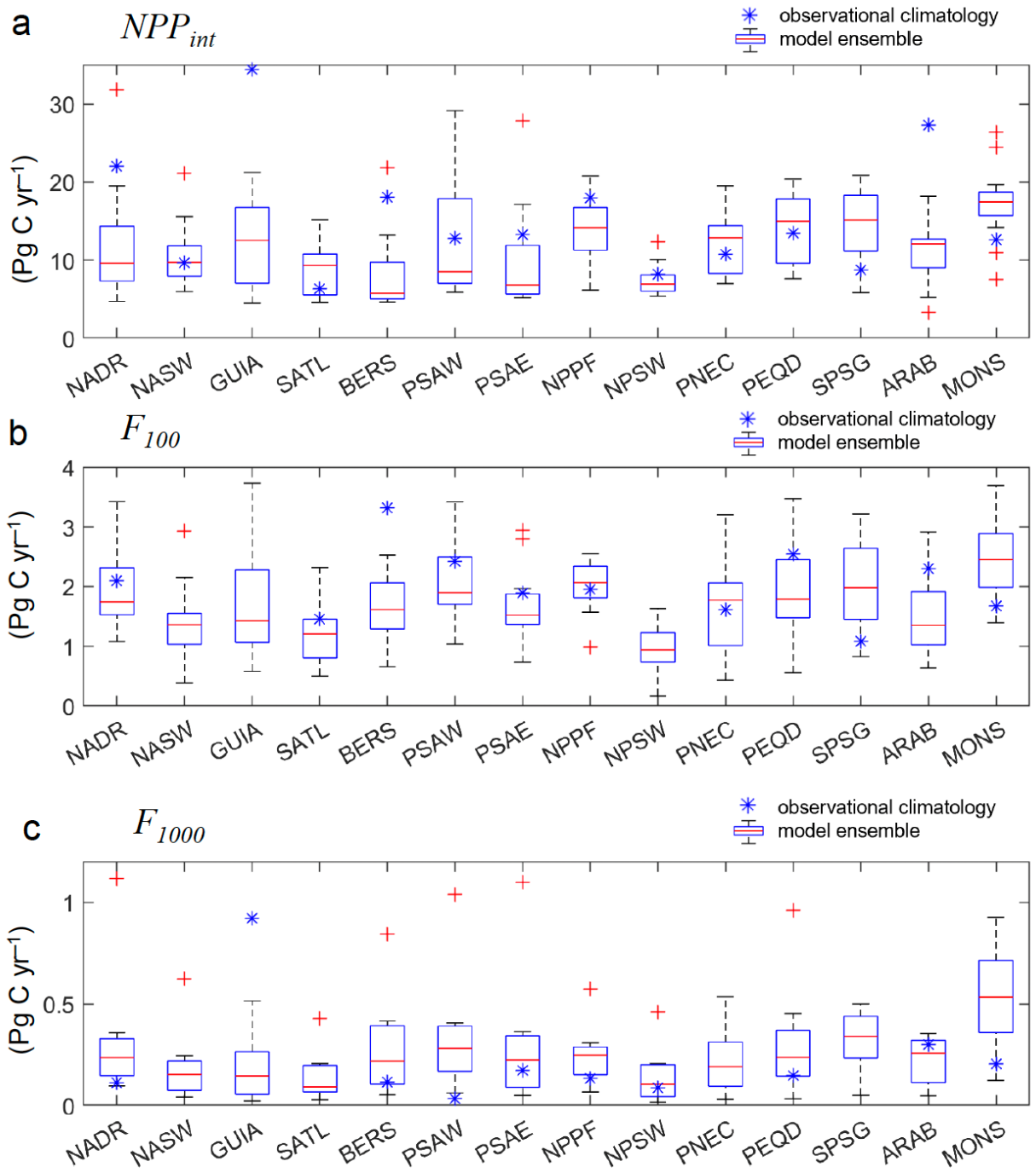

Figure 5. Box-whisker plot of RECCAP2 multi-model ensemble medians, interquartile ranges, and outliers for annual-mean (a) vertical integrated primary production (NPP_{int}), (b) sinking POC fluxes at 100m (F_{100}), and (c) sinking POC flux at 1000m (F_{1000}), all in Pg C yr^{-1}, pooled into biogeochemical Longhurst ocean provinces (Figure 4) and compared to the observational climatology for the same provinces constructed by Mouw et al. (2016b). Robust uncertainty estimates are not available for the observational climatology which averages available data that is

often spatially sparse and/or concentrated in brief time intervals. Note that only provinces with sufficient observational data are plotted (see Figure 4).

The biological carbon pump model comparison to observation-based estimates was extended in Figure 5 to a regional level using the observational data of Mouw et al. (2016a) as aggregated by Mouw et al. (2016b) into monthly climatological values for Longhurst biogeographic provinces (Figure 4). The Mouw et al. (2016a) date set aggregates the limited available field data that is often spatially sparse and locally high frequency with considerable mesoscale variability, some of which may be aliased into monthly and province scale averages. Therefore, robust uncertainty estimates are not available for the Mouw et al. (2016b) observational climatology. The variations across the RECCAP2 models are displayed as box-whisker plots. The members of the model ensemble exhibited a wide range of NPP, F_{100} and F_{1000} values for many provinces, but still the observational climatology falls within the multi-model ensemble inter-quartiles for only about half of the provinces. The substantial model-observational offsets indicate recurring regional differences consistent across multiple models in the RECCAP2 ensemble; these disagreements could be targets for future ocean biogeochemical model development and analyses of observational sampling biases. The model ensemble members also exhibited extreme model-data differences in some provinces where the observational climatology value falls outside the simulated range including model outliers. The RECCAP2 models consistently underestimated the strength of biological carbon pump metrics, relative to the observational climatology, in polar and sub-polar provinces in the North Pacific (N. Pacific epicontinental sea, BERS, low NPP and F_{100}) and North Atlantic (N. Atlantic Drift, NADR, low NPP); and in equatorial provinces in the Indian (Northwest Arabian Sea upwelling, ARAB, low NPP), Pacific (Trades-Pacific Equatorial Divergence, PEQD, low F_{100}) and Atlantic (Guianas coast, GUIA, low F_{1000}; note, the observed high Guianas coast value reflects a small, productive region that may not be well represented in global-scale models). In other provinces, the model ensemble overestimated the biological pump in the South Pacific gyre (SPSG, high NPP and F_{100}), Indian monsoon gyre (MONS, high NPP and F_{100}), and Western Pacific subarctic gyres (PSAW, high F_{1000}).

3.3 Biological pump imprint on ocean CO_2 system and biogeochemistry

The ocean biological carbon pump imprints on surface and sub-surface biogeochemistry (see Introduction), and these effects are simulated in the RECCAP2 models. A strong positive mesopelagic AOU signal is generated by cumulative biological O_2 consumption along the ventilation paths of subsurface waters (Najjar et al., 2007). AOU fields thus integrate non-local, large-scale biogeochemical dynamics and physical resupply of O_2 from the surface. A key contributor to AOU is the remineralization of sinking POC flux in the mesopelagic, quantified by the large decline between F_{100} and F_{1000} and low transfer efficiency through the mesopelagic $E_{1000/100}$ (Figures 1–3; Tables 3 and 4). For the RECCAP2 model ensemble, there was generally good model-data agreement in the geographic pattern in AOU averaged over the mesopelagic (100–1000 m) (Figure 6). The model ensemble captured the regional AOU variation of <50 to >250 μmol kg^{-1}, though substantial disagreement arose on the scale of Longhurst provinces where the model-ensemble interquartile spans the observational data for only a handful of provinces (Figure 6c). The RECCAP2 models did not exhibit a strong inter-model relationship between global mean AOU and F_{100} (not shown). The weak relationship between AOU and F_{100} across models likely highlights the influence on AOU of substantial variations in the strength of model

thermocline ventilation rates that could also influence simulated anthropogenic CO_2 uptake (e.g., Dutay et al., 2002; Matsumoto et al., 2004). Model deep-ocean AOU was not evaluated because model spin-up time scales were too short for the simulations to reach steady-state (Séférian et al., 2019), an issue that also would affect simulated deep-ocean preindustrial DIC (Mikaloff Fletcher et al., 2007). Some imprint of the observational fields used for model initial conditions could also be retained in the simulated mesopelagic AOU depending on the model spin-up procedure.

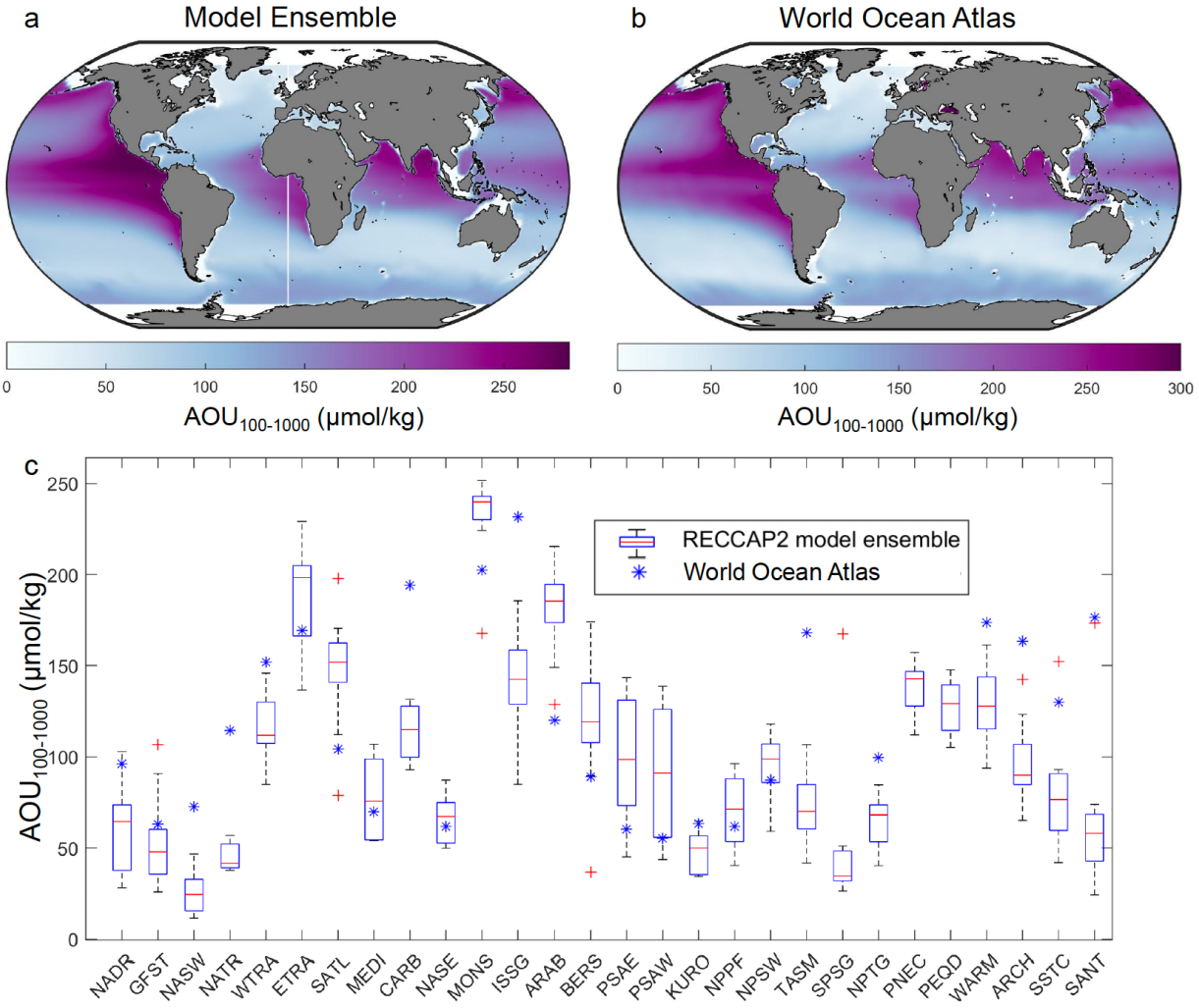

Figure 6. Analysis of apparent oxygen utilization (AOU, µmol kg^{-1}) vertically averaged over the mesopelagic zone (100-1000 m): (a) spatial map of RECCAP2 multi-model ensemble average, and (b) spatial map from WOA observational data set, and (c) box-whisker plot of RECCAP2 multi-model ensemble medians, interquartile ranges, and outliers pooled into biogeochemical Longhurst ocean provinces (Figure 4).

The simulated regional patterns and global integrated surface POC export F_{100} (Figures 1–3; Tables 3 and 4) must be balanced on appropriate time and space scales by new production and external nutrient supply, largely from physical upwelling and mixing for most ocean regions

(Ducklow and Doney, 2013). As an indicator of physical controls on export associated with nutrient supply, the individual RECCAP2 model, global-integrated F_{100} values exhibited a positive correlation with global-ocean anthropogenic CO_2 uptake (Figure 7) (DeVries et al., 2023). This is consistent with findings from previous model intercomparison exercises where models with stronger thermocline ventilation had both larger export flux and anthropogenic CO_2 uptake (Najjar et al., 2007). The F_{100}–anthropogenic CO_2 uptake correlation, therefore, is indirect through a common underlying physical mechanism whereby stronger ventilation enhances both the downward transport of anthropogenic CO_2 correlation and the upward transport of nutrients and thus F_{100}. The physical-chemical solubility mechanisms controlling ocean anthropogenic CO_2 uptake are well documented, and there is no evidence of any significant role for biogeochemical processes, though climate-change biogeochemical feedbacks on ocean carbon storage may become more important in the future (Canadell et al., 2021).

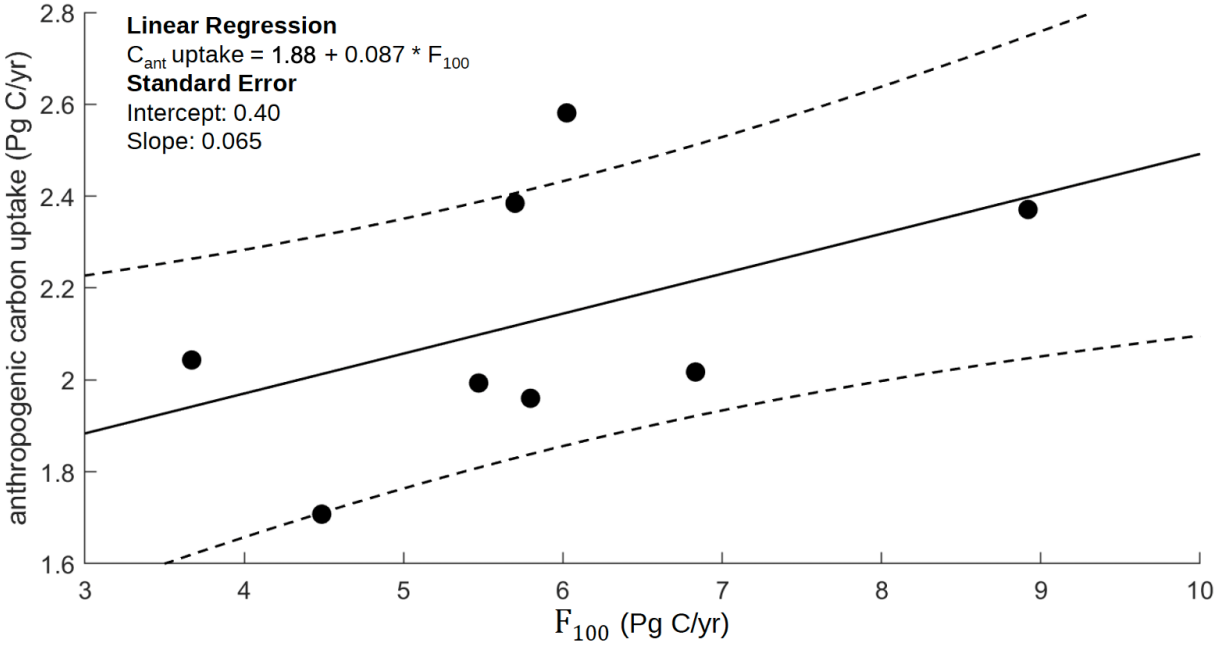

Figure 7. Scatter plot of global-integrated ocean anthropogenic CO_2 uptake (mean of 1985-2018) (Pg C yr^{-1}) versus particulate organic carbon (POC) export flux (F_{100}, Pg C yr^{-1}) for individual RECCAP2 models. Anthropogenic CO_2 uptake for the same RECCAP2 models was taken from DeVries et al. (2023) A linear regression and confidence intervals for the regression are overlain. The F_{100}–anthropogenic CO_2 uptake correlation was indirect through a common underlying physical mechanism whereby stronger ventilation enhances both the downward transport of anthropogenic CO_2 correlation and the upward transport of nutrients and thus F_{100}.

Seasonal variations in upper-ocean biogeochemistry were used as a metric of the physical controls associated with seasonal mixing and nutrient supply, which are reflected in simulated POC export. By correcting for seasonal thermal variations in pCO_2 (Equation 3), we used model monthly pCO_2 fields to quantify the combined effects of seasonal biogeochemical, gas-exchange and physical processes through the seasonal amplitude of non-thermal pCO_2, $\Delta pCO_{2,\text{non-thermal}}$ (Takahashi et al., 2002). The geographic pattern of $\Delta pCO_{2,\text{non-thermal}}$ from the RECCAP2 model

599 ensemble was similar to the pattern from the mean of the pCO_2 observational products (Figure 8a
600 and 8b). Both the model ensemble and observational products exhibited regional variations of
601 $\Delta pCO_{2,non\text{-}thermal}$ that ranged from 30 to >150 μatm with elevated values in mid- to high latitudes
602 as well as equatorial and eastern boundary current upwelling regions. However, the magnitude of
603 $\Delta pCO_{2,non\text{-}thermal}$ in the model ensemble was considerably lower in the mid- to high latitude northern
604 hemisphere, eastern tropical Pacific, and Brazil-Malvinas convergence region, suggesting a
605 generally weaker modeled seasonal cycling of DIC. The same low bias in the RECCAP2 models
606 was evident on the scale of Longhurst provinces where the observational products fell at the top
607 end or well above the model-ensemble interquartile (Figure 8c). In many ocean regions, strong
608 seasonality in mixed layer depth modulates vertical nutrient supply and annual-mean biological
609 productivity. The weaker model ensemble $\Delta pCO_{2,non\text{-}thermal}$ values (Figure 8), therefore, may be
610 linked to regional patterns of lower NPP and F_{100} relative to observations (Figure 5) in the North
611 Pacific (BERS province), North Atlantic (NADR province), eastern equatorial Pacific (PEQD),
612 and Brazil-Malvinas convergence (western part of SATL province).
613

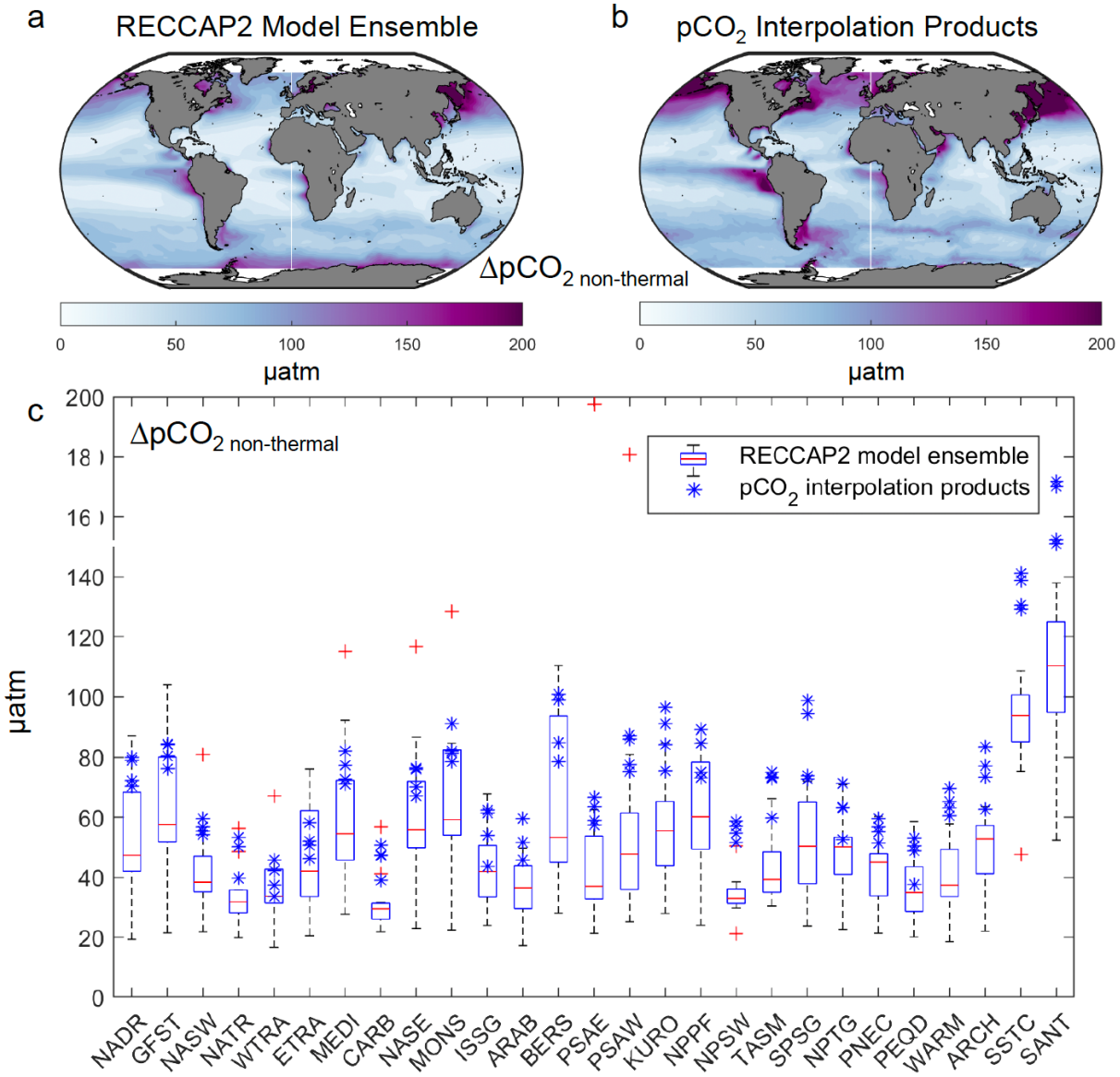

Figure 8. Analysis characterizing the combined effects of seasonal biogeochemical, gas-exchange and physical processes using the seasonal amplitude of non-thermal $\Delta pCO_{2_{non-thermal}}$ (a) spatial map of RECCAP2 multi-model ensemble average, (b) spatial map from pCO_2 observational data products, and (c) box-whisker plot of RECCAP2 multi-model ensemble medians, interquartile ranges, and outliers pooled into biogeochemical Longhurst ocean provinces (Figure 4). The province means from each observational product are plotted in panel (c) as individual points rather than as box-whiskers because of the limited number of observational products.

4 Discussion and Conclusions

Our analysis of the ocean biological carbon pump fields from the RECCAP2 multi-model ensemble revealed generally encouraging agreement with many aspects of observed patterns.

Global-integrated NPP and surface export flux (F_{100}) from the RECCAP2 models tended to fall at the lower end of observational estimates (Figure 3 and Table 4), and geographic patterns in NPP were generally consistent with observational data products (Figures 1 and 5). Similar to previous model intercomparison studies (Laufkötter et al., 2015; Laufkötter et al., 2016), we found substantial within-ensemble variation in global biological carbon pump metrics, including the presence of model outliers (Figure 3), indicating that these aspect of biogeochemical models have not necessarily converged with time.

Regional patterns in the RECCAP2 model-mean ensemble included elevated NPP, surface export flux (F_{100}) and export efficiency (E_{100}) in high-latitudes and coastal and equatorial upwelling regions, with lower values in more oligotrophic regions. These results are in line with previous studies that found that a substantial proportion of NPP in nutrient-rich regions is driven by large phytoplankton such as diatoms and, combined with an active zooplankton population, this can generate a significant export flux in the form of both dense aggregates and fecal pellets. High-latitude elevated biomass, colder temperatures (Dunne et al., 2005), and strong seasonality also have been implicated in observations of higher POC export fluxes in spring and/or summer months contributing to the annual mean (Buesseler et al., 2001; Lampitt et al., 2001; Bol et al., 2018; Henson et al., 2023). In low nutrient regimes, such as the lower latitude oligotrophic gyres, previous studies report export flux to be low (Henson et al., 2012) but relatively constant throughout the year with small seasonal increases in fluxes (Karl et al., 2012). Future studies of the RECCAP2 ensemble could investigate in more detail the seasonality in NPP, F_{100}, and E_{100}, exploring, for example, the seasonal variability in export ratio that can be substantial due in part to the time lag between NPP and export flux (Henson et al., 2015; Giering et al., 2017; Laws and Maiti, 2019; Henson et al., 2015).

The sinking POC flux into the deep ocean (F_{1000}) and mesopelagic transfer efficiency across the mesopelagic zone ($E_{1000/100}$) in the RECCAP2 multi-model ensemble (Figures 1 and 5) exhibited different spatial patterns than found for surface export, similar to findings of previous studies (e.g., Henson et al., 2012). Simulated F_{1000} and $E_{1000/100}$ were greater in the tropical eastern Pacific, eastern Atlantic, and Arabian Sea, and $E_{1000/100}$ was also elevated in the western tropical North Atlantic and, to a lesser extent, Southern Ocean. Previous model studies have also found substantial regional variations due to particle size and composition effects (Lima et al., 2014) that modify empirical power curves used for modeling POC sinking and remineralization (Martin et al., 1987). Model parameterizations tend to increase the effective remineralization length scales and thus transfer to depth in regions with high mineral fluxes (e.g., dust, $CaCO_3$, silica) (Armstrong et al., 2002) or in tropical oxygen minimum zones (Laufkötter et al., 2017; Dinauer et al., 2022). The RECCAP2 regional variations in mesopelagic transfer efficiency, modulated with basin-scale variations in physical circulation-driven sequestration time-scale (Siegel et al., 2021), influence the effect of the biological pump on ocean carbon storage (Kwon et al., 2009).

While we focused primarily on long-term mean NPP and export fluxes, the RECCAP2 models also exhibited year-to-year variability (Table S1), though typically much lower than within-ensemble model differences (Figure 2), and small long-term temporal trends (Table S2). No consistent positive or negative trend was observed across the models in simulated NPP and sinking POC fluxes at 100m and 1000m, with NPP trends of order ±0.01 Pg C yr^{-1}/year over the 33 years of the time series (1985-2018). Although these trends could contain a signal from climate change, the relatively short duration of the RECCAP2 analysis period resulted in large signal to noise due to interannual variability. Previous modeling studies indicate that chlorophyll and NPP

time series of 30-40 years length are needed to distinguish climate change trends from natural variability (Henson et al., 2010). Hence, the RECCAP2 analysis period may indeed not be long enough to separate trends from interannual variability. While a recent study suggests that climate-change trends can emerge more rapidly in ocean color remote-sensing reflectance (Cael et al., 2023), any actual climate change signal in models may be masked by temporal biases associated with incomplete model spin-up and resulting temporal drift (Séférian et al., 2016).

Our analysis of the biological carbon pump was relevant in several ways to the primary focus of the RECCAP2 ocean project on air-sea CO_2 fluxes and ocean uptake of anthropogenic CO_2 (DeVries et al., 2023). Biological net CO_2 uptake and carbon export modulate the background, pre-industrial and contemporary spatial and seasonal patterns of surface ocean pCO_2 and sea-air CO_2 flux that must be accounted for to determine anthropogenic CO_2 perturbations. The low model F_{100} values globally (Figure 3) and for mid- to high-latitude Northern Hemisphere and eastern equatorial Pacific provinces (Figure 5), relative to observations, suggested that the RECCAP2 model ensemble may have underestimated biological CO_2 drawdown in high productivity regions. Potential issues were also identified in simulated seasonal biogeochemical, gas-exchange and physical dynamics as captured in the seasonal amplitude of non-thermal pCO_2 variations, with weaker $\Delta pCO_{2,\text{non-thermal}}$ values found at mid- to high-latitudes and in the eastern equatorial Pacific in the model ensemble relative to observations (Figure 8). Future work with more detailed model diagnostics could explore the connections between regional biases in simulated annual-mean and seasonal export production and biases in air-sea CO_2 flux as observed in other RECCAP2 studies (DeVries et al., 2023; Hauck et al., 2023).

Ocean circulation modulates biological export flux on basin to global scales (Najjar et al., 2007), and the range in RECCAP2 global-integrated F_{100} values indicated that substantial differences exist in simulated ocean physics within the RECCAP2 marine biogeochemical models (Doney et al., 2004). The same ocean circulation variations also likely influenced the anthropogenic CO_2 uptake estimates from DeVries et al. (2023) as indicated by the positive correlation between anthropogenic CO_2 uptake and F_{100} across individual RECCAP2 models (Figure 7). This is supported by further analysis of the RECCAP2 models demonstrating that the rate of ocean overturning circulation is strongly correlated with anthropogenic CO_2 uptake in the models (Terhaar et al., 2023). Variations in model export could also be compared against metrics of physical stratification (Fu et al., 2022). The substantial inter-model spread in both physical and biogeochemical metrics likely reflects common factors resulting from differences in simulated thermocline ventilation and exchange between the surface and mid-depth ocean.

A set of additional model development recommendations emerge from our analyses. One path forward would leverage independent model skill evaluation for inert chemical tracers (e.g., CFC-11, CFC-12, SF_6) using standard ocean model intercomparison protocols (e.g., CMIP6 Ocean Model Intercomparison Project; Orr et al., 2017). The transient tracer simulations would help decipher the physical-biological factors controlling simulated AOU (Figure 6). Remineralization of sinking biological organic matter structures sub-surface ocean dissolved inorganic carbon, O_2, and nutrient fields, a signal that must be addressed in observational estimates of anthropogenic CO_2. While the predominant pathway for ocean anthropogenic CO_2 uptake involves physical-chemical dynamics, rather than biological dynamics, the same physical circulation and mixing processes influence biogeochemical rates such as nutrient supply. Therefore, evaluation and improvement of the ocean biological pump may provide additional insight.

716 The substantial variation in biological pump metrics shown here highlighted the need to
717 reconcile inter-model and model-observational differences. Challenges arise for model
718 improvement because there is limited agreement on the appropriate parameterizations for many
719 key processes of biological carbon export (Henson et al., 2022), subsurface particle sinking, and
720 remineralization. Many global models include detailed representation of euphotic zone processes
721 but rather more simplistic representation of mesopelagic processes. Thus, the simulated global-
722 scale biological carbon pump responses to interannual variability, let alone decadal climate
723 change, remain poorly constrained (Henson et al., 2016). Following the mechanistic approach
724 reported in previous model intercomparison studies for primary production (Laufkötter et al.,
725 2015) and export production (Laufkötter et al., 2016), future studies could emphasize how overall
726 model behavior reflects differences in model parameterizations, functional equations, and
727 parameter values in both the euphotic and mesopelagic zones.

728 Opportunities exist to leverage process-level information from lab and field studies to
729 improve model treatment of POC production, sinking POC flux and extension of export pathways
730 beyond POC gravitational sinking, for example physical subduction and active migration by
731 organisms (Boyd et al., 2019; Siegel et al., 2016; Henson et al., 2022; Siegel et al., 2023).
732 Phytoplankton community structure, captured to some degree in many models, influences
733 magnitude and composition of export flux from the euphotic zone, the heterotrophic consumers of
734 sinking POC and zooplankton community structure (Boyd and Newton, 1995; Cavan et al., 2019).
735 Model treatments could be improved for grazers, such as zooplankton, that act to decrease particle
736 flux by consuming phytoplankton and sinking POC, while also increasing flux by packaging POC
737 into fecal pellets with a wide range of sinking speeds (Turner, 2015; Steinberg and Landry, 2017).
738 Grazer diel vertical migration may also need to be incorporated as a carbon shunt below the depth
739 horizons of most intense heterotrophic activity (i.e., upper mesopelagic zone), consuming POC in
740 the surface ocean and respiring it at grazer resident daytime depth (Bianchi et al., 2013). More
741 mechanistic treatment of particle dynamics may also be feasible. Particle disaggregation,
742 physically through shear or biologically through fragmentation by grazers, likely contributes
743 substantially to the decline in POC flux with depth while also providing a POC source for
744 mesopelagic microbes (Laurenceau-Cornec et al., 2020; Briggs et al., 2020). Microbes also can
745 reduce POC flux directly, as they constantly attach and detach from sinking POC (Kiørboe et al.,
746 2002; Kiørboe et al., 2003), hydrolyzing and respiring the POC. While variable particle sinking
747 speed is included in some model parameterizations, large meta-analyses of empirical data have
748 struggled to find a strong link between sinking rate and size of particles, because of the vast
749 variability in particle type, methods used to measure sinking rate, and environment the particles
750 were collected from (Cael et al., 2021).

751 Many of these process-level insights are already driving progress on mechanistic
752 parameterizations for sinking particle flux (e.g., Dinauer et al., 2022), vertical migration (e.g.,
753 Archibald et al., 2019), and other key factors in the marine biological pump. Together with global-
754 scale ocean biogeochemical data compilations and syntheses (e.g., Mouw et al., 2016a; Mouw et
755 al., 2016b, Clements et al., 2023) there are now promising new opportunities to evaluate, constrain,
756 and improve ocean biological carbon pump simulations. Based on the model-data analysis
757 presented here, the RECCAP2 multi-model ensemble exhibited relatively good agreement with
758 observed biological carbon pump metrics, where there is sufficient data. The analysis also
759 identified model-data biases and substantial differences among some of the models included in
760 RECCAP2. These biases should be used to guide directions for future model development.

Funding

S.C. Doney and K.A. Mitchell acknowledge support from the U.S. National Science Foundation via the Center for Chemical Currencies of a Microbial Planet (NSF 2019589). S.A. Henson received support from a European Research Council Consolidator grant (GOCART, agreement number 724416). S. Henson and J. Hauck received support from the European Union's Horizon 2020 research and innovation programme under grant agreement no. 820989 (COMFORT), and the European Union's Horizon Europe research and innovation programme under grant agreement no. 101083922 (OceanICU). Funding to J. Hauck was provided by the Initiative and Networking Fund of the Helmholtz Association (Helmholtz Young Investigator Group Marine Carbon and Ecosystem Feedbacks in the Earth System, MarESys, Grant VH-NG-1301). J.D. Müller and N. Gruber acknowledge support from the European Union's Horizon 2020 research and innovation programme under grant agreement no. 821003 (project 4C) and no. 820989 (project COMFORT). T. DeVries acknowledges support from NSF grant OCE-1958955. E.L. Cavan was funded by an Imperial College Research Fellowship.

Acknowledgements

Conceptualization (Ideas; formulation or evolution of overarching research goals and aims): S.C.D, S.A.H.

Data curation (Management activities to annotate (produce metadata), scrub data and maintain research data (including software code, where it is necessary for interpreting the data itself) for initial use and later re-use): K.A.M, J.D.M.

Formal analysis (Application of statistical, mathematical, computational, or other formal techniques to analyze or synthesize study data): S.C.D., K.A.M., S.A.H.

Funding acquisition (Acquisition of the financial support for the project leading to this publication): S.C.D, S.A.H.

Investigation (Conducting a research and investigation process, specifically performing the experiments, or data/evidence collection): All co-authors

Methodology (Development or design of methodology; creation of models): S.C.D., K.A.M., S.A.H.

Project administration (Management and coordination responsibility for the research activity planning and execution): S.C.D., S.A.H., J.D.M.

Software (Programming, software development; designing computer programs; implementation of the computer code and supporting algorithms; testing of existing code components): K.A.M., J.D.M.

Supervision (Oversight and leadership responsibility for the research activity planning and execution, including mentorship external to the core team): S.C.D, S.A.H., J.D.M.

Visualization (Preparation, creation and/or presentation of the published work, specifically visualization/data presentation): S.C.D., K.A.M.

Writing – original draft (Preparation, creation and/or presentation of the published work, specifically writing the initial draft (including substantive translation)): S.C.D., K.A.M., S.A.H., E.C.

Writing – review and editing (Preparation, creation and/or presentation of the published work by those from the original research group, specifically critical review, commentary or revision – including pre- or post-publication stages): All co-authors

Open Research

The RECCAP2 ocean data collection can be found in Müller (2023).

Müller, Jens Daniel. (2023). RECCAP2-ocean data collection [Data set]. Zenodo. 1631 https://doi.org/10.5281/zenodo.7990823

References

Archibald, K., Siegel, D. A., & Doney, S. C. (2019) Modeling the impact of zooplankton diel vertical migration on the carbon export flux of the biological pump. *Global Biogeochemical Cycles*, *33*, 181–199. https://doi.org/10.1029/2018GB005983

Armstrong, R. A., Lee, C., Hedges, J. I., Honjo, S., & Wakeham, S. G. (2001). A new, mechanistic model for organic carbon fluxes in the ocean based on the quantitative association of POC with ballast minerals, *Deep Sea Research Part II*, *49*, 219–236. https://doi.org/10.1016/S0967-0645(01)00101-1

Aumont, O., Ethé, C., Tagliabue, A., Bopp, L., & Gehlen, M. (2015). PISCES-v2: An ocean biogeochemical model for carbon and ecosystem studies. *Geoscientific Model Development, 8*, 2465–2513. https://doi.org/10.5194/gmd-8-2465-2015

Bacastow, R., & Maier-Reimer, E. (1990). Ocean-circulation model of the carbon cycle. *Climate Dynamics*, *4*, 95–125. https://doi.org/10.1007/BF00208905

Behrenfeld, M. J., & Falkowski, P. G. (1997). Photosynthetic rates derived from satellite-based chlorophyll concentration. *Limnology and Oceanography*, *42*, 1–20. https://doi.org/10.4319/lo.1997.42.1.0001

Behrenfeld, M. J., Boss, E., Siegel, D. A., & Shea, D. M. (2005). Carbon-based ocean productivity and phytoplankton physiology from space, *Global Biogeochemical Cycles*, *19*, GB1006. https://doi.org/10.1029/2004GB002299.

Berthet, S., Séférian, R., Bricaud, C., Chevallier, M., Voldoire, A., & Ethé, C. (2019). Evaluation of an online grid-coarsening algorithm in a global eddy-admitting ocean-biogeochemical model. *Journal of Advances in Modeling Earth Systems*, *11*(6), 1759–1783. https://doi.org/10.1029/2019ms001644

Bianchi, D., Stock, C., Galbraith, E. D., & Sarmiento, J. L. (2013). Diel vertical migration: Ecological controls and impacts on the biological pump in a one-dimensional ocean model. *Global Biogeochemical Cycles*, *27*, 478–491. https://doi.org/10.1002/gbc.20031

Bol, R., Henson, S. A., Rumyantseva, A., & Briggs, N. (2018). High-frequency variability of small-particle carbon export flux in the Northeast Atlantic. Global Biogeochemical Cycles, 32, 1803–1814. https://doi.org/10.1029/2018GB005963

Boyd, P., & Newton, P. (1995). Evidence of the potential influence of planktonic community structure on the interannual variability of particulate organic carbon flux, Deep Sea Research Part I, 42, 619–639. https://doi.org/10.1016/0967-0637(95)00017-Z

Boyd, P.W., Claustre, H., Levy, M., Siegel, D. A., & Weber, T. (2019). Multi-faceted particle pumps drive carbon sequestration in the ocean. *Nature*, *568*, 327–335. https://doi.org/10.1038/s41586-019-1098-2

Briggs, N., Dall'Olmo, G., & Claustre, H. (2020). Major role of particle fragmentation in regulating biological sequestration of CO_2 by the oceans, *Science*, *367*, 791–793. https://doi.org/10.1126/science.aay1790

Broecker, W. S. and T. H. Peng (1982). *Tracers in the Sea*, Eldigio Press, Palisades, NY, 690 pp. https://www.ldeo.columbia.edu/~broecker/Home_files/TracersInTheSea_searchable.pdf

Buesseler, K. O., Ball, K. O. L., Andrews, J., Cochran, J. K., Hirschberg, D. J., Bacon, M. P., et al. (2001). Upper ocean export of particulate organic carbon and biogenic silica in the Southern Ocean along 170°W, *Deep Sea Research Part II*, *48*, 4275–4297. https://doi.org/10.1016/S0967-0645(01)00089-3

Burd, A. B. (2024). Modeling the vertical flux of organic carbon in the global ocean, *Annual Review of Marine Science*, *16*, 135–161, https://doi.org/10.1146/annurev-marine-022123-102516

Cael, B. B., Cavan, E. L., & Britten, G. L. (2021). Reconciling the size-dependence of marine particle sinking speed. *Geophysical Research Letters*, *48*, e2020GL091771. https://doi.org/10.1029/2020GL091771

Cael, B. B., Bisson, K., Boss, E., Dutkiewicz, S., & Henson. S. (2023). Global climate-change trends detected in indicators of ocean ecology. *Nature*, *619*, 551–554. https://doi.org/10.1038/s41586-023-06321-z

Canadell, J. G., Monteiro, P. M. S., Costa, M. H., Cotrim da Cunha, L., Cox, P. M., Eliseev, A. V., et al. (2021). Global Carbon and other Biogeochemical Cycles and Feedbacks. In Climate Change 2021: The Physical Science Basis. Contribution of Working Group I to the Sixth Assessment Report of the Intergovernmental Panel on Climate Change [Masson-Delmotte, V., P. Zhai, A. Pirani, S.L. Connors, C. Péan, S. Berger, N. Caud, Y. Chen, L. Goldfarb, M.I. Gomis, M. Huang, K. Leitzell, E. Lonnoy, J.B.R. Matthews, T.K. Maycock, T. Waterfield, O. Yelekçi, R. Yu, and B. Zhou (eds.)]. Cambridge University Press, Cambridge, United Kingdom and New York, NY, USA, pp. 673–816. https://doi.org/10.1017/9781009157896.007

Carroll, D., Menemenlis, D., Adkins, J. F., Bowman, K. W., Brix, H., Dutkiewicz, S., et al. (2020). The ECCO-Darwin data-assimilative global ocean biogeochemistry model: Estimates of

seasonal to multidecadal surface ocean pCO_2 and air-sea CO_2 flux. *Journal of Advances in Modeling Earth Systems*, *12*(10), e2019MS001888.

Carroll, D., Menemenlis, D., Dutkiewicz, S., Lauderdale, J. M., Adkins, J. F., Bowman, K. W., et al. (2022). Attribution of space-time variability in global-ocean dissolved inorganic carbon. *Global Biogeochemical Cycles*, *36*(3), e2021GB007162.

Carr, M. E. (2002). Estimation of potential productivity in Eastern Boundary Currents using remote sensing, *Deep Sea Research Part II*, *49*(1–3), 59–80.

Carr, M., Friedrichs, M., Schmeltz, M., Noguchiaita, M., Antoine, D., Arrigo, K., & et al. (2006). A comparison of global estimates of marine primary production from ocean color. *Deep-Sea Research Part II*, *53*, 741–770. https://doi.org/10.1016/j.dsr2.2006.01.028

Cavan, E. L., Laurenceau-Cornec, E. C., Bressac, M., Boyd, P. W. (2019). Exploring the ecology of the mesopelagic biological pump. *Progress in Oceanography*, *176*, 102125. https://doi.org/10.1016/j.pocean.2019.102125

Chau, T. T. T., Gehlen, M., & Chevallier, F. (2022). A seamless ensemble-based reconstruction of surface ocean pCO_2 and air–sea CO_2 fluxes over the global coastal and open oceans. *Biogeosciences*, *19*(4), 1087–1109. https://doi.org/10.5194/bg-19-1087-2022

Clements, D. J., Yang, S., Weber, T., McDonnell, A. M. P., Kiko, R., Stemmann, L., Bianchi, D. (2023). New estimate of organic carbon export from optical measurements reveals the role of

particle size distribution and export horizon. *Global Biogeochemical Cycles*, *37*, e2022GB007633. https://doi.org/10.1029/2022GB007633

Cram, J. A., Weber, T., Leung, S. W., McDonnell, A. M. P., Liang, J.-H., & Deutsch, C. (2018). The role of particle size, ballast, temperature, and oxygen in the sinking flux to the deep sea. *Global Biogeochemical Cycles*, *32*, 858–876. https://doi.org/10.1029/2017GB005710

Crisp, D., Dolman, H., Tanhua, T., McKinley, G. A., Hauck, J., Bastos, A., et al. (2022). How well do we understand the land-ocean-atmosphere carbon cycle? *Reviews of Geophysics*, *60*, e2021RG000736. https://doi.org/10.1029/2021RG000736

DeVries, T., (2022). The ocean carbon cycle, *Annual Review of Environment and Resources*, *47*, 317–341. https://doi.org/10.1146/annurev-environ-120920-111307

DeVries, T., & Weber, T. (2017). The export and fate of organic matter in the ocean: New constraints from combining satellite and oceanographic tracer observations. *Global Biogeochemical Cycles*, *31*, 535–555. https://doi.org/10.1002/2016GB005551

DeVries, T., Le Quéré, C., Andrews, O., Berthet, S., Hauck, J., Ilyina, T., et al. (2019). Decadal trends in the ocean carbon sink. *Proceedings of the National Academy of Sciences*, *116*(24), 11646–11651. https://doi.org/10.1073/pnas.1900371116

DeVries, T., Yamamoto, K., Wanninkhof, R., Gruber, N., Hauck, J., Müller, J. D., et al. (2023). Magnitude, trends, and variability of the global ocean carbon sink from 1985-2018, *Global Biogeochemical Cycles*, *37* e2023GB007780. https://doi.org/10.1029/2023GB007780

Dinauer, A., Laufkötter, C., Doney, S. C., & Joos, F. (2022). What controls the large-scale efficiency of carbon transfer through the ocean's mesopelagic zone? Insights from a new, mechanistic model (MSPACMAM). *Global Biogeochemical Cycles*, *36*, e2021GB007131. https://doi.org/10.1029/2021GB007131

Doney, S. C., Lindsay, K., Caldeira, K., Campin, J.-M., Drange, H., Dutay, J. C., et al. (2004). Evaluating global ocean carbon models: The importance of realistic physics. *Global Biogeochemical Cycles*, *18*(3), GB3017. https://doi.org/10.1029/2003GB002150

Doney, S. C., Lindsay, K., Fung, I., J. John, J. (2006). Natural variability in a stable 1000 year coupled climate-carbon cycle simulation. *Journal of Climate*, *19*(13), 3033–3054. https://doi.org/10.1175/JCLI3783.1

Doney, S. C., Yeager, S., Danabasoglu, G., Large, W. G., McWilliams, J. C. (2007). Mechanisms governing interannual variability of upper ocean temperature in a global hindcast simulation. *Journal of Physical Oceanography*, *37*, 1918–1938. https://doi.org/10.1175/JPO3089.1

Doney, S. C., Lima, I., Feely, R. A., Glover, D. M., Lindsay, K., Mahowald, N., Moore, J. K., Wanninkhof, R. (2009): Mechanisms governing interannual variability in upper-ocean inorganic carbon system and air–sea CO_2 fluxes: Physical climate and atmospheric dust. *Deep Sea*

Research Part II: Topical Studies in Oceanography, *56*(8–10) 640–655. https://doi.org/10.1016/j.dsr2.2008.12.006

Döscher, R., Acosta, M., Alessandri, A., Anthoni, P., Arsouze, T., Bergman, T., et al. (2022). The EC-Earth3 Earth system model for the Coupled Model Intercomparison Project 6. *Geoscientific Model Development*, *15*(7), 2973–3020. https://doi.org/10.5194/gmd-15-2973-2022

Ducklow, H. W., & Doney, S. C. (2013). What is the metabolic state of the oligotrophic ocean? A debate. *Annual Review of Marine Science*, *5*, 525–533. https://doi.org/10.1146/annurev-marine-121211-172331

Dunne, J. P., Armstrong, R. A., Gnanadesikan, A., & Sarmiento, J. L. (2005). Empirical and mechanistic models for theparticle export ratio, *Global Biogeochemical Cycles*, *19*, GB4026. https://doi.org/10.1029/2004GB002390.

Dunne, J. P., Sarmiento, J. L., & Gnanadesikan, A. (2007). A synthesis of global particle export from the surface ocean and cycling through the ocean interior and on the seafloor. *Global Biogeochemical Cycles*, *21*, GB4006. https://doi.org/10.1029/2006GB002907

Dutay, J.-C., Bullister, J. L., Doney, S. C., Orr, J. C., Najjar, R., Caldeira, K., et al. (2002). Evaluation of ocean model ventilation with CFC-11: comparison of 13 global ocean models. *Ocean Modelling*, 4, 89–120. https://doi.org/10.1016/S1463-5003(01)00013-0

Falkowski, P. G., Barber, R. T., & Smetacek, V. (1998). Biogeochemical controls and feedbacks on ocean primary production. *Science*, *281*(5374), 200–206. https://doi.org/10.1126/science.281.5374.200

Fay, A. R., & McKinley, G. A. (2014). Global open-ocean biomes: mean and temporal variability. *Earth System Science Data*, *6*, 273–284. https://doi.org/10.5194/essd-6-273-2014.

Fennel, K., Mattern, J. P., Doney, S. C., Bopp, L., Moore, A. M., Wang, B., & Yu, L. (2022). Ocean biogeochemical modelling. *Nature Reviews Methods Primers*, *2*, 76. https://doi.org/10.1038/s43586-022-00154-2

Friedlingstein, P., O'Sullivan, M., Jones, M. W., Andrew, R. M., Gregor, L., Hauck, J., et al. (2022). Global carbon budget 2022. *Earth System Science Data*, *14*, 4811–4900. https://doi.org/10.5194/essd-14-4811-2022

Fu, W., Moore, J. K., Primeau, F., Collier, N., Ogunro, O. O., Hoffman, F. M., & Randerson, J. T. (2022). Evaluation of ocean biogeochemistry and carbon cycling in CMIP earth system models with the International Ocean Model Benchmarking (IOMB) software system. *Journal of Geophysical Research: Oceans*, *127*, e2022JC018965. https://doi.org/10.1029/2022JC018965

Garcia, H. E., Weathers, K., Paver, C. R., Smolyar, I., Boyer, T. P., Locarnini, R. A., et al. (2019). World Ocean Atlas 2018, Volume 3: Dissolved Oxygen, Apparent Oxygen Utilization, and

Oxygen Saturation. A. Mishonov Technical Ed., *NOAA Atlas NESDIS 83*, 38pp. https://www.ncei.noaa.gov/sites/default/files/2020-04/woa18_vol3.pdf

Giering, S., Sanders, R., Lampitt, R., Anderson, T. R., Tamburini, C., Boutrif, M., et al. (2014). Reconciliation of the carbon budget in the ocean's twilight zone. *Nature*, *507*, 480–483. https://doi.org/10.1038/nature13123

Giering, S. L. C., Sanders, R., Martin, A. P., Henson, S. A., Riley, J. S., Marsay, C. M., & Johns, D. G. (2017). Particle flux in the oceans: Challenging the steady state assumption, Global Biogeochemical Cycles, 31, 159–171. https://doi.org/10.1002/2016GB005424

Gloege, L., Yan, M., Zheng, T., & McKinley, G. A. (2022). Improved quantification of ocean carbon uptake by using machine learning to merge global models and pCO_2 data. *Journal of Advances in Modeling Earth Systems, 14*(2), e2021MS002620. https://doi.org/10.1029/2021ms002620

Glover, D. M., Jenkins, W. J., & Doney, S. C. (2011). *Modeling Methods for Marine Science*. Cambridge, United Kingdom: Cambridge University Press. https://doi.org/10.1017/CBO9780511975721

Gregor, L., & Gruber, N. (2021). OceanSODA-ETHZ: A global gridded data set of the surface ocean carbonate system for seasonal to decadal studies of ocean acidification. *Earth System Science Data*, *13*(2), 777–808. https://doi.org/10.5194/essd-13-777-2021

Gruber, N., Bakker, D.C.E., DeVries, T., Gregor, L., Hauck, J., Landschützer, P., McKinley, G. A., & Müller, J. D. (2023). Trends and variability in the ocean carbon sink. *Nature Reviews Earth and Environment*, *4*, 119–134. https://doi.org/10.1038/s43017-022-00381-x

Guidi, L., Legendre, L., Reygondeau, G., Uitz, J., Stemmann, L., & Henson, S. A. (2015). A new look at ocean carbon remineralization for estimating deep water sequestration. *Global Biogeochemical Cycles*, *29*, 1044–1059. https://doi.org/10.1002/2014GB005063

Hauck, J., Zeising, M., Le Quéré, C., Gruber, N., Bakker, D. C. E., Bopp, L., et al. (2020). Consistency and challenges in the ocean carbon sink estimate for the global carbon budget. *Frontiers in Marine Science*, *7*, 571720. https://doi.org/10.3389/fmars.2020.571720

Hauck, J., Gregor, L., Nissen, C., Patara, L., Hague, M., Mongwe, P., et al. (2023). The Southern Ocean carbon cycle 1985–2018: Mean, seasonal cycle, trends, and storage. *Global Biogeochemical Cycles, 37*, e2023GB007848. https://doi.org/10.1029/2023GB007848

Henson, S. A., Sarmiento, J. L., Dunne, J. P., Bopp, L., Lima, I., Doney, S. C., et al. (2010). Detection of anthropogenic climate change in satellite records of ocean chlorophyll and productivity. *Biogeosciences*, *7*, 621–640. https://doi.org/10.5194/bg-7-621-2010

Henson, S. A., Sanders, R., & Madsen, E. (2012). Global patterns in efficiency of particulate organic carbon export and transfer to the deep ocean. *Global Biogeochemical Cycles*, *26*, GB1028. https://doi.org/10.1029/2011GB004099

Henson, S. A., Yool, A., & Sanders, R. (2015). Variability in efficiency of particulate organic carbon export: A model study, *Global Biogeochemical Cycles*, *29*, 33–45. doi:10.1002/2014GB004965

Henson, S. A., Beaulieu, C., & Lampitt, R. (2016). Observing climate change trends in ocean biogeochemistry: When and where. *Global Change Biology*, *22*(4), 1561–1571. https://doi.org/10.1111/gcb.13152

Henson, S. A., Laufkötter, C., Leung, S. Giering, S. L. C., Palevsky, H. I., & Cavan, E. L. (2022). Uncertain response of ocean biological carbon export in a changing world. *Nature Geoscience*, *15*, 248–254. https://doi.org/10.1038/s41561-022-00927-0

Henson, S. A., Briggs, N., Carvalho, F., Manno, C., Mignot, A., Thomalla, S. (2023). A seasonal transition in biological carbon pump efficiency in the northern Scotia Sea, Southern Ocean. *Deep Sea Research Part II*, *208*, 105274. https://doi.org/10.1016/j.dsr2.2023.105274

Henson, S. A., Kelsey Bisson, K., Hammond, M. L., Martin, A., Mouw, C., Yool, A. (2024). Effect of sampling bias on global estimates of ocean carbon export. *Environmental Research Letters*, *19*, 024009. http://dx.doi.org/10.1088/1748-9326/ad1e7f

Ilyina, T., Six, K. D., Segschneider, J., Maier-Reimer, E., Li, H., & Núñez-Riboni, I. (2013). Global ocean biogeochemistry model HAMOCC: Model architecture and performance as component of the MPI-Earth system model in different CMIP5 experimental realizations. *Journal of Advances in Modeling Earth Systems*, *5*(2), 287–315. https://doi.org/10.1029/2012ms000178

Iversen, M. H. (2023). Carbon export in the ocean: a biologist's perspective. *Annual Review of Marine Science*, *15*, 357–381. https://doi.org/10.1146/annurev-marine-032122-035153

Karl, D. M., Church, M. J., Dore, J. E., Letelier, R., & Mahaffey, C. (2012). Predictable and efficient carbon sequestration in the North Pacific Ocean supported by symbiotic nitrogen fixation, *Proceedings of the National Academy of Sciences USA*, *109*, 1842–1849. https://doi.org/10.1073/pnas.1120312109

Khatiwala, S., Tanhua, T., Mikaloff Fletcher, S., Gerber, M., Doney, S. C., Graven, H. D., et al. (2013). Global ocean storage of anthropogenic carbon, *Biogeosciences*, *10*, 2169–2191. https://doi.org/10.5194/bg-10-2169-2013

Kiørboe, T., Grossart, H.-P., Ploug, H., & Tang, K. (2002). Mechanisms and rates of bacterial colonization of sinking aggregates, *Applied and Environmental Microbiology*, *68*, 3996–4006. https://doi.org/10.1128/AEM.68.8.3996-4006.2002

Kiørboe, T., Tang, K., Grossart, H.-P., & Ploug, H. (2003). Dynamics of microbial communities on marine snow aggregates: colonization, growth, detachment, and grazing mortality of attached bacteria, *Applied and Environmental Microbiology*, *69*, 3036–3047. https://doi.org/10.1128/AEM.69.6.3036-3047.2003

Kwon, E., Primeau, F., & Sarmiento, J. (2009). The impact of remineralization depth on the air–sea carbon balance, *Nature Geoscience*, *2*, 630–635. https://doi.org/10.1038/ngeo612

Lam, P. J., Doney, S. C., & Bishop, J. K. B. (2011). The dynamic ocean biological pump: Insights from a global compilation of particulate organic carbon, $CaCO_3$, and opal concentration profiles from the mesopelagic. *Global Biogeochemical Cycles*, *25*, GB3009. https://doi.org/10.1029/2010GB003868.

Lampitt, R. S., Bett, B. J., Kiriakoulakis, K., Popova, E. E., Ragueneau, O., Vangriesheim, A., & Wolff, G. A. (2001). Material supply to the abyssal seafloor in the Northeast Atlantic, *Progress in Oceanography*, *50*, 27–63. https://doi.org/10.1016/S0079-6611(01)00047-7

Landschützer, P., Gruber, N., & Bakker, D. C. (2016). Decadal variations and trends of the global ocean carbon sink. Global Biogeochemical Cycles, *30*(10), 1396–1417. https://doi.org/10.1002/2015gb005359

Landschützer, P., Gruber, N., Bakker, D. C. E., Stemmler, I., Six, K. D. (2018). Strengthening seasonal marine CO_2 variations due to increasing atmospheric CO_2. *Nature Climate Change*, *8*, 146–150. https://doi.org/10.1038/s41558-017-0057-x

Laufkötter, C., Vogt, M., Gruber, N., Aita-Noguchi, M., Aumont, O., Bopp, L., et al. (2015). Drivers and uncertainties of future global marine primary production in marine ecosystem models. *Biogeosciences*, *12*(23), 6955–6984. https://doi.org/10.5194/bg-12-6955-2015

Laufkötter, C., Vogt, M., Gruber, N., Aumont, O., Bopp, L., Doney, S. C., et al. (2016). Projected decreases in future marine export production: The role of the carbon flux through the upper ocean ecosystem. *Biogeosciences*, *13*, 4023–4047. https://doi.org/10.5194/bg-13-4023-2016

Laufkötter, C., John, J. G., Stock, C. A., & Dunne, J. P. (2017). Temperature and oxygen dependence of the remineralization of organic matter. *Global Biogeochemical Cycles*, *31*, 1038–1050. https://doi.org/10.1002/2017GB005643

Laurenceau-Cornec, E. C., Le Moigne, F. A. C., Gallinari, M., Moriceau, B., Toullec, J., Iversen, M. I., Engel, A., & De La Rocha, C. L. (2020). New guidelines for the application of Stokes' models to the sinking velocity of marine aggregates, *Limnology and Oceanography*, *65*, 1264–1285. https://doi.org/10.1002/lno.11388

Laws, E. A., Falkowski, P. G., Smith Jr, W. O., Ducklow, H., & McCarthy, J. J. (2000). Temperature effects on export production in the open ocean. *Global Biogeochemical Cycles*, *14*, 1231–1246. https://doi.org/10.1029/1999GB001229

Laws, E. A., & Maiti, K. (2019). The relationship between primary production and export production in the ocean: Effects of time lags and temporal variability, *Deep Sea Research Part I*, *148*, 100–107. https://doi.org/10.1016/j.dsr.2019.05.006

Laws, E. A., D'sa, E., & Naik, P. (2011). Simple equations to estimate ratios of new or export production to total production from satellite-derived estimates of sea surface temperature and primary production. *Limnology and Oceanography: Methods*, *9*(12), 593–601. https://doi.org/10.4319/lom.2011.9.593

Le Quéré, C., Buitenhuis, E. T., Moriarty, R., Alvain, S., Aumont, O., Bopp, L., et al. (2016). Role of zooplankton dynamics for Southern Ocean phytoplankton biomass and global biogeochemical cycles. *Biogeosciences*, *13*(14), 4111–4133. https://doi.org/10.5194/bg-13-4111-2016

Liao, E., Resplandy, L., Liu, J., & Bowman, K. W. (2020). Amplification of the ocean carbon sink during El Niños: Role of poleward Ekman transport and influence on atmospheric CO_2. *Global Biogeochemical Cycles*, *34*(9), e2020GB006574. https://doi.org/10.1029/2020gb006574

Lima, I. D., Lam, P. J., & Doney, S. C. (2014). Dynamics of particulate organic carbon flux in a global ocean model, *Biogeosciences*, *11*, 1177–1198. https://doi.org/10.5194/bg-11-1177-2014

Lindsay, K., Bonan, G. B., Doney, S. C., Hoffman, F. M., Lawrence, D. M., Long, M. C., et al. (2014). Preindustrial-control and twentieth-century carbon cycle experiments with the Earth System Model CESM1(BGC). *Journal of Climate*, *27*(24), 8981–9005. https://doi.org/10.1175/jcli-d-12-00565.1

Lutz, M. J., Caldeira, K., Dunbar, R. B., & Behrenfeld, M. J. (2007). Seasonal rhythms of net primary production and particulate organic carbon flux to depth describe the efficiency of biological pump in the global ocean. *Journal of Geophysical Research Oceans*, *112*, C10011. https://doi.org/10.1029/2006JC003706

Maier-Reimer, E. (1993). Geochemical cycles in an ocean general circulation model. Preindustrial tracer distributions, *Global Biogeochemical Cycles*, *7*, 645–677. https://doi.org/10.1029/93GB01355

Marinov, I., Gnanadesikan, A., Sarmiento, J. L., Toggweiler, J. R., Follows, M., & Mignone, B. K. (2008). Impact of oceanic circulation on biological carbon storage in the ocean and atmospheric pCO_2, *Global Biogeochemical Cycles*, *22*, GB3007. https://doi.org/10.1029/2007GB002958

Marra, J., Ho, C., & Trees, C. C. (2003). An alternative algorithm for the calculation of primary production from remote sensing data, Rep. LDEO 2003–1, Lamont-Doherty Earth Observatory, Palisades, New York. https://www.ldeo.columbia.edu/~marra/MarraAlgorithm.pdf (Accessed August, 2022).

Marsay, C. M., Sanders, R. J., Henson, S. A., Pabortsava, K., Achterberg, E. P., & Lampitt, R. S. (2015). Attenuation of sinking particulate organic carbon flux through the mesopelagic ocean, *Proceedings of the National Academy of Sciences USA*, *112*(4) 1089–1094. https://doi.org/10.1073/pnas.1415311112

Martin, J. H., Knauer, G. A., Karl, D. M., & Broenkow, W. W. (1987). VERTEX: carbon cycling in the northeast Pacific, *Deep-Sea Research*, *34*, 267–285. https://doi.org/10.1016/0198-0149(87)90086-0

Matsumoto, K., Sarmiento, J. L., Key, R. M., Bullister, J. L., Caldeira, K., Campin, J.-M., et al. (2004). Evaluation of ocean carbon cycle models with data-based metrics, *Geophysical Research Letters*, *31*, L07303. https://doi.org/10.1029/2003GL018970

Mauritsen, T., Bader, J., Becker, T., Behrens, J., Bittner, M., Brokopf, R., et al. (2019). Developments in the MPI-M Earth system model version 1.2 (MPI-ESM1. 2) and its response to increasing CO_2. *Journal of Advances in Modeling Earth Systems*, *11*(4), 998–1038. https://doi.org/10.1029/2018ms001400

Mayor, D. J., Sanders, R., Giering, S. L. C., & Anderson, T. R. (2014). Microbial gardening in the ocean's twilight zone: Detritivorous metazoans benefit from fragmenting, rather than ingesting, sinking detritus, *BioEssays*, *36*, 1132–1137. https://doi.org/10.1002/bies.201400100

Mikaloff Fletcher, S. E., Gruber, N., Jacobson, A. R., Gloor, M., Doney, S. C., Dutkiewicz, S., et al. (2007). Inverse estimates of the oceanic sources and sinks of natural CO_2 and their implied oceanic transport. *Global Biogeochemical Cycles*, *21*, GB1010. https://doi.org/10.1029/2006GB002751

Mouw, C. B., Barnett, A., McKinley, G. A., Gloege, L., & Pilcher, D. (2016a). Global ocean particulate organic carbon flux merged with satellite parameters, *Earth System Science Data*, *8*, 531–541. https://doi.org/10.5194/essd-8-531-2016

Mouw, C. B., Barnett, A., McKinley, G. A., Gloege, L., & Pilcher, D. (2016b). Phytoplankton size impact on export flux in the global ocean, *Global Biogeochemical Cycles*, *30*, 1542–1562. https://doi.org/10.1002/2015GB005355

Müller, Jens Daniel. (2023). RECCAP2-ocean data collection [Data set]. Zenodo. 1631. https://doi.org/10.5281/zenodo.7990823

Najjar, R. G., X. Jin, F. Louanchi, O. Aumont, K. Caldeira, S.C. Doney, et al. (2007). Impact of circulation on export production, dissolved organic matter and dissolved oxygen in the ocean: Results from Phase II of the Ocean Carbon-cycle Model Intercomparison Project (OCMIP-2), *Global Biogeochemical Cycles*, *21*, GB3007. https://doi.org/10.1029/2006GB002857.

Nowicki, M., DeVries, T., & Siegel, D. A. (2022). Quantifying the carbon export and sequestration pathways of the ocean's biological carbon pump. *Global Biogeochemical Cycles*, *36*, e2021GB007083. https://doi.org/10.1029/2021GB007083

Omand, M. M., Govindarajan, R., He, J., & Mahadevan, A. (2020). Sinking flux of particulate organic matter in the oceans: Sensitivity to particle characteristics. *Scientific Reports*, *10*, 5582. https://doi.org/10.1038/s41598-020-60424-5

Orr, J. C., R.G. Najjar, O. Aumount, L. Bopp, J.L. Bullister, G. Danabasoglu, et al. (2017). Biogeochemical protocols and diagnostics for the CMIP6 Ocean Model Intercomparison Project (OMIP). *Geoscientific Model Development*, *10*, 2169–2199. https://doi.org/10.5194/gmd-10-2169-2017

RECCAP2 Ocean Science Team (2022). RECCAP2 Ocean Protocols, accessed August 3rd, 2022. https://reccap2-ocean.github.io/protocols/

Reygondeau, G., Longhurst, A., Martinez, E., Beaugrand, G., Antoine, D., & Maury, O. (2013), Dynamic biogeochemical provinces in the global ocean, *Global Biogeochemical Cycles*, *27*, 1046–1058. https://doi.org/10.1002/gbc.20089

Rödenbeck, C., DeVries, T., Hauck, J., Le Quéré, C., & Keeling, R. F. (2022). Data-based estimates of interannual sea–air CO_2 flux variations 1957–2020 and their relation to environmental drivers. *Biogeosciences*, *19*(10), 2627–2652. https://doi.org/10.5194/bg-19-2627-2022

Rödenbeck, C., Keeling, R. F., Bakker, D. C., Metzl, N., Olsen, A., Sabine, C., & Heimann, M. (2013). Global surface-ocean pCO_2 and sea–air CO_2 flux variability from an observation-driven ocean mixed-layer scheme. *Ocean Science*, *9*(2), 193–216. https://doi.org/10.5194/os-9-193-2013

Rodgers, K. B., Schwinger, J., Fassbender, A. J., Landschützer, P., Yamaguchi, R., Frenzel, H., et al. (2023). Seasonal variability of the surface ocean carbon cycle: A synthesis. *Global Biogeochemical Cycles*, 37, e2023GB007798. https://doi.org/10.1029/2023GB007798

Sarmiento, J. L., & Gruber, N. (2002). Anthropogenic carbon sinks. *Physics Today*, 55(8), 30–36. https://doi.org/10.1063/1.1510279

Sarmiento, J. L., & Gruber, N. (2006). *Ocean Biogeochemical Dynamics*. Princeton University Press. https://doi.org/10.1017/S0016756807003755

Schlitzer, R. (2000). Applying the adjoint method for biogeochemical modeling: Export of particulate organic matter in the World Ocean, *Inverse methods in biogeochemical cycles*, ed. P. Kasibhata, AGU Monograph 114, pp. 107-124.

Schwinger, J., Goris, N., Tjiputra, J. F., Kriest, I., Bentsen, M., Bethke, I., et al. (2016). Evaluation of NorESM-OC (versions 1 and 1.2), the ocean carbon-cycle stand-alone configuration of the Norwegian Earth System Model (NorESM1). *Geoscientific Model Development*, *9*(8), 2589–2622. https://doi.org/10.5194/gmd-9-2589-2016

Séférian, R., Gehlen, M., Bopp, L., Resplandy, L., Orr, J. C., Marti, O., et al. (2016). Inconsistent strategies to spin up models in CMIP5: implications for ocean biogeochemical model performance assessment, *Geoscientific Model Development*, *9*, 1827–1851. https://doi.org/10.5194/gmd-9-1827-2016

Séférian, R., Berthet, S., Yool, A., Palmiéri, J., Bopp, L., Tagliabue, A., et al. (2020). Tracking improvement in simulated marine biogeochemistry between CMIP5 and CMIP6. *Current Climate Change Reports*, 6(3), 95–119. https://doi.org/10.1007/s40641-020-00160-0

Séférian, R., Nabat, P., Michou, M., Saint-Martin, D., Voldoire, A., Colin, J., et al. (2019). Evaluation of CNRM Earth-System model, CNRM-ESM2-1: Role of Earth system processes in present-day and future climate. *Journal of Advances in Modeling Earth Systems*, *11*(12), 4182–4227. https://doi.org/10.1029/2019ms001791

Siegel, D. A., Buesseler, K. O., Doney, S. C., Sailley, S. F., Behrenfeld, M. J., & Boyd, P. W. (2014). Global assessment of ocean carbon export by combining satellite observations and food-web models. *Global Biogeochemical Cycles*, *28*(3), 181–196. https://doi.org/10.1002/2013gb004743

Siegel, D. A., Buesseler, K. O., Behrenfeld, M. J., Benitez-Nelson, C. R., Boss, E., Brzezinski, M. A., et al. (2016). Prediction of the export and fate of global ocean net primary production: the EXPORTS science plan, *Frontiers in Marine Science*, *3*, 22. http://doi.org/10.3389/fmars.2016.00022

Siegel, D. A., DeVries, T., Doney, S. C., & T. Bell, T. (2021). Assessing the sequestration time scales of some ocean-based carbon dioxide reduction strategies, *Environmental Research Letters*, *16*, 104003. https://doi.org/10.1088/1748-9326/ac0be0

Siegel, D. A., DeVries, T., Cetinić, I., & K Bisson, K. M. (2023). Quantifying the ocean's biological pump and Its carbon cycle impacts on global scales, *Annual Review of Marine Science*, *15*, 329–356. https://doi.org/10.1146/annurev-marine-040722-115226

Silsbe, G. M., Behrenfeld, M. J., Halsey, K. H., Milligan, A. J., & Westberry, T. K. (2016). The CAFE model: A net production model for global ocean phytoplankton, *Global Biogeochemical Cycles*, *30*, 1756–1777. doi:10.1002/2016GB005521

Steinberg, D. K., & M.R. Landry, M. R. (2017). Zooplankton and the ocean carbon cycle, *Annual Review of Marine Science*, *9*, 413–444. https://doi.org/10.1146/annurev-marine-010814-015924

Stock, C. A., Dunne, J. P., Fan, S., Ginoux, P., John, J., Krasting, J. P., et al. (2020). Ocean biogeochemistry in GFDL's Earth system model 4.1 and its response to increasing atmospheric CO_2. *Journal of Advances in Modeling Earth Systems*, *12*(10), e2019MS002043. https://doi.org/10.1029/2019ms002043

Stukel, M. R., Ohman, M. D., Kelly, T. B., & Biard, T. (2019). The roles of suspension-feeding and flux-feeding zooplankton as gatekeepers of particle flux into the mesopelagic ocean in the Northeast Pacific. *Frontiers in Marine Science*, *6*, 397. https://doi.org/10.3389/fmars.2019.00397

Takahashi, T., Olafsson, J., Goddard, J. G., Chipman, D. W., & Sutherland, S. C. (1993). Seasonal variation of CO_2 and nutrients in the high-latitude surface oceans: A comparative study, *Global Biogeochemical Cycles*, *7*(4), 843–878. https://doi.org/10.1029/93GB02263

Takahashi, T., Sutherland, S. C., Sweeney, C., Poisson, A., Metzl, N., Tilbrook, B., et al. (2002). Global sea–air CO_2 flux based on climatological surface ocean pCO_2, and seasonal biological and temperature effects. *Deep Sea Research Part II: Topical Studies in Oceanography*, *49*(9–10), 1601–1622. https://doi.org/10.1016/S0967-0645(02)00003-6

Terhaar, T., Goris, N., Müller, J. D., DeVries, T., Gruber, N., Hauck, J., et al. (2023). Assessment of global ocean biogeochemistry models for ocean carbon sink estimates in RECCAP2 and recommendations for future studies. *ESS Open Archive*. https://doi.org/10.22541/essoar.168394734.41886821/v1

Turner, J. T. (2015). Zooplankton fecal pellets, marine snow, phytodetritus and the ocean's biological pump, *Progress in Oceanography*, *130*, 205–248. https://doi.org/10.1016/j.pocean.2014.08.005

Tsujino, H., Nakano, H., Sakamoto, K., Urakawa, S., Hirabara, M., Ishizaki, H., & Yamanaka, G. (2017). Reference manual for the meteorological research institute community ocean model version 4 (MRI. COMv4) (Vol. 80, p. 306). Technical Reports of the Meteorological Research Institute.

Urakawa, L. S., Tsujino, H., Nakano, H., Sakamoto, K., Yamanaka, G., & Toyoda, T. (2020). The sensitivity of a depth-coordinate model to diapycnal mixing induced by practical implementations of the isopycnal tracer diffusion scheme. *Ocean Modelling*, *154*, 101693. https://doi.org/10.1016/j.ocemod.2020.101693

Volk, T., & Hoffert, M. I. (1985). Ocean carbon pumps: Analysis of relative strengths and efficiencies in ocean-driven atmospheric CO_2 changes. In E. Sundquist & W. Broecker (Eds.), *The carbon cycle and atmospheric CO_2: Natural variations archean to present* (Vol. 32, pp. 99–110). American Geophysical Union (AGU). https://doi.org/10.1029/GM032P0099

Wanninkhof, R., Park, G.-H., Takahashi, T., Sweeney, C., Feely, R., Nojiri, Y., et al. (2013). Global ocean carbon uptake: magnitude, variability and trends, *Biogeosciences*, *10*, 1983–2000. https://doi.org/10.5194/bg-10-1983-2013

Watson, A. J., Schuster, U., Shutler, J. D., Holding, T., Ashton, I. G., Landschützer, P., et al. (2020). Revised estimates of ocean-atmosphere CO_2 flux are consistent with ocean carbon inventory. *Nature Communications*, *11*(1), 1–6. https://doi.org/10.1038/s41467-020-18203-3

Weber, T., Cram, J. A., Leung, S. W., DeVries, T., & Deutsch, C. (2016). Deep ocean nutrients imply large latitudinal variation in particle transfer efficiency, *Proceedings of the National Academy of Sciences*, *113*, 8606–8611. https://doi.org/10.1073/pnas.1604414113

Wilson, J. D., Andrews, O., Katavouta, A., de Melo Viríssimo, F., Death, R. M., Adloff, M., et al. (2022). The biological carbon pump in CMIP6 models: 21st century trends and uncertainties. *Proceedings of the National Academy of Sciences USA*, *119*(29), e2204369119. https://doi.org/10.1073/pnas.2204369119

Wright, R. M., Le Quéré, C., Buitenhuis, E., Pitois, S., & Gibbons, M. J. (2021). Role of jellyfish in the plankton ecosystem revealed using a global ocean biogeochemical model. *Biogeosciences*, *18*(4), 1291–1320. https://doi.org/10.5194/bg-18-1291-2021

Yang, S., & Gruber, N. (2016). The anthropogenic perturbation of the marine nitrogen cycle by atmospheric deposition: Nitrogen cycle feedbacks and the ^{15}N Haber-Bosch effect. *Global Biogeochemical Cycles*, *30*(10), 1418–1440. https://doi.org/10.1002/2016gb005421

Zeng, J., Iida, Y., Matsunaga, T., & Shirai, T. (2022). Surface ocean CO_2 concentration and air-sea flux estimate by machine learning with modelled variable trends. *Frontiers in Marine Science*, *9*, 989233. https://doi.org/10.3389/fmars.2022.989233

Supporting Information:
Observational and numerical modeling constraints on the global ocean biological carbon pump

Scott C. Doney[1], Kayla A. Mitchell[1,2], Stephanie A. Henson[3], Emma Cavan[4], Tim DeVries[5], Nicolas Gruber[6], Judith Hauck[7], Colleen B. Mouw[8], Jens D. Müller[6], and Francois W. Primeau[2]

February 4th, 2024

[1] Department of Environmental Sciences, University of Virginia, Charlottesville, VA, USA,

[2] Department of Earth System Science, University of California, Irvine, Irvine, CA, USA,

[3] National Oceanography Centre, Southampton, UK,

[4] Department of Life Sciences, Silwood Park Campus, Imperial College London, Berkshire, UK,

[5] Earth Research Institute and Department of Geography, University of California, Santa Barbara, Santa Barbara, CA, USA,

[6] Environmental Physics, Institute of Biogeochemistry and Pollutant Dynamics, ETH Zurich, Zürich, Switzerland

[7] Alfred-Wegener-Institut, Helmholtz-Zentrum für Polar- und Meeresforschung, Bremerhaven, Germany

[8] Graduate School of Oceanography, University of Rhode Island, Narragansett, RI, USA.

The REgional Carbon Cycle Assessment and Processes (RECCAP) project is a coordinated, international effort to constrain contemporary ocean carbon air-sea fluxes and interior storage trends using a combination of field observations, inverse model products, and ocean biogeochemical hindcast simulations. The second phase, RECCAP2, extends the original synthesis using additional years of ocean observational data and updated numerical results (DeVries et al., 2023) as well as expanding the scope of the observational and model analysis, in this case into the biological carbon pump magnitude and efficiency.

Supplement Figures

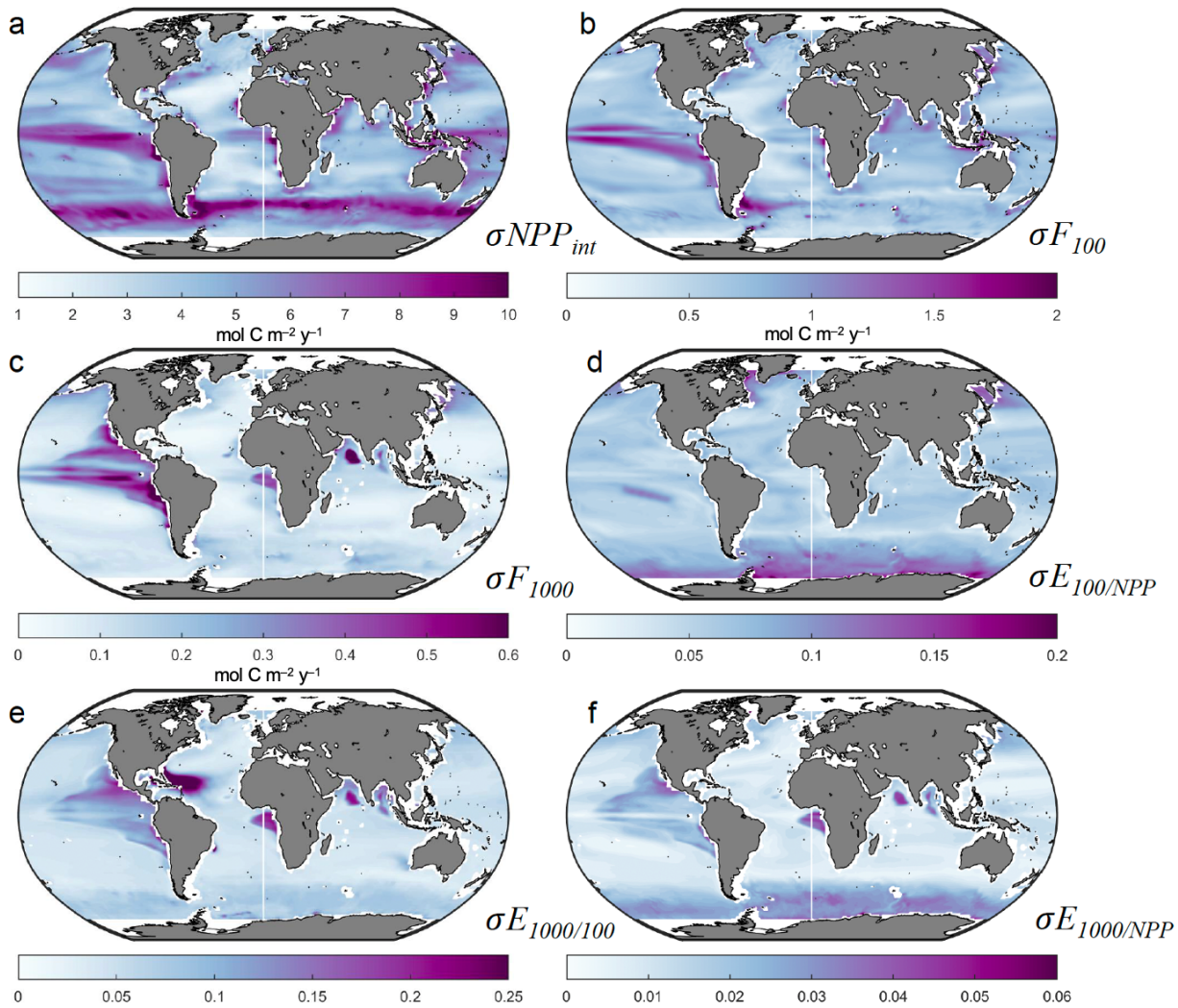

Figure S1. Maps of within-ensemble standard deviation of biological pump parameters. Standard deviations across model ensemble members are computed relative to the average model ensemble presented in Figure 1 for: (a) vertically integrated primary productivity σ_{NPP}, (b) particulate organic carbon export fluxes at 100 m σF_{100}, and (c) 1000 m σF_{1000}, all in moles C m^{-2} y^{-1}, and (d) surface export efficiency ratio $E_{100/NPP} = F_{100}/NPP$, (e) mesopelagic transfer efficiency at 1000 m $E_{1000/100} = F_{1000}/F_{100}$, and (f) export efficiency to the deep ocean $E_{1000/NPP} = F_{1000}/NPP$, all ratios unitless.

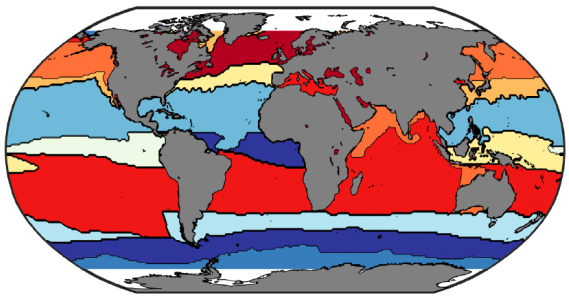

Biome Number	Biome Acronym	Biome Description
18	SOSPSS	Southern Ocean Subpolar Seasonally Stratified
17	NaAEQU	N. Atlantic Equatorial
16	SOICE	Southern Ocean Ice
15	NPICE	North Pacific Ice
14	NPSTPS	N. Pacific Subtropical Permanently Stratified
13	NaSTPS	N. Atlantic Subtropical Seasonally Stratified
12	SOSTSS	Southern Ocean Subtropical Seasonally Stratified
11	BARENTS	Barents Sea
10	PEQUE	Eastern Equatorial Pacific
9	PEQUW	Western Equatorial Pacific
8	NAICE	N. Atlantic Ice
7	NaSTSS	N. Atlantic Subtropical Seasonally Stratified
6	NPSTSS	N. Pacific Subtropical Seasonally Stratified
5	NPSPSS	N. Pacific Subpolar Seasonally Stratified
4	INDSTPS	Indian Ocean Subtropical Permanently Stratified
3	MED	Mediterranean Sea
2	SASTPS	S. Atlantic Subtropical Permanently Stratified
1	NaSPSS	N. Atlantic Subpolar Seasonally Stratified

Figure S2. Map of standard RECCAP2 biomes by ocean basin (Fay and McKinley, 2014). The biomes include polar (ICE), subpolar seasonally-stratified (SPSS), subtropical seasonally stratified (STSS), subtropical permanently stratified (STPS), and equatorial regions (EQU); note the equatorial Pacific is divided into western and eastern sub-basins. The equatorial eastern Pacific and Atlantic, monsoon-influenced Indian, and seasonally-stratified biomes generally exhibited relatively high NPP, F_{100}, and F_{1000}. Polar and sub-polar biomes exhibited relatively high E_{100}.

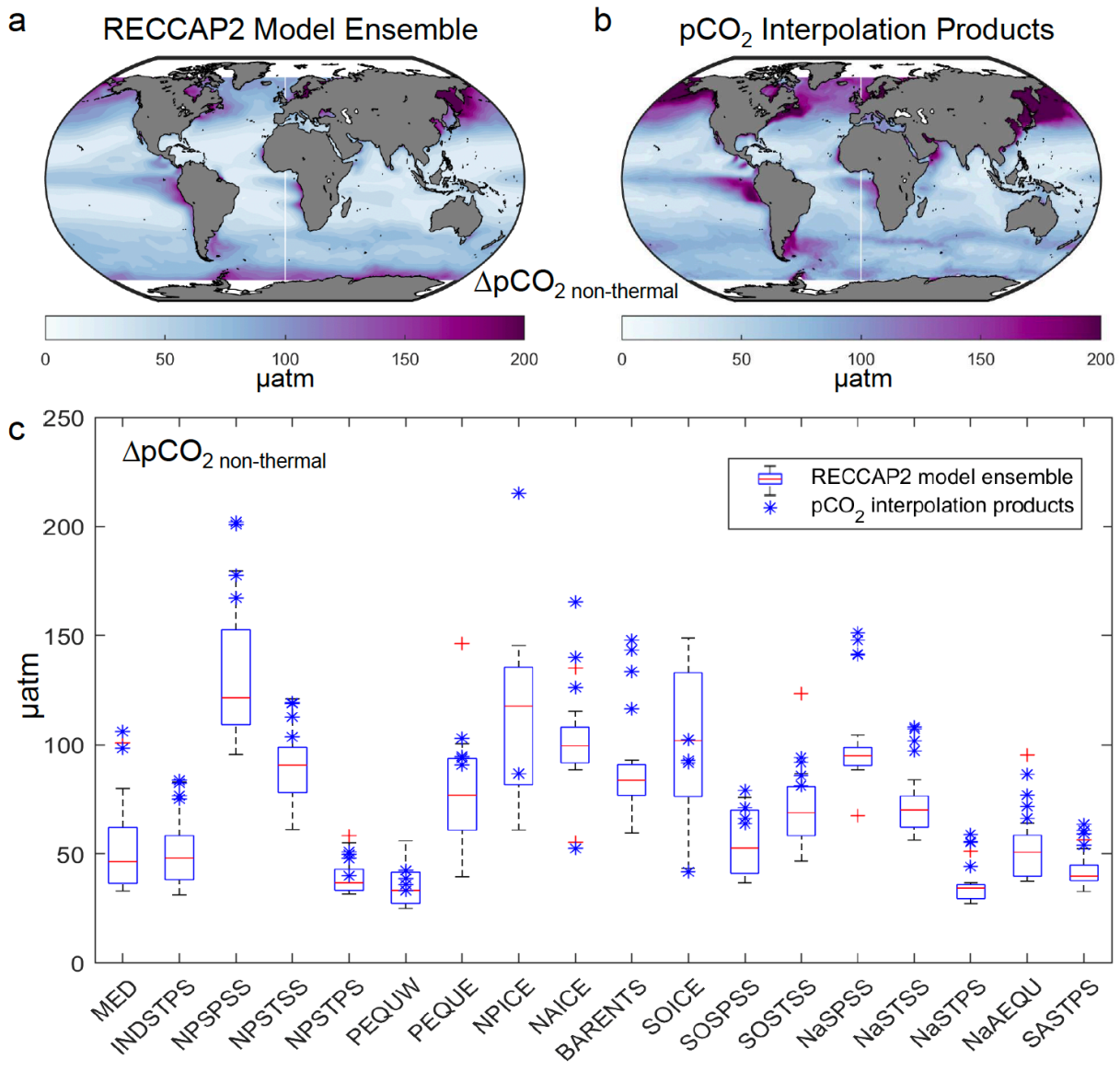

Figure S3. Analysis of the seasonal cycle of non-thermal $\Delta pCO_{2_{non-thermal}}$ (a) spatial map of RECCAP2 multi-model ensemble average, (b) spatial map from pCO_2 observational data products, and (c) box-whisker plot of RECCAP2 multi-model ensemble medians, interquartile ranges, and outliers pooled into Fay and McKinley biomes (Figure S2).

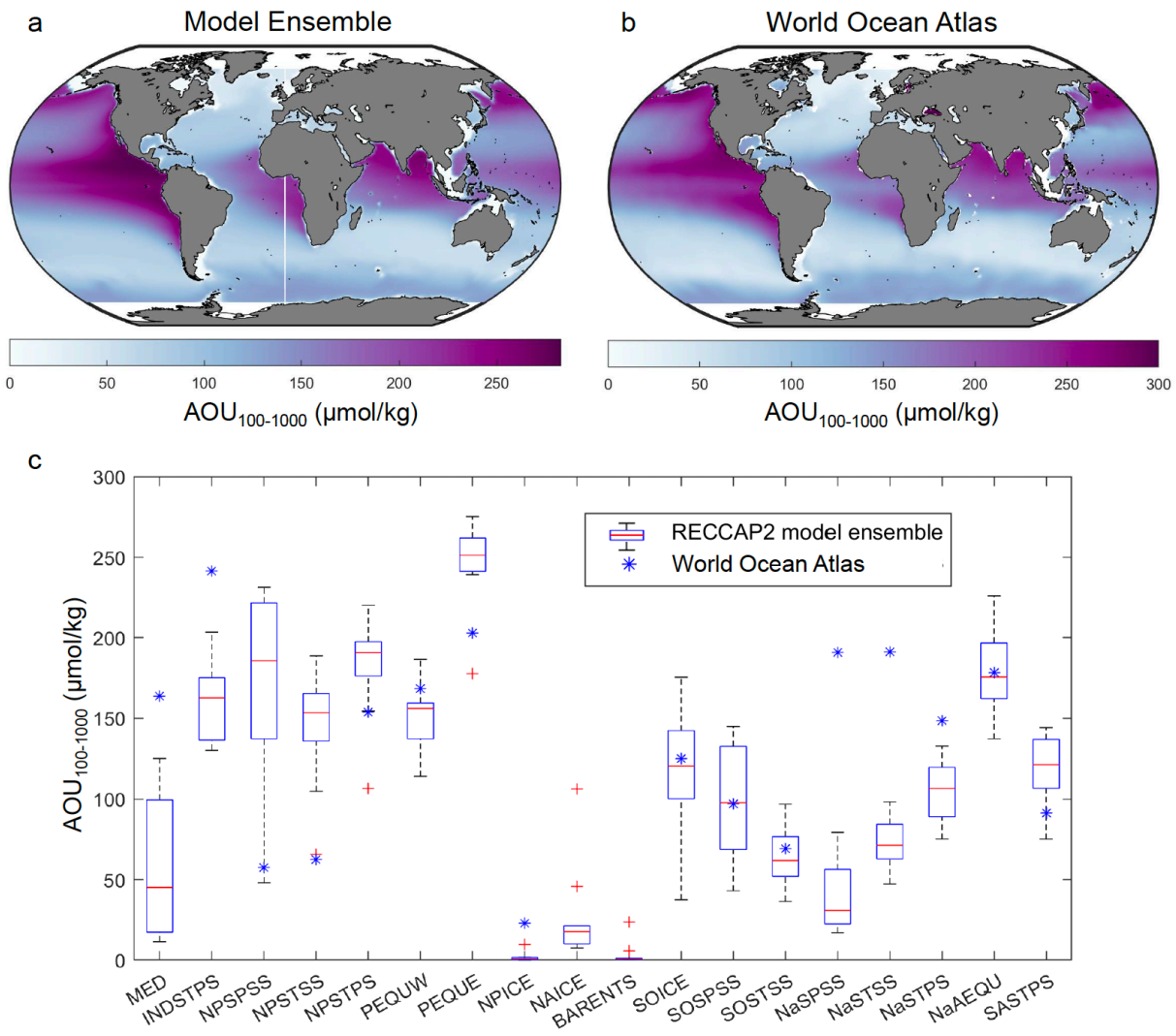

Figure S4. Analysis of apparent oxygen utilization (AOU) vertically averaged over the mesopelagic zone (100-1000 m) (a) spatial map of RECCAP2 multi-model ensemble average, and (b) spatial map from WOA observational data set, and (c) box-whisker plot of RECCAP2 multi-model ensemble medians, interquartile ranges, and outliers pooled into Fay and McKinley biomes (Figure S2).

Supporting Information Tables

Table S1. Interannual variability (1985-2018) for the RECCAP2 simulations (simulation A) for global-integrated, annual-mean variables: vertically integrated net primary productivity NPP and particulate organic carbon export fluxes at 100 m F_{100} and 1000 m depth F_{1000}. Interannual variability (standard deviation) are in Pg C y^{-1}.

	CCSM-WHOI	CESM-ETHZ	CNRM-ESM2	ECCO-Darwin	EC-Earth3	FESOM-REcoM_LR	MOM6-Princeton	MPIOM-HAMOCC	MRI-ESM2-0	Nor_ESM-OC1.2	ORCA1-LIM3-PISCES	PlankTOM12
NPP	0.1914	0.3743	0.2000	0.7272	0.2194	0.3878	0.3204	1.5377	0.4127	0.3518	0.2286	0.3655
F100	0.0352	0.0491	0.0304	0.1966	0.0412	0.1079	0.0383	0.2004	0.0736	0.0717	0.0484	0.1447
F1000	0.0024	0.0140	0.0000	0.1107	0.0000	0.0143	0.0000	0.0419	0.0103	0.0283	0.0000	0.0000

Table S2. Long-term temporal trends (1985-2018) for the RECCAP2 simulations (simulation A) for global-integrated, annual-mean variables: vertically integrated net primary productivity NPP and particulate organic carbon export fluxes at 100 m F_{100} and 1000 m depth F_{1000}. Trends are in Pg C y^{-1}/year,

	CCSM-WHOI	CESM-ETHZ	CNRM-ESM2	ECCO-Darwin	EC-Earth3	FESOM-REcoM_LR	MOM6-Princeton	MPIOM-HAMOCC	MRI-ESM2-0	Nor_ESM-OC1.2	ORCA1-LIM3-PISCES	PlankTOM12
NPP	-0.0140	-0.0172	0.0005	-0.0727	0.0017	-0.0094	0.0102	0.0028	-0.0047	0.0009	0.0190	0.0184
F100	-0.0031	-0.0020	0.0000	-0.0209	0.0000	0.0013	0.0010	0.0001	0.0002	0.0017	0.0029	0.0237
F1000	-0.0002	-0.0002	0.0000	-0.0117	0.0000	0.0004	0.0000	0.0013	0.0000	-0.0001	0.0000	0.0000

Observational and numerical modeling constraints on the global ocean biological carbon pump

Scott C. Doney[1], Kayla A. Mitchell[1,2], Stephanie A. Henson[3], Emma Cavan[4], Tim DeVries[5], Nicolas Gruber[6], Judith Hauck[7], Colleen B. Mouw[8], Jens D. Müller[6], and Francois W. Primeau[2]

Submitted, March 4th, 2024

[1] Department of Environmental Sciences, University of Virginia, Charlottesville, VA, USA,

[2] Department of Earth System Science, University of California, Irvine, Irvine, CA, USA,

[3] National Oceanography Centre, Southampton, UK,

[4] Department of Life Sciences, Silwood Park Campus, Imperial College London, Berkshire, UK,

[5] Earth Research Institute and Department of Geography, University of California, Santa Barbara, Santa Barbara, CA, USA,

[6] Environmental Physics, Institute of Biogeochemistry and Pollutant Dynamics, ETH Zurich, Zürich, Switzerland

[7] Alfred-Wegener-Institut, Helmholtz-Zentrum für Polar- und Meeresforschung, Bremerhaven, Germany

[8] Graduate School of Oceanography, University of Rhode Island, Narragansett, RI, USA.

Corresponding author: Scott Doney (sdoney@virginia.edu) ORCID: 0000-0002-3683-2437

Key Points:

- Global-scale, ocean biogeochemical simulations are compared with observation-based estimates of the marine biological carbon pump.
- A multi-model ensemble exhibits relatively good agreement with observation-based metrics for carbon export flux and transfer efficiency.
- Based on identified model-observation and inter-model differences, we provide guidance for future model evaluations and development.

Abstract

This study characterized ocean biological carbon pump metrics in the second iteration of the REgional Carbon Cycle Assessment and Processes (RECCAP2) project, a coordinated, international effort to constrain contemporary ocean carbon air-sea fluxes and interior carbon storage trends using a combination of observation-based estimates, inverse models, and global ocean biogeochemical models. The analysis here focused on comparisons of global and biome-scale regional patterns in particulate organic carbon production and sinking flux from the RECCAP2 model ensemble against observational products derived from satellite remote sensing, sediment traps, and geochemical methods. There was generally encouraging model-data agreement in large-scale spatial patterns, though with substantial spread across the model ensemble and observational products. The global-integrated, model ensemble-mean export production, taken as the sinking particulate organic carbon flux at 100 m (6.41 ± 1.52 Pg C yr^{-1}), and export ratio defined as sinking flux divided by net primary production (0.154 ± 0.026) both fell at the lower end of observational estimates. Comparison with observational constraints also suggested that the model ensemble may have underestimated regional biological CO_2 drawdown and air-sea CO_2 flux in high productivity regions. Reasonable model-data agreement was found for global-integrated, ensemble-mean sinking particulate organic carbon flux into the deep ocean at 1000 m (0.95 ± 0.64 Pg C yr^{-1}) and the transfer efficiency defined as flux at 1000m divided by flux at 100m (0.121 ± 0.035), with both variables exhibiting considerable regional variability. Future modeling studies are needed to improve system-level simulation of interaction between model ocean physics and biogeochemical response.

Plain Language Summary

Phytoplankton in the surface ocean create each year an amount of organic carbon approximately equivalent to all the annual photosynthesis by plants on land. A small fraction of this newly formed organic carbon is exported below the surface layer, and an even smaller amount makes it all the way to the deep ocean. The transport of organic carbon to the sub-surface ocean, called the biological carbon pump, influences the global-scale distributions of ocean nutrients, oxygen, and inorganic carbon as well as the amount of carbon dioxide in the atmosphere. The global rates and geographic patterns of photosynthesis and carbon flux out of the surface ocean have previously been constructed from ship measurements and satellite remote sensing. Here, we compare these observation-based estimates to a suite of three-dimensional, numerical ocean models and find broadly similar results. The model simulations also capture aspects of the biological carbon pump deeper in the water column, where there are fewer direct constraints from field observations. Our comparison of observations and simulations identifies some deficiencies in the models that should be corrected in order to better simulate climate change impacts on the biological carbon pump.

1 Introduction

Marine biogeochemical processes play a central role in the global Earth System, modulating the distribution of inorganic carbon, oxygen, and nutrients within the ocean and the partitioning of carbon between ocean and atmosphere reservoirs (Broecker and Peng, 1982; Sarmiento and Gruber, 2002; Devries, 2022; Iversen, 2023; Siegel et al., 2023). Because of the

strong oceanic influence on atmospheric CO_2 concentration and thus planetary climate, there is considerable scientific focus on quantifying both the baseline and trends in ocean carbon storage and fluxes arising from the uptake of anthropogenic CO_2 and climate change impacts on marine biogeochemical and physical dynamics (Henson et al., 2016; DeVries et al., 2019; Hauck et al., 2020; Canadell et al., 2021; Crisp et al., 2022; Wilson et al., 2022; Gruber et al., 2023). The REgional Carbon Cycle Assessment and Processes (RECCAP) project is a coordinated, international effort to constrain contemporary ocean carbon air-sea fluxes and interior storage trends using a combination of observation-based estimates, inverse models, and global ocean biogeochemical models (GOBMs) (Wanninkhof et al., 2013; Khatiwala et al., 2013). The second phase, RECCAP2, extends the original synthesis using additional years of ocean observations and updated methodology and numerical results (DeVries et al., 2023; Hauck et al., 2023) as well as expanding the scope of the analysis, in this case into biological carbon pump magnitude and efficiency.

In a simple 1-D form, the marine biological carbon pump can be viewed as the net production of particulate organic carbon (POC) and inorganic carbon (PIC) in the surface ocean, downward vertical transport of particulate carbon into the thermocline and deep sea, and subsequent respiration and remineralization of particulate carbon back into dissolved inorganic carbon (DIC) (Volk and Hoffert, 1985). The downward organic carbon transport, or export flux, drives subsurface marine biogeochemistry, fuels deep-ocean ecosystems, and influences ocean carbon storage and atmospheric CO_2. The biological pump accentuates the vertical gradient in DIC already established from CO_2 system thermal solubility and temperature gradients, and deep-ocean carbon storage reflects a net balance between the biological carbon pump source and physical ocean circulation processes that return elevated deep-ocean DIC waters back to the surface ocean via upwelling and vertical mixing (Sarmiento and Gruber, 2006). The relationship between ocean carbon storage and the strength of the biological pump is not necessarily straightforward because of physical-biological interactions; for example, stronger overturning circulation can enhance both biological export through increased nutrient supply and the physical return of high-DIC deep-ocean waters to the surface (Doney et al., 2006). The vertical structure of the biological carbon pump is also important. Sinking POC fluxes decline rapidly in the thermocline (0 to ~1000 m depth), with only a fraction of surface export flux reaching the deep ocean below 1000 m (Martin et al., 1987; Lutz et al., 2007; Lima et al., 2014; Dinauer et al., 2022). Deeper remineralization depths, that is the transport of a greater fraction of POC into the lower thermocline or deep ocean prior to respiration, enhances ocean carbon storage because of generally reduced physical return rates to the surface ocean for deeper waters, and therefore longer retention times for the remineralized DIC, although with substantial regional variations associated with circulation pathways and rates (Kwon et al., 2009; Siegel et al., 2021).

Net primary production (NPP) by surface ocean phytoplankton generates POC and dissolved organic carbon (DOC), and most marine NPP is converted rapidly back to DIC through zooplankton grazing of living biomass and detritus or through the microbial loop involving consumption of POC and DOC pools. Export fluxes require an excess of community production of organic carbon over respiration that in turn must be supported by an external supply of new nutrients over sufficient time and space scales (Ducklow and Doney, 2013). The fraction of NPP that is exported (export ratio = export flux/NPP), is modulated by the magnitude and seasonality of NPP, environmental conditions, and phytoplankton and zooplankton community composition (Laufkötter et al., 2016). Export flux from the euphotic zone occurs through multiple pathways including gravitational sinking of POC (e.g., living and dead cells; fecal pellets; marine snow),

physical subduction and mixing of POC and DOC below the surface layer, and active biological transport by vertically migrating organisms (Siegel et al., 2016). Contemporary models capture, with varying levels of sophistication and skill, biological processes involved in NPP and export flux from the upper ocean (Fennel et al., 2022), though models tend to focus on gravitational particle sinking and many do not incorporate all of the relevant export pathways (Boyd et al., 2019; Henson et al., 2022) or dynamics governing vertical carbon fluxes from the surface to the deep sea (Burd, 2024). Here we focus on simulated export via gravitational particle sinking, which is incorporated in virtually all global ocean biogeochemical models in some form. Observation-based estimates of the global export flux have a large range (~5-12 Pg C yr^{-1}; Siegel et al., 2016), which is almost identical to the range in export estimates for the modern-day era simulated by coupled climate models (4.5-12 Pg C yr^{-1}; Henson et al., 2022), i.e. the observations-based estimates of export flux provide a poor constraint for biogeochemical models. Because of differences in model climate responses and parameterizations of the ocean biological carbon pump, substantial uncertainties also plague projections of future changes in export flux in response to climate change. For example, Henson et al. (2022) found a large inter-model spread in projected changes in export flux by 2100 of between +0.16 and -1.98 Pg C yr^{-1} (+1.8 to -41%) under the high-emission SSP5-8.5 scenario.

Much of the export flux of organic carbon from the euphotic zone, taken here as the downward flux through 100m (F_{100}), is consumed by respiration in the mesopelagic zone (100 – 1000 m). The diverse mechanisms for vertical transport and remineralization of organic matter in the mesopelagic are only partially captured in models (Fennel et al., 2022). A steep decline with depth in the gravitational sinking flux of particles is well documented from mid-depth sediment traps (e.g., Lutz et al., 2007; Lima et al., 2014; Dinauer et al., 2022), but the exact processes involved are less well quantified and may include physical and biological particle fragmentation (Briggs et al., 2020) as well as particle consumption and repackaging by zooplankton (Stukel et al., 2019). Particle fluxes and the depth-scale of remineralization are affected by particle composition, size, density, and sinking speeds. Particles can vary widely from small, slowly sinking dead cells and detrital material, to large marine snow aggregates with enhanced sinking speeds from captured ballast material, to large rapidly sinking fecal pellets (Lam et al., 2011; Omand et al., 2020). Vertical migrators transport organic carbon downward from the euphotic zone into the mesopelagic, respiring CO_2 and releasing fecal pellets at depth (Archibald et al., 2019). Sinking particle fluxes and mesopelagic biological processes typically are not modeled in great mechanistic detail in contemporary global ocean biogeochemical models, and often relatively simplistic empirical relationships such as variants of the Martin power-law flux curve (Martin et al., 1987) are used in place of explicit representation of the processes controlling mesopelagic flux attenuation.

The proportion of sinking exported POC that survives remineralization in the mesopelagic zone to reach depths > 1000 meters is referred to as the transfer efficiency, given here as the ratio of sinking fluxes at 100 and 1000 meters ($E_{1000/100}$). POC reaching 1000m depth is remineralized below the main thermocline and is likely sequestered on timescales of >100 years, thus contributing to the long-term ocean carbon sink (Siegel et al., 2021). There is currently little consensus on the global magnitude or spatial patterns of transfer efficiency, with some approaches suggesting that $E_{1000/100}$ is high at high latitudes and low at low latitudes (Marsay et al., 2015; Weber et al., 2016; DeVries and Weber, 2017), whilst others imply the opposite pattern (Lam et al., 2011; Henson et al., 2012; Guidi et al., 2015; Mouw et al., 2016b; Dinauer et al. 2022). A variety of approaches have been used to generate these estimates, including paired in situ

observations of ^{234}Th-derived export flux and deep sediment trap flux (Henson et al. 2012), vertical profiles of flux from drifting sediment traps (Marsay et al., 2015) or inverting the observed nutrient and/or oxygen distributions using an inverse model (Weber et al., 2016; Devries and Weber, 2017; Cram et al., 2018). The differing approaches, and differing time and space scales that they integrate over, are likely a significant source of the uncertainty in global $E_{1000/100}$ patterns. In CMIP6 models, there are substantial differences in both the preindustrial mean $E_{1000/100}$ (varying from 3% to 25% across models) and its response to 21st century climate change, with projections showing both increases and decreases in $E_{1000/100}$ over time (Wilson et al., 2022).

Early model skill assessments relied heavily on model-data comparisons to transient tracers, ocean physics, and sub-surface nutrient and oxygen fields that reflect the imprint of biological pump fluxes and ocean circulation (e.g., Matsumoto et al., 2004; Doney et al. 2004; Najjar et al. 2007). However, observational constraints on the ocean biological carbon pump have advanced considerably since the early global 3-D ocean biogeochemical modelling efforts (e.g., Bacastow and Maier-Reimer, 1990; Maier-Reimer, 1993). Global-scale data compilations of primary production, surface export and mesopelagic sinking carbon fluxes are now available based on a wealth of satellite remote sensing, sediment traps, and geochemical methods (e.g., Henson et al. 2012; Mouw et al., 2016a). Past model-data skill assessments using multi-model ensembles have highlighted differences in simulated ocean biological carbon pump patterns, magnitudes, and mechanisms and identified model biases relative to admittedly imperfect observational estimates (Laufkötter et al., 2015; Laufkötter et al., 2016). This study expands on these past assessment efforts of the ocean biological carbon pump to include the current generation of global ocean biogeochemical models compiled for RECCAP2 (DeVries et al., 2023).

The objective of this study is to characterize the global-scale biological carbon pump from RECCAP2 models and compare the simulation results with observation-based metrics. The focus is on the spatial patterns and global-integrated rates from the multi-model ensemble mean taking into consideration inter-model spread. Key metrics include export of sinking POC from the surface euphotic zone and the efficiency of POC transfer through the mesopelagic ocean, both of which are central to ocean carbon storage. Based on identified model-observation and inter-model differences, we also provide guidance for future global ocean biogeochemical model evaluations and development that could include targeted, more detailed analyses of dynamics and biases within individual RECCAP models.

2 Methods and Data

2.1 RECCAP2 model simulations and observational data products

This study leveraged a collection of ocean simulation and observational data sets, outlined in Table 1, assembled for RECCAP2 following standardized protocols and data reporting for numerical and observation-based pCO_2 products (RECCAP2 Ocean Science Team, 2022; DeVries et al., 2023; Müller, 2023). The RECCAP2 ocean data sets included monthly surface and annual ocean interior output for the contemporary period from more than a dozen global ocean biogeochemical model hindcast simulations, including both forward and data-assimilated models, along with observation-based surface ocean pCO_2 interpolation products. Many of the models included in the RECCAP2 suite have been used in the Global Carbon Project to assess the ocean carbon sink (Hauck et al., 2020; Friedlingstein et al., 2022). Here, we present model results for

1985 to 2018 from RECCAP2 simulation A, which was forced with historical atmospheric reanalysis data and increasing atmospheric CO_2, and hence represents both steady-state and variable climate processes and both natural, pre-industrial carbon fluxes and anthropogenic carbon fluxes caused by rising atmospheric CO_2 (DeVries et al., 2023).

Table 1. Description of RECCAP2 global ocean biogeochemical hindcast models, global data-assimilated models, and observation-based products used in this study. For more details see Tables S1 and S2 in DeVries et al. (2023). The World Ocean Atlas (WOA) data set was also used in the model-data evaluation.

Global hindcast models	**Data range**	**References**
CCSM-WHOI	1958-2017	Doney et al. (2009)
CESM-ETHZ	1980-2018	Lindsay et al. (2014); Yang and Gruber (2016)
CNRM-ESM2 -1	1980-2018	Séférian et al. (2019; 2020); Berthet et al. (2019)
EC-Earth3	1980-2018	Döscher et al. (2021)
FESOM-REcoM-LR	1980-2018	Hauck et al. (2020)
MPIOM-HAMOCC	1980-2018	Ilyina et al. (2013); Mauritsen et al. (2019)
MOM6-Princeton	1980-2018	Liao et al. (2020); Stock et al. (2020)
MRI-ESM2-1	1980-2018	Urakawa et al. (2020); Tsujino et al. (2017)
NorESM-OC1.2	1980-2018	Schwinger et al. (2016)
NEMO-PlankTOM12.1	1980-2018	Le Quéré et al. (2016); Wright et al. (2021)
ORCA1-LIM3-PISCES	1980-2018	Aumont et al. (2015)
Data-assimilated models		
ECCO-Darwin	1995-2018	Carroll et al. (2020; 2022)
SIMPLE-TRIM	Climatology	DeVries and Weber (2017)
pCO_2 interpolation products		
CMEMS-LSCE-FFNN	1985-2018	Chau et al. (2022)
JenaMLS	1985-2018	Rödenbeck et al. (2013); Rödenbeck et al. (2022)
MPI-SOMFFN	1982-2018	Landschützer et al. (2016)
NIES-ML3	1980-2020	Zeng et al. (2022)
OceanSODA-ETHZ	1985-2018	Gregor and Gruber (2021)
LDEO_HPD	1985-2018	Gloege et al. (2022)
UOEX_Wat20	1985-2019	Watson et al. (2020)
World Ocean Atlas		
Oxygen and AOU	Climatology	Garcia et al. (2019)
Biological carbon pump metrics		
net primary production, export production, and sinking POC flux	Climatology	Mouw et al. (2016a; 2016b)

Spatial 2D model output and pCO_2 interpolation products were provided to RECCAP2 with 1° x 1° resolution at monthly time steps, and 3D model output was resolved at annual time

steps. All estimates derived in this study were computed on the 1° x 1° grid. Global multi-model ensembles, spatial integrals and averages were computed as needed from the gridded results. For the aggregation to sub-basin ocean regions, ocean biomes based on Fay and McKinley (2014) were used in most instances to facilitate consistent regional intercomparison across RECCAP2 studies (e.g., Hauck et al., 2023). Longhurst provinces (Supplement Figure S1; Reygondeau et al., 2013) were additionally used in some of the biological pump model-observational comparisons to be consistent with one of the key observational data synthesis products (Mouw et al., 2016a). The notation and units for the biological, chemical and physical variables used in this study are described in Table 2. More details on the RECCAP2 ocean data sets can be found in DeVries et al. (2023).

We also used an observational compilation of surface ocean export production and sinking POC flux combined with satellite ocean color data products for primary production synthesized in Mouw et al. (2016a) and as aggregated to Longhurst regional provinces in Mouw et al. (2016b). The full dataset includes over 15000 individual sediment trap and ^{234}Th POC flux measurements at 673 locations, combined with satellite-derived estimates of NPP. Chlorophyll measurements collected from the SeaWiFS sensor on the OrbView-2 ocean color satellite, spanning from August 1997 to December 2010, were used to derive NPP using the vertically generalized production model (VGPM) (Behrenfeld and Falkowski, 1997) on an equal-area grid with 9-km resolution. The climatology in Mouw et al. (2016a) used an interpolation approach to combine the satellite timeseries and short-deployment (<30 days trap cup intervals) sediment trap POC flux measurements at overlapping locations. Over 43% of the POC flux measurements were collected after 1997, overlapping with the satellite record. For each POC flux location, median monthly values are computed and binned into biogeochemical Longhurst provinces for the climatology. The POC flux climatology also has a depth dimension, with depth bins centered at 20 m for a near-surface layer, in 50 m intervals in the upper thermocline, and in 200 m intervals from 500 m to 5000 m.

Table 2. Glossary and description of modeled, observed, and derived variables including notation and units.

Variable Name	Units	Output frequency	Description
2D or surface ocean properties			
pCO_2	µatm	monthly	Surface ocean pCO_2
NPP	mol C m^{-2} yr^{-1}	monthly	Vertically-integrated net primary production of organic carbon
F_{100}	mol C m^{-2} yr^{-1}	monthly	POC sinking flux at 100 m
F_{1000}	mol C m^{-2} yr^{-1}	monthly	POC sinking flux at 1000 m
3D or Interior Ocean Properties			
T	°C	annual	Seawater potential temperature
S	-	annual	Salinity (PSS-78)
F_{3D}	mol C m^{-2} yr^{-1}	annual	3D field of POC sinking flux

O_2	mol O_2 m^{-3}	annual	Dissolved oxygen concentration
Derived Variables			
$E_{100/NPP} = F_{100}/NPP$	-	monthly	Surface Export Ratio
$E_{1000/100} = F_{1000}/F_{100}$	-	monthly	Mesopelagic Transfer Efficiency
$E_{1000/NPP} = F_{1000}/NPP$	-	monthly	Surface to Deep-sea Export Efficiency
AOU	μmol kg^{-1}	monthly	Apparent oxygen utilization

2.2 Ocean biological pump and biogeochemical metrics

Our analysis utilized biogeochemical model estimates of vertically integrated NPP and export fluxes of sinking POC flux across a shallow surface at the approximate base of the euphotic zone (100 m, F_{100}) and at the base of the main thermocline (1000 m, F_{1000}). Note that the 1000 m fluxes were not provided for all models (see Figure 2c), and therefore the ensemble means for F_{100} and F_{1000} were constructed from different subsets of RECCAP2 simulations. The export ratio, $E_{100/NPP}$, was computed as the ratio of POC sinking flux at 100 m divided by net integrated primary production:

$$E_{100/NPP} = \frac{F_{100}}{\mathrm{NPP}} \quad (1)$$

The transfer efficiency across the 1000 m depth horizon, $E_{1000/100}$, was similarly computed as the ratio of sinking POC fluxes at 100 m and 1000 m:

$$E_{1000/100} = \frac{F_{1000}}{F_{100}} \quad (2)$$

A depth of 1000 m is taken as an approximate boundary between the main thermocline with ventilation timescales of years to decades and the deep ocean with time-scales of a century and longer (Siegel et al., 2021).

The relationship between the biological pump and the inorganic CO_2 system was examined by partitioning the seasonal variability in surface seawater pCO_2 into thermal and non-thermal components following Takahashi et al. (2002). We refer readers interested in a thorough analysis of RECCAP2 CO_2 system seasonality to Rodgers et al. (2023). The temperature effect on pCO_2 was calculated for isochemical seawater using the approximation $\frac{\partial(\ln(pCO_2))}{\partial T} = 0.0423$ (°C^{-1}) from the experimental value from Takahashi et al. (1993). The seasonal cycle in monthly surface temperature anomalies relative to the annual mean surface temperature generated a corresponding seasonal variation in the thermal (temperature-dependent) pCO_2 component about the pCO_2 annual mean:

$$pCO_2^{thermal} = (pCO_2)_{mean} \times exp\left[0.0423\left(T_{monthly} - T_{mean}\right)\right] \quad (3)$$

Ocean hindcast simulations typically capture quite well the seasonal cycle of sea surface temperature because the ocean models are forced by atmospheric reanalysis products and heat flux boundary conditions that effectively contain information on the observed temperature record (Doney et al., 2007); the same model-data agreement transfers to the thermal pCO_2 seasonal component. The non-thermal pCO_2 component was computed by subtracting the thermal component from the monthly pCO_2 values, and the seasonal amplitude $\Delta pCO_{2,\text{non-thermal}}$ was calculated as the seasonal peak-to-trough difference. The non-thermal pCO_2 component reflects seasonal variations in DIC and alkalinity from biological organic and inorganic carbon production and remineralization, air-sea CO_2 gas exchange, and physical transport and mixing. Note that the seasonal phasing of the non-thermal pCO_2 component can be distinct from the phasing of the total pCO_2 cycle. This is especially the case in the low latitudes, where the thermal component dominates the seasonal cycle (Takahashi et al., 1993; Landschützer et al., 2018; Rodgers et al., 2023).

We also computed apparent oxygen utilization (AOU) using modeled dissolved oxygen, salinity, and potential temperature fields. Modeled average AOU at 100 m (AOU_{100}) and 1000 m depth (AOU_{1000}) were found using nearest depth bins in model products (bins centered within 50 m of depths). The simulated AOU fields are compared against the World Ocean Atlas (WOA) data product (Garcia et al., 2019).

3 Results

3.1 Simulated ocean biological carbon pump metrics

Global spatial fields of present-day biological carbon pump variables are displayed in Figure 1 for the RECCAP2 model ensemble mean with the corresponding ensemble standard deviation in Figure S1. Biome-scale ensemble-mean averages and within-ensemble standard deviation values for the biological pump metrics are reported in Table 3 using the standard RECCAP2 biomes by ocean basin (Figure S2; Fay and McKinley, 2014).

The magnitude and spatial patterns of simulated annual mean NPP and export flux from sinking POC (F_{100}) (Figure 1a and 1b) are broadly similar to observational estimates (Section 3.2). Simulated upper-ocean biological pump variables showed large geographic variations with annual-mean NPP ranging on biome scales (Table 3) from 8 to 21 mol C m^{-2} yr^{-1} and F_{100} ranging from 1.1 to 2.9 mol C m^{-2} yr^{-1}. The simulated spatial patterns reflect euphotic zone temperature, nutrient supply, and grazing and loss rates that govern phytoplankton standing stock in the models (Falkowski et al., 1998; Laufkötter et al., 2015; Laufkötter et al., 2016). The imprint of nutrient supply was particularly evident in the elevated NPP and export fluxes found in equatorial and coastal upwelling regions, western boundary currents, and mid-latitude bands of deep seasonal mixing. Within-ensemble standard deviations (σ) of NPP and F_{100} were elevated in the equatorial band, and high σ_{NPP} values were found also in the Southern Ocean indicating substantial model disagreement within the ensemble (Figure S1a and S1b). Biome-scale σ_{NPP} values ranged from 2.1 to 6.6 mol C m^{-2} yr^{-1} (from as low as 0.22 to nearly 0.72 times the ensemble mean in parts of the Southern Ocean); biome-scale σ_{F100} values varied from 0.4 to >1.0 mol C m^{-2} yr^{-1} with the largest absolute and fractional within-ensemble variation of >0.7 times the ensemble mean occurring in the western equatorial Pacific.

359 The local POC sinking flux at the base of the mesopelagic (F_{1000}) ranged at biome scale
360 from 0.09 to 0.54 mol C m^{-2} yr^{-1} with broadly similar patterns to F_{100}, though with some notable
361 exceptions such as the high F_{1000} values in tropical low-oxygen zones in the eastern tropical Pacific
362 and Arabian Sea (Figure 1c). Note the roughly half to full order of magnitude decline in scale in
363 Figure 1 from NPP to F_{100} and then F_{100} to F_{1000}. This indicates first that the bulk of simulated
364 NPP is recycled within the euphotic zone above 100 m, rather than exported as sinking POC flux,
365 and second that most of the sinking POC flux at 100 m is remineralized in the mesopelagic, rather
366 than reaching the deep ocean below 1000 m. As for NPP and F_{100}, some correspondence was found
367 for the spatial patterns of ensemble-mean F_{1000} and σ_{F1000}. Highest biome-scale σ_{F1000} values of
368 0.26 to 0.29 mol C m^{-2} yr^{-1} occurred in the North Pacific and eastern equatorial Pacific, equal to
369 0.85 and 0.53 times the ensemble-mean F_{1000} for those biomes; biome-scale σ_{F1000} values of ~0.5
370 or more of the ensemble-mean were common, with even higher fractional values locally such is in
371 the eastern subtropical North Pacific (Figure S1c; Table 3).

372 The fraction of NPP exported across 100 m, or export ratio ($E_{100/NPP}$, Figure 1d; Table 3)
373 varies at the biome scale in the ensemble mean from 0.12 to 0.21 with elevated values in high
374 latitudes. The spatial patterns for within-ensemble $E_{100/NPP}$ standard deviation (Figure S1d) mirror
375 that of the mean $E_{100/NPP}$ with biome-mean standard deviations of 0.035 to 0.050 in most biomes
376 and up to 0.091 in the sub-polar Southern Ocean biome where there is more within-ensemble
377 model spread.
378
379
380

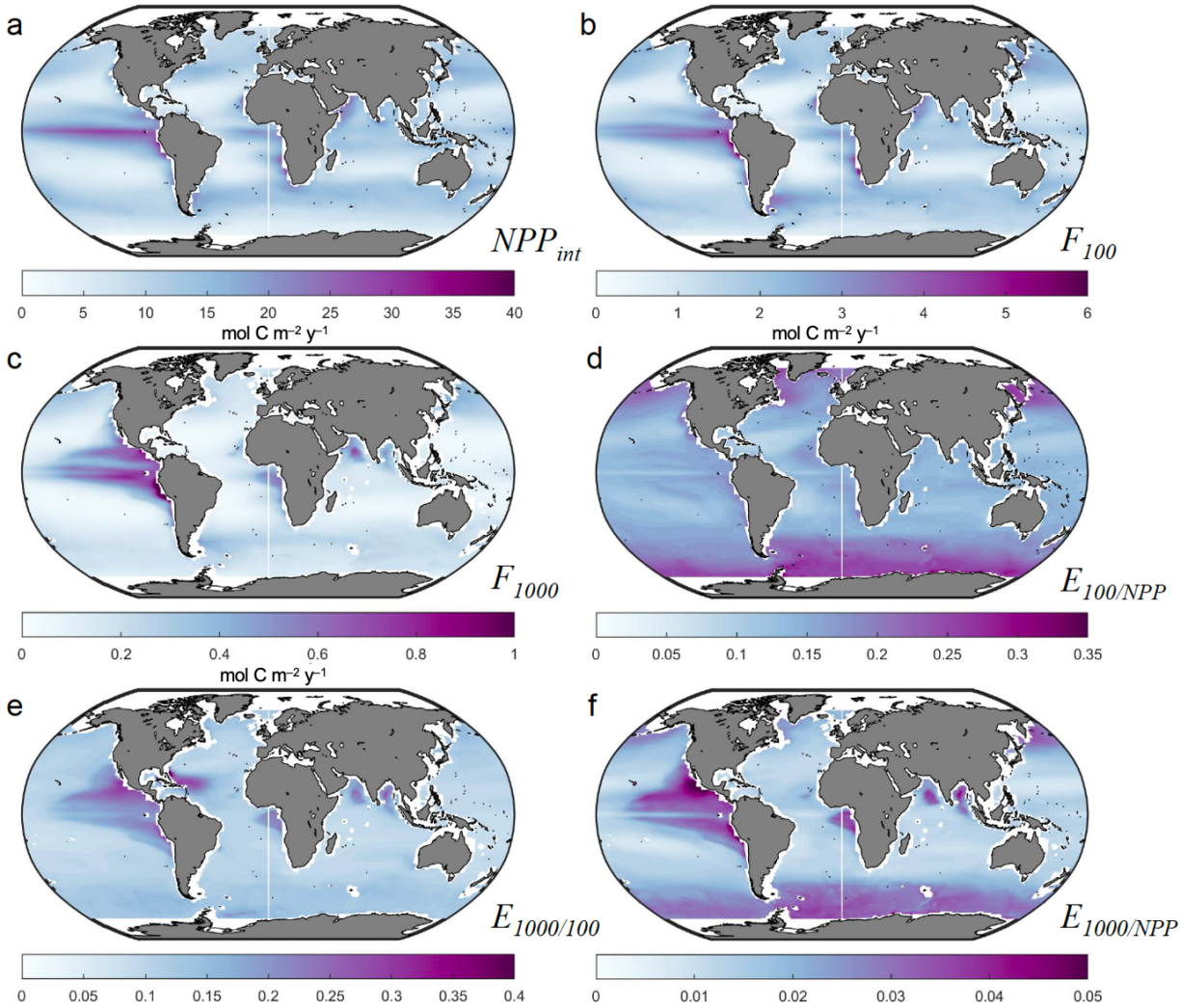

Figure 1. Multi-model ensemble averages of biological pump parameters from 1985 to 2018 across all RECCAP2 model simulations (simulation A). Maps of annual mean (a) integrated net primary productivity NPP, (b) particulate organic carbon export fluxes at 100 m F_{100}, and (c) 1000 m depth F_{1000}, all in mol C m^{-2} yr^{-1}. Ensemble mean (d) surface export efficiency ratio $E_{100/NPP} = F_{100}/NPP$ (Eq. 1), (e) mesopelagic transfer efficiency at 1000 m $E_{1000/100} = F_{1000}/F_{100}$ (Eq. 2), and (f) export efficiency to the deep ocean $E_{1000/NPP} = F_{1000}/NPP$, all ratios unitless.

The ensemble-mean transfer efficiency through the mesopelagic, $E_{1000/100}$ (Figure 1e; Table 3), exhibited background levels at the biome-scale of 0.09-0.14 for most biomes and ranging as high as 0.18 in the eastern equatorial Pacific biome; sub-biome regional values up to 0.3 occurred in the eastern tropical Pacific, western and eastern tropical Atlantic, and Arabian Sea and Bay of Bengal. Some ocean biogeochemical models reduce sub-surface POC remineralization in low-oxygen zones, using a parameterization based on local oxygen concentrations, driving higher $E_{1000/100}$ values in low-oxygen regions such as the eastern tropical Pacific, Arabian Sea and Bay of Bengal. Furthermore, POC flux mineral ballasting from Saharan dust deposition, prescribed as an

external forcing, is likely an important contributor in at least some models (CCSM-WHOI and CESM-ETHZ) to high $E_{1000/100}$ in the western tropical Atlantic (Lima et al., 2014). The ensemble $E_{1000/100}$ standard deviation (Figure S1e) generally followed $E_{1000/100}$ with particularly large $\sigma E_{1000/100}$ values up to 0.3 in the western tropical Atlantic reflecting differences across models in the parameterization of POC sinking in the presence of desert dust. The metric $E_{1000/NPP}$ (Figure 1f), combining surface export and mesopelagic transfer efficiencies, had generally similar spatial patterns to $E_{1000/100}$ but with lower values, reflecting the small fraction of NPP that sinks below 1000 m and is sequestered in the deep ocean. More than a factor of two variation was found for metric $E_{1000/NPP}$ across biomes (0.012 to 0.027) with large within-ensemble variation for some biomes where the standard deviation approached or exceeded the ensemble mean.

Table 3. Model ensemble averages and standard deviations of biological pump parameters by RECCAP2 regional biomes (Figure S2) (see also Figure 1) grouped as Sub-Polar Seasonally Stratified (SPSS), Sub-Tropical Seasonally Stratified (STSS), Sub-Tropical Permanently Stratified (STPS), Equatorial (EQU), and Mediterranean (MED). Table includes annual means and standard deviations for vertically integrated net primary productivity NPP, particulate organic carbon export fluxes at 100 m F_{100}, and 1000 m depth F_{1000}, all in mol C m^{-2} yr^{-1}, and average surface export efficiency ratio $E_{100/NPP} = F_{100}/NPP$, mesopelagic transfer efficiency at 1000 m $E_{1000/100} = F_{1000}/F_{100}$, and export efficiency to the deep ocean $E_{1000/NPP} = F_{1000}/NPP$, all ratios unitless. Ensemble were not computed for the small, high-latitude polar ice biomes due to noisy and/or missing data across the full ensemble.

	NPP	F_{100}	F_{1000}	$E_{100/NPP}$	$E_{1000/100}$	$E_{1000/NPP}$
SPSS						
N. PACIFIC	11.89±4.81	2.21±0.65	0.307±0.263	0.206±0.076	0.124±0.071	0.018±0.012
N. ATLANTIC	9.30±3.00	1.77±0.65	0.177±0.156	0.211±0.075	0.116±0.060	0.014±0.009
SOUTHERN	9.24±6.64	1.59±0.60	0.197±0.119	0.213±0.091	0.132±0.071	0.023±0.025
STSS						
N. PACIFIC	13.53±3.68	2.04±0.70	0.206±0.117	0.161±0.040	0.114±0.049	0.014±0.006
N. ATLANTIC	12.98±3.28	1.93±0.54	0.165±0.069	0.162±0.049	0.099±0.036	0.014±0.006
SOUTHERN	13.91±5.02	2.12±0.39	0.222±0.087	0.173±0.053	0.109±0.040	0.016±0.009
STPS						
N. PACIFIC	8.92±3.24	1.18±0.61	0.177±0.102	0.131±0.047	0.132±0.049	0.017±0.010
N. ATLANTIC	7.70±2.37	0.97±0.44	0.092±0.057	0.121±0.051	0.140±0.097	0.013±0.008
S. ATLANTIC	9.78±2.16	1.33±0.41	0.138±0.090	0.130±0.043	0.104±0.040	0.012±0.008
INDIAN	16.67±4.75	2.25±0.85	0.284±0.162	0.143±0.035	0.130±0.063	0.016±0.008
EQU						
W. PACIFIC	11.03±5.31	1.44±1.06	0.10±0.078	0.134±0.059	0.089±0.050	0.013±0.011
E. PACIFIC	21.16±5.16	2.91±0.74	0.542±0.288	0.151±0.043	0.178±0.086	0.027±0.015
ATLANTIC	14.33±4.71	1.94±0.65	0.272±0.137	0.145±0.039	0.140±0.043	0.019±0.010
MED	9.21±3.71	1.34±0.79	0.074±0.062	0.141±0.060	0.119± 0.107	0.011± 0.008

420

421 To illustrate differences among the models making up the RECCAP2 multi-model
422 ensemble, global integrals of the annual average biological pump metrics are displayed in Figure
423 2. A box-whisker plot is shown for each model ensemble member quantifying the interannual
424 variability for each model for the RECCAP2 reporting period (1985-2018). Note that some
425 RECCAP2 models did not report F_{1000}, resulting in missing estimates for $E_{1000/100}$ and $E_{1000/NPP}$.
426 Some models stood out as either anomalously low (e.g. FESOM-REcoM-LR for NPP) or high
427 (e.g. NEMO-PlankTOM12.1 for F_{100}) relative to the other RECCAP2 ensemble members, though
428 inter-model agreement alone was not necessarily a robust indicator of model skill (see Section
429 3.2). For global $E_{100/NPP}$, the models were roughly split into low (0.10-0.12) and high (0.16-0.19)
430 groups (Figure 2d). Global F_{1000}, $E_{1000/100}$, and $E_{1000/NPP}$ varied widely for the smaller number of
431 available models (Figure 2c, 2e, and 2f).
432

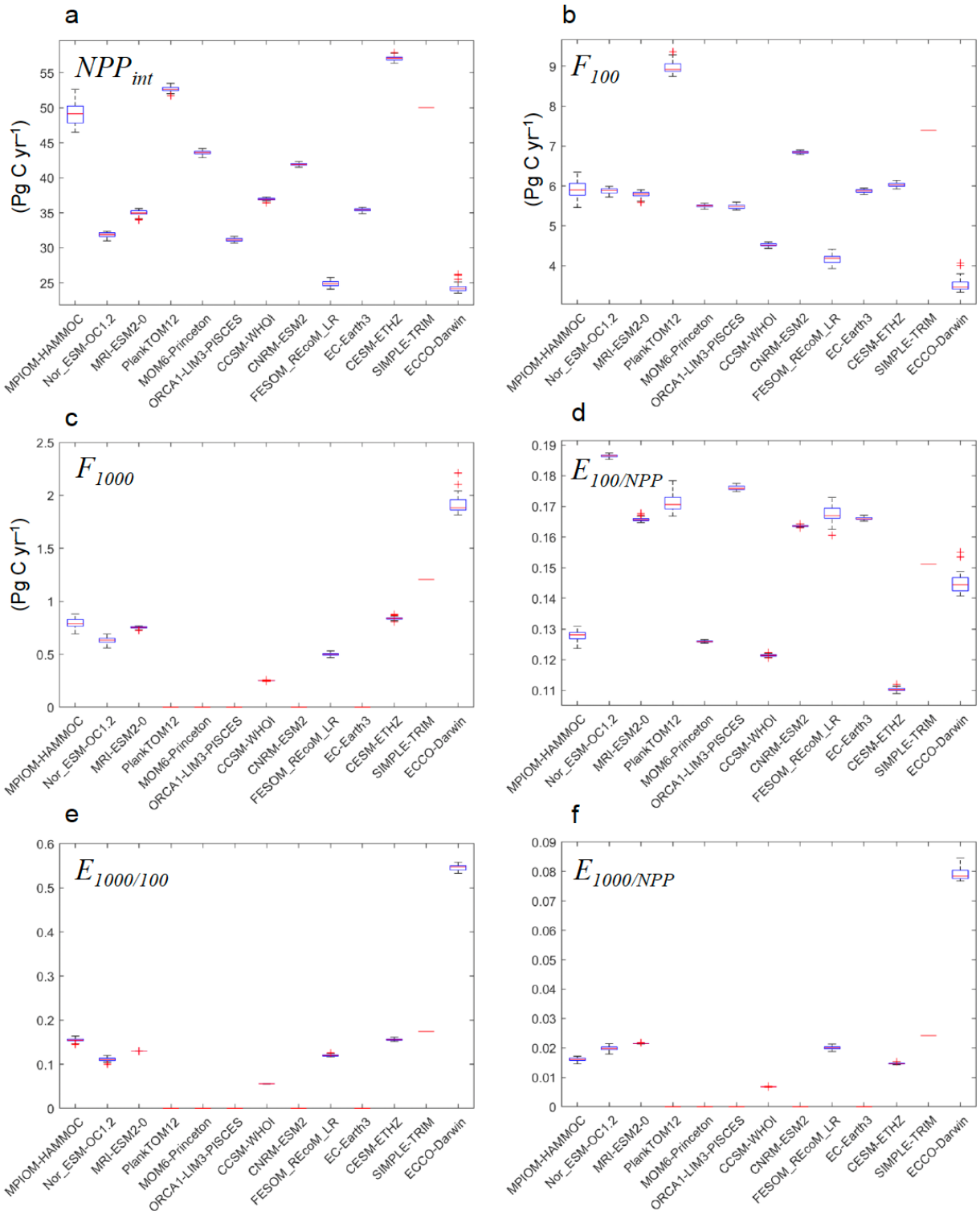

Figure 2. Boxplots showing median values (1985-2018), interannual interquartile ranges, and outliers of biological pump metrics across model products in RECCAP2 ensemble (simulation A). Globally integrated, annual (a) net primary productivity NPP, (b) particulate organic carbon export fluxes at 100 m F_{100}, and (c) 1000 m depth F_{1000} , all in Pg C y^{-1}. Global and annual average (d)

surface export efficiency ratio $E_{100/NPP} = F_{100}/NPP$ (Eq. 1), (e) mesopelagic transfer efficiency at 1000 m $E_{1000/100} = F_{1000}/F_{100}$ (Eq. 2), and (f) export efficiency to the deep ocean $E_{1000/NPP} = F_{1000}/NPP$, all ratios unitless. CCSM-WHOI output does not include the year 2018 and SIMPLE-TRIM does not simulate interannual variability. Efficiency ratios are not given in panels d, e, and f for models lacking the corresponding *NPP*, F_{100}, or F_{1000}.

3.2 Model-observational comparisons

The global ocean biological carbon pump metrics from the RECCAP2 multi-model ensemble were compared against corresponding literature values in Table 4 and Figure 3. The RECCAP2 multi-model ensemble global-integrated NPP value, 42.7 ± 10.9 Pg C yr^{-1}, was at the lower end of literature estimates (43.5-68 Pg C yr^{-1}), and the inter-quartiles have limited overlap. Similarly, global-integrated F_{100} from the multi-model ensemble of 6.41 ± 1.52 Pg C yr^{-1} was lower than the mean of the literature estimates of sinking POC flux (~8 Pg C yr^{-1}, range 4-13 Pg C yr^{-1}), though the inter-quartiles overlapped substantially because of the large range in observation-based estimates. The global-integrated model ensemble F_{1000} value of 0.95 ± 0.64 Pg C yr^{-1} fell between one low estimate of 0.66 Pg C yr^{-1} (Henson et al., 2012) and two other literature estimates of 1.1 Pg C yr^{-1}. The global multi-model ensemble-mean export and transfer efficiencies, $E_{100/NPP}$ (0.15 ± 0.03) and $E_{1000/100}$ (0.12 ± 0.04), were within the range of literature values after removing the high E_{100} values (0.3 and 0.38) from Laws et al. (2000) and acknowledging one low outlier model for global $E_{1000/100}$ (~0.05; CCSM-WHOI; Figure 2e).

The wide range of literature estimates reflects differences in measurement methodologies, biases, and uncertainties in the datasets used for biological carbon pump metric estimation, as well as uncertainties introduced by data sampling biases, aggregation, time/space interpolation and modeling approaches. At global scales, in situ observational sampling for some variables remains sparse and regionally patchy, and satellites, empirical relationships, and numerical models have been used to gap-fill for global-scale product generation. For example, even with field data sets available for ocean NPP based on ^{14}C uptake incubation studies, satellite remote sensing has been required to create uniform global NPP products, which have been calibrated/validated against ^{14}C NPP field data. A variety of in situ methods have been used to estimate surface ocean export flux estimates (~F_{100}) – drifting sediment traps, ^{234}Th deficit, etc. To derive global-scale fields of export, extrapolation from the limited in situ data is required which generates uncertainties in the derived estimates due to the underlying data sparsity (Henson et al., 2024). Typically, satellite data is used to build an empirical relationship between flux and readily derived variables, such as sea surface temperature or chlorophyll concentration. Other approaches include merging satellite data with food-web models (e.g., Siegel et al., 2014). Observation-based global F_{1000} estimates have been generated from sediment trap data (Mouw et al., 2016a), and estimates of both global F_{100} and F_{1000} have been derived from inverse and data-assimilation ocean models (e.g., Devries and Weber, 2017; Nowicki et al., 2022).

478 **Table 4**. Comparison of literature-based, global observation-based ocean biological carbon pump
479 metrics with the RECCAP2 model ensemble means and within-ensemble standard deviations.
480 Note that SIMPLE-TRIM data assimilation results from Devries and Weber (2017) are also
481 included in the RECCAP-2 model ensemble.

482

Net Primary Production *NPP* (Pg C yr^{-1})	**References**
43.5	VGPM Behrenfeld & Falkowski (1997)
52	CAFÉ Silsbe et al. 2016
68	Carr (2002) & Carr et al. 2006
49	Marra et al. (2003)
52	CbPM2 Behrenfeld et al. 2005
42.7 ± 10.9	**RECCAP2 model ensemble mean and STD**
POC Export ~F_{100} (Pg C yr^{-1})	
4	Henson et al. (2012)
9.6	Dunne et al. (2007)
11.1-12.9	Laws et al. (2000)
5.7	Siegel et al. (2014)
9.6	Schlitzer (2000); inversion
9-13	Laws et al. (2011)
8.8 (7.3 at 100 m)	DeVries & Weber (2017); data assimilating
7.3 (6.4 at 100 m)	Nowicki et al. (2022)
6.41 ± 1.52	**RECCAP2 model ensemble-mean and STD**
POC Flux 1000 m F_{1000} (Pg C yr^{-1})	
0.66	Henson et al. (2012)
1.1	DeVries & Weber (2017)
1.1	Nowicki et al. (2022)
0.95 ± 0.64	**RECCAP2 model ensemble mean and STD**
Export Ratio ~$E_{100/NPP}$	
0.1	Henson et al. (2012)
0.19	Dunne et al. (2007)
0.3	Laws et al. (2000); food web
0.38	Laws et al. (2000); empirical
0.103	Siegel et al. (2014)
0.17	Devries & Weber (2017)

0.13 (for POC only) 0.18 (for POC + DOC + vertical migration)	Nowicki et al. (2022)
0.154 ± 0.026	**RECCAP2 model ensemble mean and STD**
Transfer Flux Efficiency $E_{1000/100}$	
0.19	Henson et al. (2012)
0.13	DeVries & Weber (2017)
0.15	Nowicki et al. (2022)
0.121 ± 0.035	**RECCAP2 model ensemble mean**

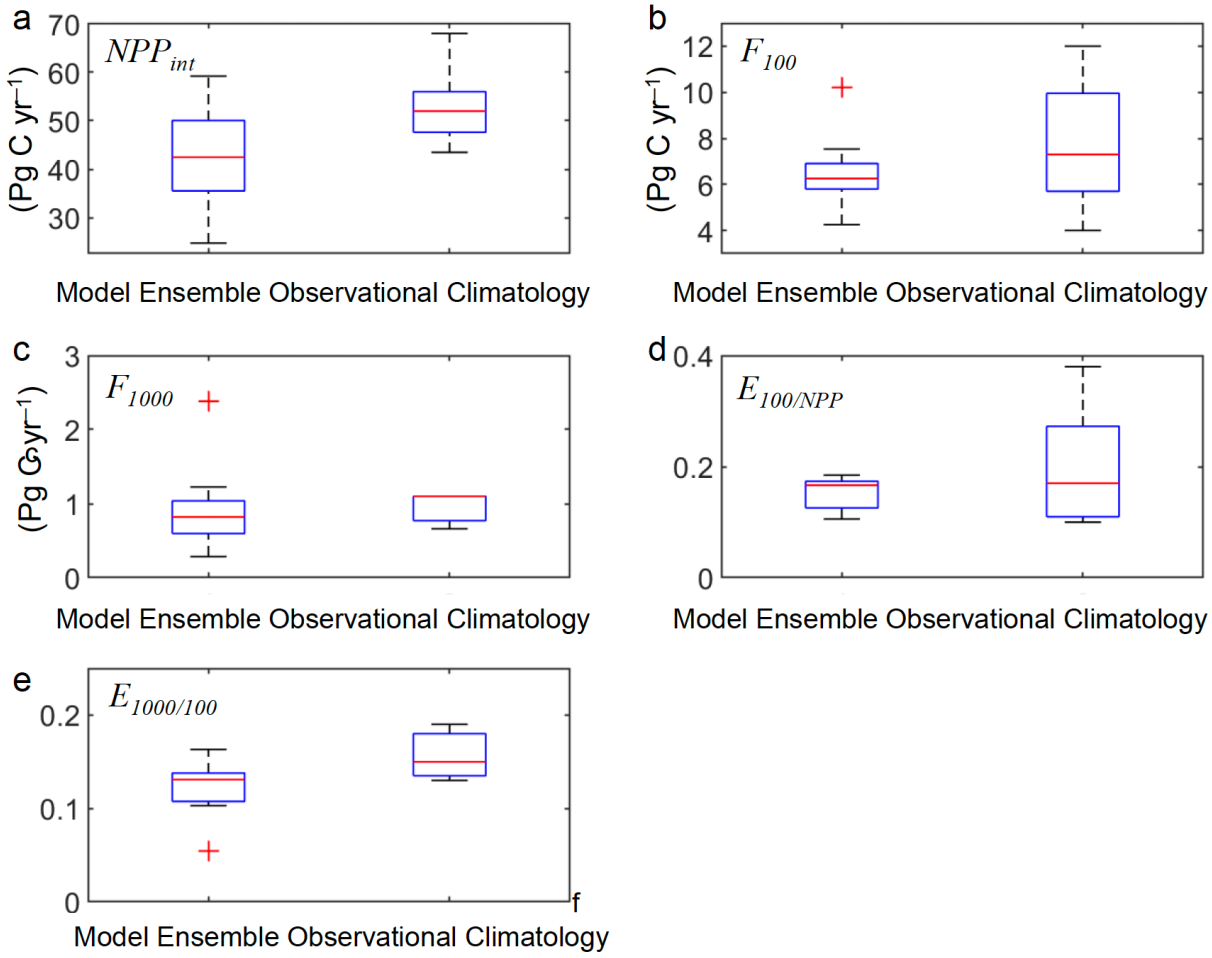

Figure 3. Box-whisker plots showing median values and interquartile ranges of biological pump parameters from 1985-2018 averaged across model products in RECCAP2 ensemble (simulation A). Global integrated, annual (a) net primary productivity *NPP*, (b) particulate organic carbon export fluxes at 100 m F_{100}, and (c) 1000 m depth F_{1000} , all in Pg C yr^{-1} (note that the median line for F_{1000} is also the upper interquartile because two of the three observational estimates match).

491 Global and annual average surface export efficiency ratio (d) $E_{100/NPP} = F_{100}/NPP$ (Eq. 1), and (e)
492 mesopelagic transfer efficiency at 1000 m $E_{1000/100} = F_{1000}/F_{100}$ (Eq. 2), all ratios unitless.

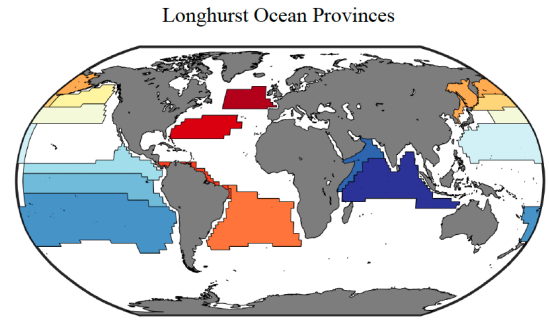

Province Number	Province Code	Province Description
1	NADR	Westerlies - N. Atlantic Drift Province
2	NASW	Westerlies - N. Atlantic Subtropical Gyral Province (West)
3	GUIA	Coastal - Guianas Coastal Province
4	SATL	Trades - South Atlantic Gyral Province (SATG)
5	BERS	Polar - N. Pacific Epicontinental Province
6	PSAW	Westerlies - Pacific Subarctic Gyres Province (West)
7	PSAE	Westerlies - Pacific Subarctic Gyres Province (East)
8	NPPF	Westerlies - N. Pacific Polar Front Province
9	NPSW	Westerlies - N. Pacific Subtropical Gyre Province (West)
10	PNEC	Trades - N. Pacific Equatorial Countercurrent Province
11	PEQD	Trades - Pacific Equatorial Divergence Province
12	SPSG	Westerlies - S. Pacific Subtropical Gyre Province
13	ARAB	Coastal - NW Arabian Upwelling Province
14	MONS	Trades - Indian Monsoon Gyres Province

Figure 4. Map of Longhurst provinces (Reygondeau et al., 2013) used in analysis of biological pump field observations and model results (Mouw et al., 2016a).

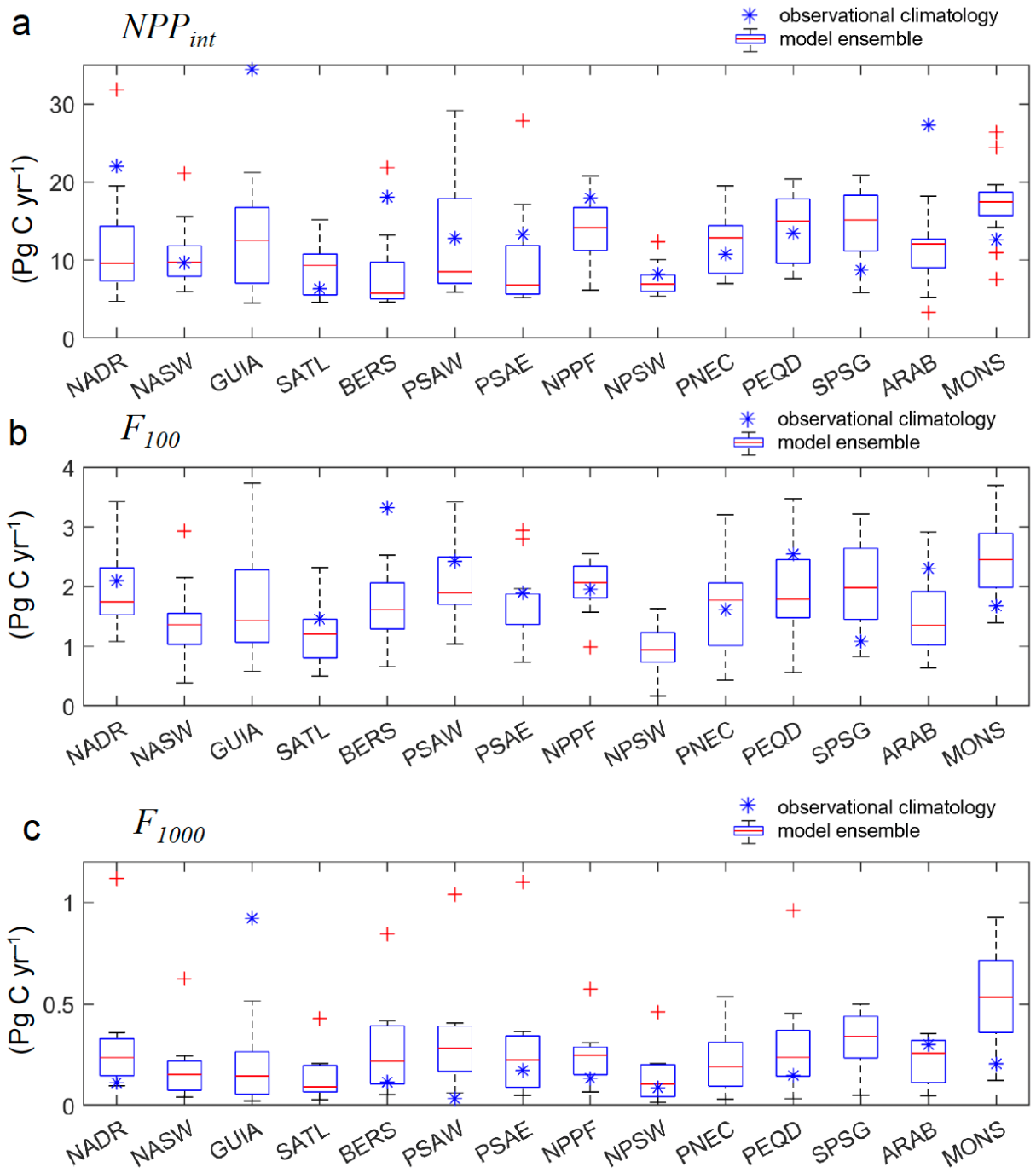

Figure 5. Box-whisker plot of RECCAP2 multi-model ensemble medians, interquartile ranges, and outliers for annual-mean (a) vertical integrated primary production (NPP_{int}), (b) sinking POC fluxes at 100m (F_{100}), and (c) sinking POC flux at 1000m (F_{1000}), all in Pg C yr^{-1}, pooled into biogeochemical Longhurst ocean provinces (Figure 4) and compared to the observational climatology for the same provinces constructed by Mouw et al. (2016b). Robust uncertainty estimates are not available for the observational climatology which averages available data that is

often spatially sparse and/or concentrated in brief time intervals. Note that only provinces with sufficient observational data are plotted (see Figure 4).

The biological carbon pump model comparison to observation-based estimates was extended in Figure 5 to a regional level using the observational data of Mouw et al. (2016a) as aggregated by Mouw et al. (2016b) into monthly climatological values for Longhurst biogeographic provinces (Figure 4). The Mouw et al. (2016a) date set aggregates the limited available field data that is often spatially sparse and locally high frequency with considerable mesoscale variability, some of which may be aliased into monthly and province scale averages. Therefore, robust uncertainty estimates are not available for the Mouw et al. (2016b) observational climatology. The variations across the RECCAP2 models are displayed as box-whisker plots. The members of the model ensemble exhibited a wide range of NPP, F_{100} and F_{1000} values for many provinces, but still the observational climatology falls within the multi-model ensemble inter-quartiles for only about half of the provinces. The substantial model-observational offsets indicate recurring regional differences consistent across multiple models in the RECCAP2 ensemble; these disagreements could be targets for future ocean biogeochemical model development and analyses of observational sampling biases. The model ensemble members also exhibited extreme model-data differences in some provinces where the observational climatology value falls outside the simulated range including model outliers. The RECCAP2 models consistently underestimated the strength of biological carbon pump metrics, relative to the observational climatology, in polar and sub-polar provinces in the North Pacific (N. Pacific epicontinental sea, BERS, low NPP and F_{100}) and North Atlantic (N. Atlantic Drift, NADR, low NPP); and in equatorial provinces in the Indian (Northwest Arabian Sea upwelling, ARAB, low NPP), Pacific (Trades-Pacific Equatorial Divergence, PEQD, low F_{100}) and Atlantic (Guianas coast, GUIA, low F_{1000}; note, the observed high Guianas coast value reflects a small, productive region that may not be well represented in global-scale models). In other provinces, the model ensemble overestimated the biological pump in the South Pacific gyre (SPSG, high NPP and F_{100}), Indian monsoon gyre (MONS, high NPP and F_{100}), and Western Pacific subarctic gyres (PSAW, high F_{1000}).

3.3 Biological pump imprint on ocean CO_2 system and biogeochemistry

The ocean biological carbon pump imprints on surface and sub-surface biogeochemistry (see Introduction), and these effects are simulated in the RECCAP2 models. A strong positive mesopelagic AOU signal is generated by cumulative biological O_2 consumption along the ventilation paths of subsurface waters (Najjar et al., 2007). AOU fields thus integrate non-local, large-scale biogeochemical dynamics and physical resupply of O_2 from the surface. A key contributor to AOU is the remineralization of sinking POC flux in the mesopelagic, quantified by the large decline between F_{100} and F_{1000} and low transfer efficiency through the mesopelagic $E_{1000/100}$ (Figures 1–3; Tables 3 and 4). For the RECCAP2 model ensemble, there was generally good model-data agreement in the geographic pattern in AOU averaged over the mesopelagic (100–1000 m) (Figure 6). The model ensemble captured the regional AOU variation of <50 to >250 μmol kg^{-1}, though substantial disagreement arose on the scale of Longhurst provinces where the model-ensemble interquartile spans the observational data for only a handful of provinces (Figure 6c). The RECCAP2 models did not exhibit a strong inter-model relationship between global mean AOU and F_{100} (not shown). The weak relationship between AOU and F_{100} across models likely highlights the influence on AOU of substantial variations in the strength of model

thermocline ventilation rates that could also influence simulated anthropogenic CO_2 uptake (e.g., Dutay et al., 2002; Matsumoto et al., 2004). Model deep-ocean AOU was not evaluated because model spin-up time scales were too short for the simulations to reach steady-state (Séférian et al., 2019), an issue that also would affect simulated deep-ocean preindustrial DIC (Mikaloff Fletcher et al., 2007). Some imprint of the observational fields used for model initial conditions could also be retained in the simulated mesopelagic AOU depending on the model spin-up procedure.

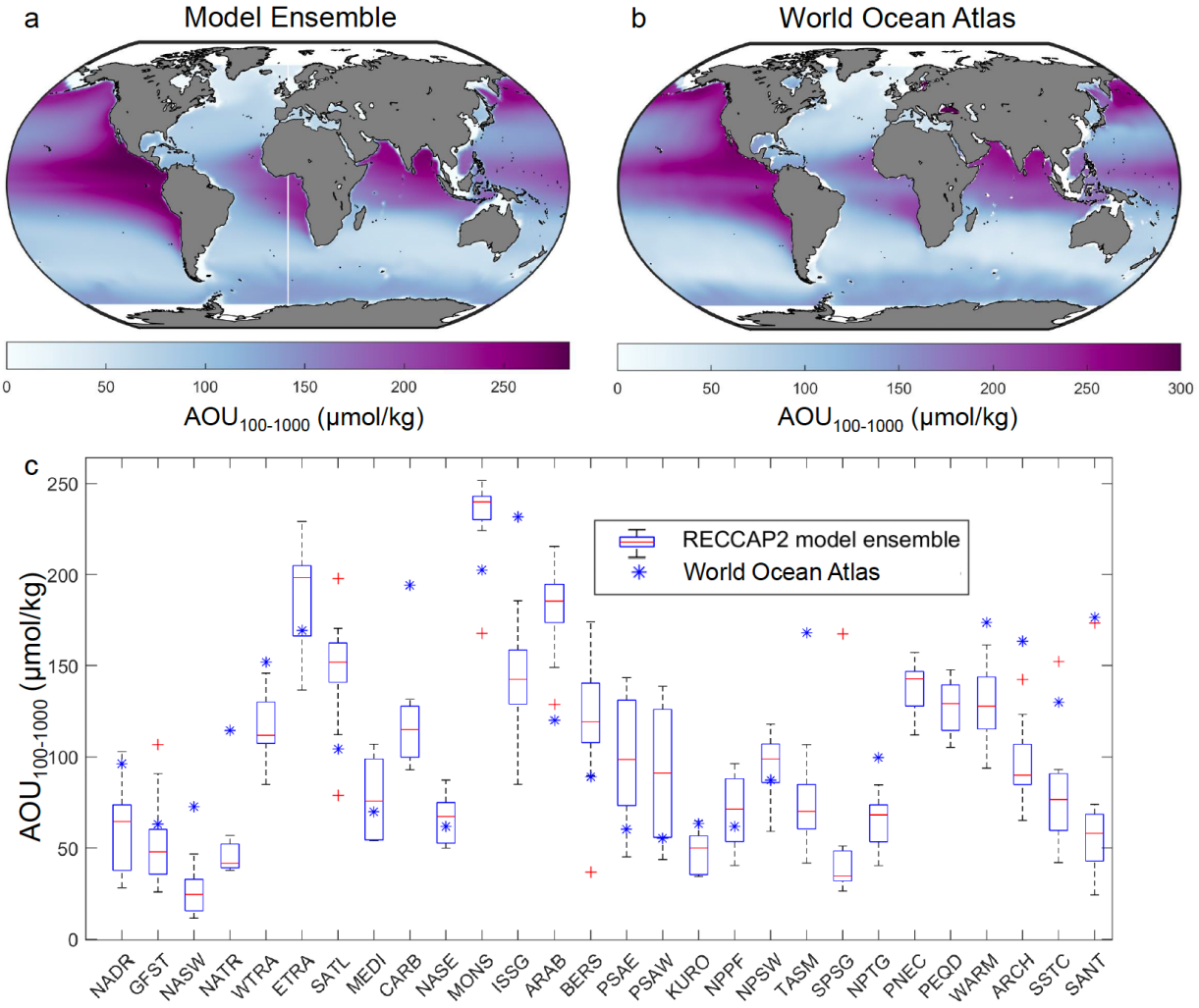

Figure 6. Analysis of apparent oxygen utilization (AOU, µmol kg^{-1}) vertically averaged over the mesopelagic zone (100-1000 m): (a) spatial map of RECCAP2 multi-model ensemble average, and (b) spatial map from WOA observational data set, and (c) box-whisker plot of RECCAP2 multi-model ensemble medians, interquartile ranges, and outliers pooled into biogeochemical Longhurst ocean provinces (Figure 4).

The simulated regional patterns and global integrated surface POC export F_{100} (Figures 1–3; Tables 3 and 4) must be balanced on appropriate time and space scales by new production and external nutrient supply, largely from physical upwelling and mixing for most ocean regions

(Ducklow and Doney, 2013). As an indicator of physical controls on export associated with nutrient supply, the individual RECCAP2 model, global-integrated F_{100} values exhibited a positive correlation with global-ocean anthropogenic CO_2 uptake (Figure 7) (DeVries et al., 2023). This is consistent with findings from previous model intercomparison exercises where models with stronger thermocline ventilation had both larger export flux and anthropogenic CO_2 uptake (Najjar et al., 2007). The F_{100}–anthropogenic CO_2 uptake correlation, therefore, is indirect through a common underlying physical mechanism whereby stronger ventilation enhances both the downward transport of anthropogenic CO_2 correlation and the upward transport of nutrients and thus F_{100}. The physical-chemical solubility mechanisms controlling ocean anthropogenic CO_2 uptake are well documented, and there is no evidence of any significant role for biogeochemical processes, though climate-change biogeochemical feedbacks on ocean carbon storage may become more important in the future (Canadell et al., 2021).

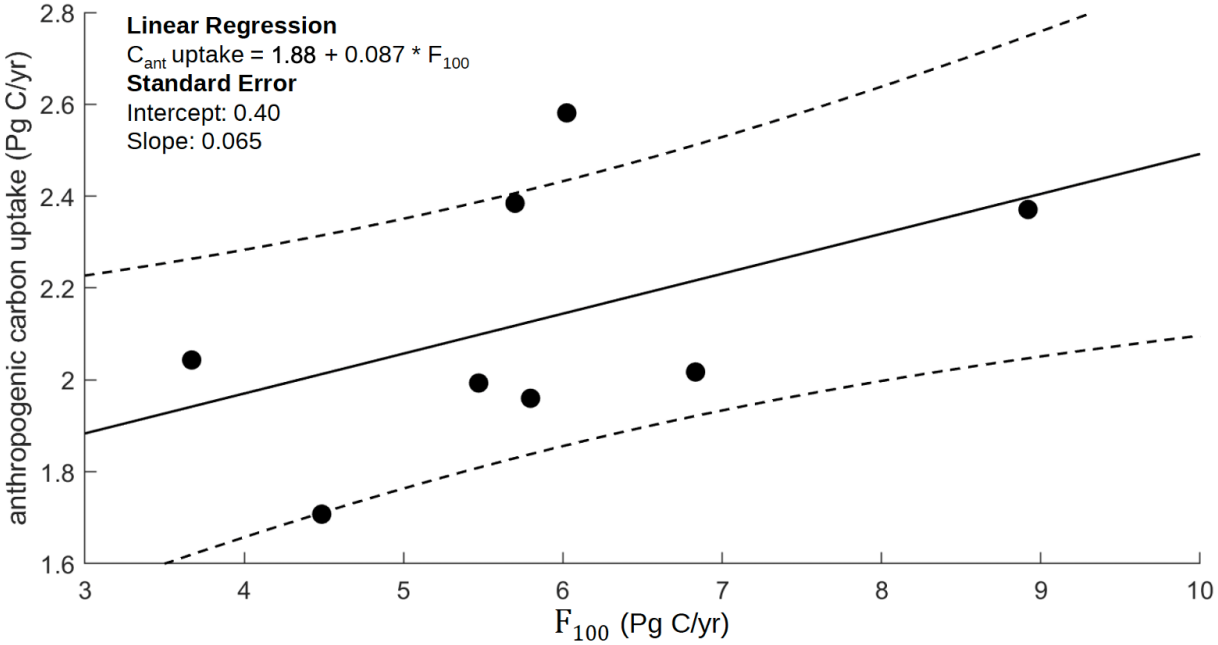

Figure 7. Scatter plot of global-integrated ocean anthropogenic CO_2 uptake (mean of 1985-2018) (Pg C yr^{-1}) versus particulate organic carbon (POC) export flux (F_{100}, Pg C yr^{-1}) for individual RECCAP2 models. Anthropogenic CO_2 uptake for the same RECCAP2 models was taken from DeVries et al. (2023) A linear regression and confidence intervals for the regression are overlain. The F_{100}–anthropogenic CO_2 uptake correlation was indirect through a common underlying physical mechanism whereby stronger ventilation enhances both the downward transport of anthropogenic CO_2 correlation and the upward transport of nutrients and thus F_{100}.

Seasonal variations in upper-ocean biogeochemistry were used as a metric of the physical controls associated with seasonal mixing and nutrient supply, which are reflected in simulated POC export. By correcting for seasonal thermal variations in pCO_2 (Equation 3), we used model monthly pCO_2 fields to quantify the combined effects of seasonal biogeochemical, gas-exchange and physical processes through the seasonal amplitude of non-thermal pCO_2, $\Delta pCO_{2,\text{non-thermal}}$ (Takahashi et al., 2002). The geographic pattern of $\Delta pCO_{2,\text{non-thermal}}$ from the RECCAP2 model

599 ensemble was similar to the pattern from the mean of the pCO_2 observational products (Figure 8a
600 and 8b). Both the model ensemble and observational products exhibited regional variations of
601 $\Delta pCO_{2,non\text{-}thermal}$ that ranged from 30 to >150 μatm with elevated values in mid- to high latitudes
602 as well as equatorial and eastern boundary current upwelling regions. However, the magnitude of
603 $\Delta pCO_{2,non\text{-}thermal}$ in the model ensemble was considerably lower in the mid- to high latitude northern
604 hemisphere, eastern tropical Pacific, and Brazil-Malvinas convergence region, suggesting a
605 generally weaker modeled seasonal cycling of DIC. The same low bias in the RECCAP2 models
606 was evident on the scale of Longhurst provinces where the observational products fell at the top
607 end or well above the model-ensemble interquartile (Figure 8c). In many ocean regions, strong
608 seasonality in mixed layer depth modulates vertical nutrient supply and annual-mean biological
609 productivity. The weaker model ensemble $\Delta pCO_{2,non\text{-}thermal}$ values (Figure 8), therefore, may be
610 linked to regional patterns of lower NPP and F_{100} relative to observations (Figure 5) in the North
611 Pacific (BERS province), North Atlantic (NADR province), eastern equatorial Pacific (PEQD),
612 and Brazil-Malvinas convergence (western part of SATL province).
613

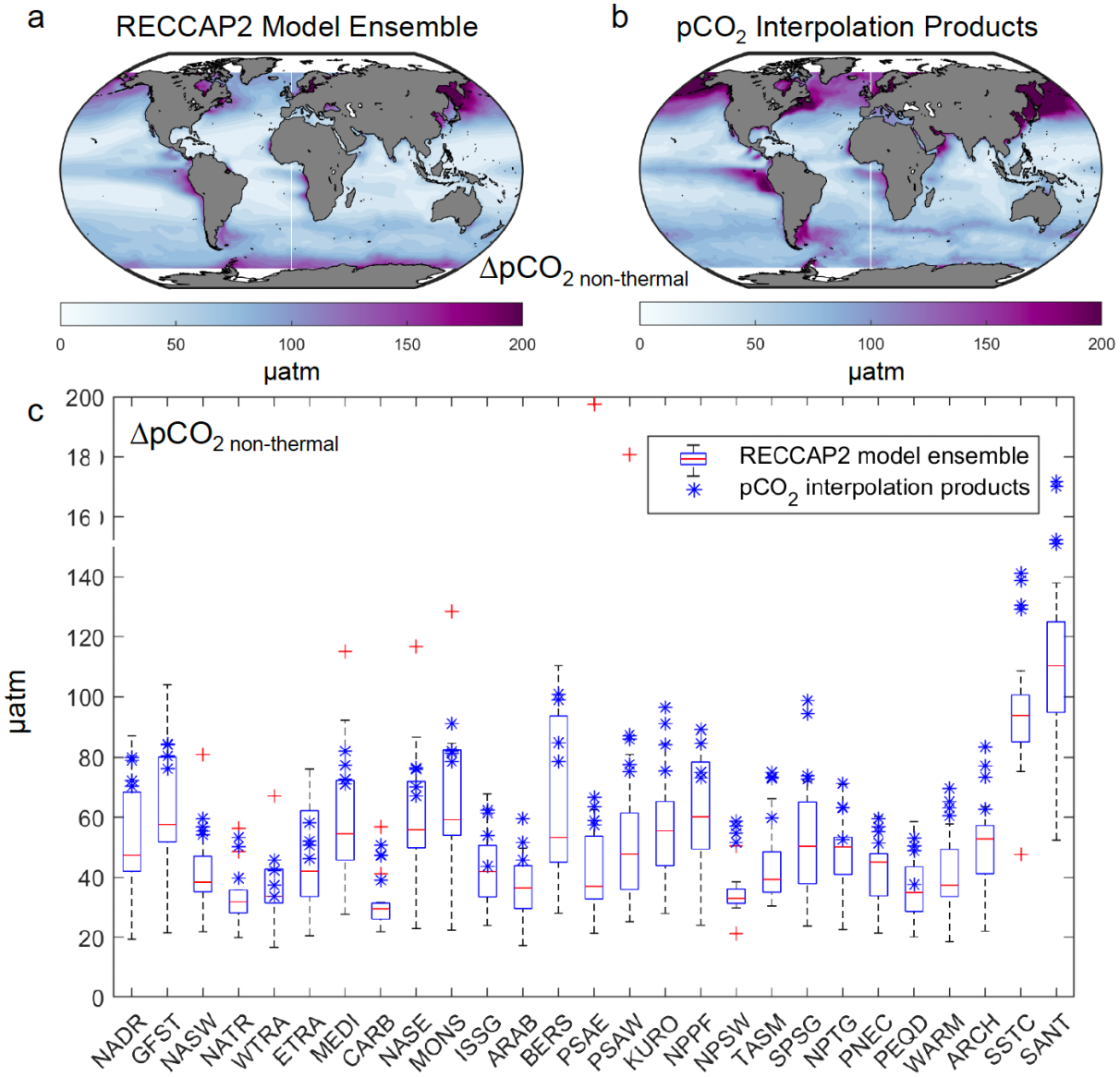

Figure 8. Analysis characterizing the combined effects of seasonal biogeochemical, gas-exchange and physical processes using the seasonal amplitude of non-thermal $\Delta pCO_{2_{non-thermal}}$ (a) spatial map of RECCAP2 multi-model ensemble average, (b) spatial map from pCO_2 observational data products, and (c) box-whisker plot of RECCAP2 multi-model ensemble medians, interquartile ranges, and outliers pooled into biogeochemical Longhurst ocean provinces (Figure 4). The province means from each observational product are plotted in panel (c) as individual points rather than as box-whiskers because of the limited number of observational products.

4 Discussion and Conclusions

Our analysis of the ocean biological carbon pump fields from the RECCAP2 multi-model ensemble revealed generally encouraging agreement with many aspects of observed patterns.

Global-integrated NPP and surface export flux (F_{100}) from the RECCAP2 models tended to fall at the lower end of observational estimates (Figure 3 and Table 4), and geographic patterns in NPP were generally consistent with observational data products (Figures 1 and 5). Similar to previous model intercomparison studies (Laufkötter et al., 2015; Laufkötter et al., 2016), we found substantial within-ensemble variation in global biological carbon pump metrics, including the presence of model outliers (Figure 3), indicating that these aspect of biogeochemical models have not necessarily converged with time.

Regional patterns in the RECCAP2 model-mean ensemble included elevated NPP, surface export flux (F_{100}) and export efficiency (E_{100}) in high-latitudes and coastal and equatorial upwelling regions, with lower values in more oligotrophic regions. These results are in line with previous studies that found that a substantial proportion of NPP in nutrient-rich regions is driven by large phytoplankton such as diatoms and, combined with an active zooplankton population, this can generate a significant export flux in the form of both dense aggregates and fecal pellets. High-latitude elevated biomass, colder temperatures (Dunne et al., 2005), and strong seasonality also have been implicated in observations of higher POC export fluxes in spring and/or summer months contributing to the annual mean (Buesseler et al., 2001; Lampitt et al., 2001; Bol et al., 2018; Henson et al., 2023). In low nutrient regimes, such as the lower latitude oligotrophic gyres, previous studies report export flux to be low (Henson et al., 2012) but relatively constant throughout the year with small seasonal increases in fluxes (Karl et al., 2012). Future studies of the RECCAP2 ensemble could investigate in more detail the seasonality in NPP, F_{100}, and E_{100}, exploring, for example, the seasonal variability in export ratio that can be substantial due in part to the time lag between NPP and export flux (Henson et al., 2015; Giering et al., 2017; Laws and Maiti, 2019; Henson et al., 2015).

The sinking POC flux into the deep ocean (F_{1000}) and mesopelagic transfer efficiency across the mesopelagic zone ($E_{1000/100}$) in the RECCAP2 multi-model ensemble (Figures 1 and 5) exhibited different spatial patterns than found for surface export, similar to findings of previous studies (e.g., Henson et al., 2012). Simulated F_{1000} and $E_{1000/100}$ were greater in the tropical eastern Pacific, eastern Atlantic, and Arabian Sea, and $E_{1000/100}$ was also elevated in the western tropical North Atlantic and, to a lesser extent, Southern Ocean. Previous model studies have also found substantial regional variations due to particle size and composition effects (Lima et al., 2014) that modify empirical power curves used for modeling POC sinking and remineralization (Martin et al., 1987). Model parameterizations tend to increase the effective remineralization length scales and thus transfer to depth in regions with high mineral fluxes (e.g., dust, $CaCO_3$, silica) (Armstrong et al., 2002) or in tropical oxygen minimum zones (Laufkötter et al., 2017; Dinauer et al., 2022). The RECCAP2 regional variations in mesopelagic transfer efficiency, modulated with basin-scale variations in physical circulation-driven sequestration time-scale (Siegel et al., 2021), influence the effect of the biological pump on ocean carbon storage (Kwon et al., 2009).

While we focused primarily on long-term mean NPP and export fluxes, the RECCAP2 models also exhibited year-to-year variability (Table S1), though typically much lower than within-ensemble model differences (Figure 2), and small long-term temporal trends (Table S2). No consistent positive or negative trend was observed across the models in simulated NPP and sinking POC fluxes at 100m and 1000m, with NPP trends of order ±0.01 Pg C yr^{-1}/year over the 33 years of the time series (1985-2018). Although these trends could contain a signal from climate change, the relatively short duration of the RECCAP2 analysis period resulted in large signal to noise due to interannual variability. Previous modeling studies indicate that chlorophyll and NPP

time series of 30-40 years length are needed to distinguish climate change trends from natural variability (Henson et al., 2010). Hence, the RECCAP2 analysis period may indeed not be long enough to separate trends from interannual variability. While a recent study suggests that climate-change trends can emerge more rapidly in ocean color remote-sensing reflectance (Cael et al., 2023), any actual climate change signal in models may be masked by temporal biases associated with incomplete model spin-up and resulting temporal drift (Séférian et al., 2016).

Our analysis of the biological carbon pump was relevant in several ways to the primary focus of the RECCAP2 ocean project on air-sea CO_2 fluxes and ocean uptake of anthropogenic CO_2 (DeVries et al., 2023). Biological net CO_2 uptake and carbon export modulate the background, pre-industrial and contemporary spatial and seasonal patterns of surface ocean pCO_2 and sea-air CO_2 flux that must be accounted for to determine anthropogenic CO_2 perturbations. The low model F_{100} values globally (Figure 3) and for mid- to high-latitude Northern Hemisphere and eastern equatorial Pacific provinces (Figure 5), relative to observations, suggested that the RECCAP2 model ensemble may have underestimated biological CO_2 drawdown in high productivity regions. Potential issues were also identified in simulated seasonal biogeochemical, gas-exchange and physical dynamics as captured in the seasonal amplitude of non-thermal pCO_2 variations, with weaker $\Delta pCO_{2,\text{non-thermal}}$ values found at mid- to high-latitudes and in the eastern equatorial Pacific in the model ensemble relative to observations (Figure 8). Future work with more detailed model diagnostics could explore the connections between regional biases in simulated annual-mean and seasonal export production and biases in air-sea CO_2 flux as observed in other RECCAP2 studies (DeVries et al., 2023; Hauck et al., 2023).

Ocean circulation modulates biological export flux on basin to global scales (Najjar et al., 2007), and the range in RECCAP2 global-integrated F_{100} values indicated that substantial differences exist in simulated ocean physics within the RECCAP2 marine biogeochemical models (Doney et al., 2004). The same ocean circulation variations also likely influenced the anthropogenic CO_2 uptake estimates from DeVries et al. (2023) as indicated by the positive correlation between anthropogenic CO_2 uptake and F_{100} across individual RECCAP2 models (Figure 7). This is supported by further analysis of the RECCAP2 models demonstrating that the rate of ocean overturning circulation is strongly correlated with anthropogenic CO_2 uptake in the models (Terhaar et al., 2023). Variations in model export could also be compared against metrics of physical stratification (Fu et al., 2022). The substantial inter-model spread in both physical and biogeochemical metrics likely reflects common factors resulting from differences in simulated thermocline ventilation and exchange between the surface and mid-depth ocean.

A set of additional model development recommendations emerge from our analyses. One path forward would leverage independent model skill evaluation for inert chemical tracers (e.g., CFC-11, CFC-12, SF_6) using standard ocean model intercomparison protocols (e.g., CMIP6 Ocean Model Intercomparison Project; Orr et al., 2017). The transient tracer simulations would help decipher the physical-biological factors controlling simulated AOU (Figure 6). Remineralization of sinking biological organic matter structures sub-surface ocean dissolved inorganic carbon, O_2, and nutrient fields, a signal that must be addressed in observational estimates of anthropogenic CO_2. While the predominant pathway for ocean anthropogenic CO_2 uptake involves physical-chemical dynamics, rather than biological dynamics, the same physical circulation and mixing processes influence biogeochemical rates such as nutrient supply. Therefore, evaluation and improvement of the ocean biological pump may provide additional insight.

716 The substantial variation in biological pump metrics shown here highlighted the need to
717 reconcile inter-model and model-observational differences. Challenges arise for model
718 improvement because there is limited agreement on the appropriate parameterizations for many
719 key processes of biological carbon export (Henson et al., 2022), subsurface particle sinking, and
720 remineralization. Many global models include detailed representation of euphotic zone processes
721 but rather more simplistic representation of mesopelagic processes. Thus, the simulated global-
722 scale biological carbon pump responses to interannual variability, let alone decadal climate
723 change, remain poorly constrained (Henson et al., 2016). Following the mechanistic approach
724 reported in previous model intercomparison studies for primary production (Laufkötter et al.,
725 2015) and export production (Laufkötter et al., 2016), future studies could emphasize how overall
726 model behavior reflects differences in model parameterizations, functional equations, and
727 parameter values in both the euphotic and mesopelagic zones.

728 Opportunities exist to leverage process-level information from lab and field studies to
729 improve model treatment of POC production, sinking POC flux and extension of export pathways
730 beyond POC gravitational sinking, for example physical subduction and active migration by
731 organisms (Boyd et al., 2019; Siegel et al., 2016; Henson et al., 2022; Siegel et al., 2023).
732 Phytoplankton community structure, captured to some degree in many models, influences
733 magnitude and composition of export flux from the euphotic zone, the heterotrophic consumers of
734 sinking POC and zooplankton community structure (Boyd and Newton, 1995; Cavan et al., 2019).
735 Model treatments could be improved for grazers, such as zooplankton, that act to decrease particle
736 flux by consuming phytoplankton and sinking POC, while also increasing flux by packaging POC
737 into fecal pellets with a wide range of sinking speeds (Turner, 2015; Steinberg and Landry, 2017).
738 Grazer diel vertical migration may also need to be incorporated as a carbon shunt below the depth
739 horizons of most intense heterotrophic activity (i.e., upper mesopelagic zone), consuming POC in
740 the surface ocean and respiring it at grazer resident daytime depth (Bianchi et al., 2013). More
741 mechanistic treatment of particle dynamics may also be feasible. Particle disaggregation,
742 physically through shear or biologically through fragmentation by grazers, likely contributes
743 substantially to the decline in POC flux with depth while also providing a POC source for
744 mesopelagic microbes (Laurenceau-Cornec et al., 2020; Briggs et al., 2020). Microbes also can
745 reduce POC flux directly, as they constantly attach and detach from sinking POC (Kiørboe et al.,
746 2002; Kiørboe et al., 2003), hydrolyzing and respiring the POC. While variable particle sinking
747 speed is included in some model parameterizations, large meta-analyses of empirical data have
748 struggled to find a strong link between sinking rate and size of particles, because of the vast
749 variability in particle type, methods used to measure sinking rate, and environment the particles
750 were collected from (Cael et al., 2021).

751 Many of these process-level insights are already driving progress on mechanistic
752 parameterizations for sinking particle flux (e.g., Dinauer et al., 2022), vertical migration (e.g.,
753 Archibald et al., 2019), and other key factors in the marine biological pump. Together with global-
754 scale ocean biogeochemical data compilations and syntheses (e.g., Mouw et al., 2016a; Mouw et
755 al., 2016b, Clements et al., 2023) there are now promising new opportunities to evaluate, constrain,
756 and improve ocean biological carbon pump simulations. Based on the model-data analysis
757 presented here, the RECCAP2 multi-model ensemble exhibited relatively good agreement with
758 observed biological carbon pump metrics, where there is sufficient data. The analysis also
759 identified model-data biases and substantial differences among some of the models included in
760 RECCAP2. These biases should be used to guide directions for future model development.

Funding

S.C. Doney and K.A. Mitchell acknowledge support from the U.S. National Science Foundation via the Center for Chemical Currencies of a Microbial Planet (NSF 2019589). S.A. Henson received support from a European Research Council Consolidator grant (GOCART, agreement number 724416). S. Henson and J. Hauck received support from the European Union's Horizon 2020 research and innovation programme under grant agreement no. 820989 (COMFORT), and the European Union's Horizon Europe research and innovation programme under grant agreement no. 101083922 (OceanICU). Funding to J. Hauck was provided by the Initiative and Networking Fund of the Helmholtz Association (Helmholtz Young Investigator Group Marine Carbon and Ecosystem Feedbacks in the Earth System, MarESys, Grant VH-NG-1301). J.D. Müller and N. Gruber acknowledge support from the European Union's Horizon 2020 research and innovation programme under grant agreement no. 821003 (project 4C) and no. 820989 (project COMFORT). T. DeVries acknowledges support from NSF grant OCE-1958955. E.L. Cavan was funded by an Imperial College Research Fellowship.

Acknowledgements

Conceptualization (Ideas; formulation or evolution of overarching research goals and aims): S.C.D, S.A.H.

Data curation (Management activities to annotate (produce metadata), scrub data and maintain research data (including software code, where it is necessary for interpreting the data itself) for initial use and later re-use): K.A.M, J.D.M.

Formal analysis (Application of statistical, mathematical, computational, or other formal techniques to analyze or synthesize study data): S.C.D., K.A.M., S.A.H.

Funding acquisition (Acquisition of the financial support for the project leading to this publication): S.C.D, S.A.H.

Investigation (Conducting a research and investigation process, specifically performing the experiments, or data/evidence collection): All co-authors

Methodology (Development or design of methodology; creation of models): S.C.D., K.A.M., S.A.H.

Project administration (Management and coordination responsibility for the research activity planning and execution): S.C.D., S.A.H., J.D.M.

Software (Programming, software development; designing computer programs; implementation of the computer code and supporting algorithms; testing of existing code components): K.A.M., J.D.M.

Supervision (Oversight and leadership responsibility for the research activity planning and execution, including mentorship external to the core team): S.C.D, S.A.H., J.D.M.

Visualization (Preparation, creation and/or presentation of the published work, specifically visualization/data presentation): S.C.D., K.A.M.

Writing – original draft (Preparation, creation and/or presentation of the published work, specifically writing the initial draft (including substantive translation)): S.C.D., K.A.M., S.A.H., E.C.

Writing – review and editing (Preparation, creation and/or presentation of the published work by those from the original research group, specifically critical review, commentary or revision – including pre- or post-publication stages): All co-authors

Open Research

The RECCAP2 ocean data collection can be found in Müller (2023).

Müller, Jens Daniel. (2023). RECCAP2-ocean data collection [Data set]. Zenodo. 1631 https://doi.org/10.5281/zenodo.7990823

References

Archibald, K., Siegel, D. A., & Doney, S. C. (2019) Modeling the impact of zooplankton diel vertical migration on the carbon export flux of the biological pump. *Global Biogeochemical Cycles*, *33*, 181–199. https://doi.org/10.1029/2018GB005983

Armstrong, R. A., Lee, C., Hedges, J. I., Honjo, S., & Wakeham, S. G. (2001). A new, mechanistic model for organic carbon fluxes in the ocean based on the quantitative association of POC with ballast minerals, *Deep Sea Research Part II*, *49*, 219–236. https://doi.org/10.1016/S0967-0645(01)00101-1

Aumont, O., Ethé, C., Tagliabue, A., Bopp, L., & Gehlen, M. (2015). PISCES-v2: An ocean biogeochemical model for carbon and ecosystem studies. *Geoscientific Model Development, 8*, 2465–2513. https://doi.org/10.5194/gmd-8-2465-2015

Bacastow, R., & Maier-Reimer, E. (1990). Ocean-circulation model of the carbon cycle. *Climate Dynamics*, *4*, 95–125. https://doi.org/10.1007/BF00208905

Behrenfeld, M. J., & Falkowski, P. G. (1997). Photosynthetic rates derived from satellite-based chlorophyll concentration. *Limnology and Oceanography*, *42*, 1–20. https://doi.org/10.4319/lo.1997.42.1.0001

Behrenfeld, M. J., Boss, E., Siegel, D. A., & Shea, D. M. (2005). Carbon-based ocean productivity and phytoplankton physiology from space, *Global Biogeochemical Cycles*, *19*, GB1006. https://doi.org/10.1029/2004GB002299.

Berthet, S., Séférian, R., Bricaud, C., Chevallier, M., Voldoire, A., & Ethé, C. (2019). Evaluation of an online grid-coarsening algorithm in a global eddy-admitting ocean-biogeochemical model. *Journal of Advances in Modeling Earth Systems*, *11*(6), 1759–1783. https://doi.org/10.1029/2019ms001644

Bianchi, D., Stock, C., Galbraith, E. D., & Sarmiento, J. L. (2013). Diel vertical migration: Ecological controls and impacts on the biological pump in a one-dimensional ocean model. *Global Biogeochemical Cycles*, *27*, 478–491. https://doi.org/10.1002/gbc.20031

Bol, R., Henson, S. A., Rumyantseva, A., & Briggs, N. (2018). High-frequency variability of small-particle carbon export flux in the Northeast Atlantic. Global Biogeochemical Cycles, 32, 1803–1814. https://doi.org/10.1029/2018GB005963

Boyd, P., & Newton, P. (1995). Evidence of the potential influence of planktonic community structure on the interannual variability of particulate organic carbon flux, Deep Sea Research Part I, 42, 619–639. https://doi.org/10.1016/0967-0637(95)00017-Z

Boyd, P.W., Claustre, H., Levy, M., Siegel, D. A., & Weber, T. (2019). Multi-faceted particle pumps drive carbon sequestration in the ocean. *Nature*, *568*, 327–335. https://doi.org/10.1038/s41586-019-1098-2

Briggs, N., Dall'Olmo, G., & Claustre, H. (2020). Major role of particle fragmentation in regulating biological sequestration of CO_2 by the oceans, *Science*, *367*, 791–793. https://doi.org/10.1126/science.aay1790

Broecker, W. S. and T. H. Peng (1982). *Tracers in the Sea*, Eldigio Press, Palisades, NY, 690 pp. https://www.ldeo.columbia.edu/~broecker/Home_files/TracersInTheSea_searchable.pdf

Buesseler, K. O., Ball, K. O. L., Andrews, J., Cochran, J. K., Hirschberg, D. J., Bacon, M. P., et al. (2001). Upper ocean export of particulate organic carbon and biogenic silica in the Southern Ocean along 170°W, *Deep Sea Research Part II*, *48*, 4275–4297. https://doi.org/10.1016/S0967-0645(01)00089-3

Burd, A. B. (2024). Modeling the vertical flux of organic carbon in the global ocean, *Annual Review of Marine Science*, *16*, 135–161, https://doi.org/10.1146/annurev-marine-022123-102516

Cael, B. B., Cavan, E. L., & Britten, G. L. (2021). Reconciling the size-dependence of marine particle sinking speed. *Geophysical Research Letters*, *48*, e2020GL091771. https://doi.org/10.1029/2020GL091771

Cael, B. B., Bisson, K., Boss, E., Dutkiewicz, S., & Henson. S. (2023). Global climate-change trends detected in indicators of ocean ecology. *Nature*, *619*, 551–554. https://doi.org/10.1038/s41586-023-06321-z

Canadell, J. G., Monteiro, P. M. S., Costa, M. H., Cotrim da Cunha, L., Cox, P. M., Eliseev, A. V., et al. (2021). Global Carbon and other Biogeochemical Cycles and Feedbacks. In Climate Change 2021: The Physical Science Basis. Contribution of Working Group I to the Sixth Assessment Report of the Intergovernmental Panel on Climate Change [Masson-Delmotte, V., P. Zhai, A. Pirani, S.L. Connors, C. Péan, S. Berger, N. Caud, Y. Chen, L. Goldfarb, M.I. Gomis, M. Huang, K. Leitzell, E. Lonnoy, J.B.R. Matthews, T.K. Maycock, T. Waterfield, O. Yelekçi, R. Yu, and B. Zhou (eds.)]. Cambridge University Press, Cambridge, United Kingdom and New York, NY, USA, pp. 673–816. https://doi.org/10.1017/9781009157896.007

Carroll, D., Menemenlis, D., Adkins, J. F., Bowman, K. W., Brix, H., Dutkiewicz, S., et al. (2020). The ECCO-Darwin data-assimilative global ocean biogeochemistry model: Estimates of

seasonal to multidecadal surface ocean pCO_2 and air-sea CO_2 flux. *Journal of Advances in Modeling Earth Systems*, *12*(10), e2019MS001888.

Carroll, D., Menemenlis, D., Dutkiewicz, S., Lauderdale, J. M., Adkins, J. F., Bowman, K. W., et al. (2022). Attribution of space-time variability in global-ocean dissolved inorganic carbon. *Global Biogeochemical Cycles*, *36*(3), e2021GB007162.

Carr, M. E. (2002). Estimation of potential productivity in Eastern Boundary Currents using remote sensing, *Deep Sea Research Part II*, *49*(1–3), 59–80.

Carr, M., Friedrichs, M., Schmeltz, M., Noguchiaita, M., Antoine, D., Arrigo, K., & et al. (2006). A comparison of global estimates of marine primary production from ocean color. *Deep-Sea Research Part II*, *53*, 741–770. https://doi.org/10.1016/j.dsr2.2006.01.028

Cavan, E. L., Laurenceau-Cornec, E. C., Bressac, M., Boyd, P. W. (2019). Exploring the ecology of the mesopelagic biological pump. *Progress in Oceanography*, *176*, 102125. https://doi.org/10.1016/j.pocean.2019.102125

Chau, T. T. T., Gehlen, M., & Chevallier, F. (2022). A seamless ensemble-based reconstruction of surface ocean pCO_2 and air–sea CO_2 fluxes over the global coastal and open oceans. *Biogeosciences*, *19*(4), 1087–1109. https://doi.org/10.5194/bg-19-1087-2022

Clements, D. J., Yang, S., Weber, T., McDonnell, A. M. P., Kiko, R., Stemmann, L., Bianchi, D. (2023). New estimate of organic carbon export from optical measurements reveals the role of

particle size distribution and export horizon. *Global Biogeochemical Cycles*, *37*, e2022GB007633. https://doi.org/10.1029/2022GB007633

Cram, J. A., Weber, T., Leung, S. W., McDonnell, A. M. P., Liang, J.-H., & Deutsch, C. (2018). The role of particle size, ballast, temperature, and oxygen in the sinking flux to the deep sea. *Global Biogeochemical Cycles*, *32*, 858–876. https://doi.org/10.1029/2017GB005710

Crisp, D., Dolman, H., Tanhua, T., McKinley, G. A., Hauck, J., Bastos, A., et al. (2022). How well do we understand the land-ocean-atmosphere carbon cycle? *Reviews of Geophysics*, *60*, e2021RG000736. https://doi.org/10.1029/2021RG000736

DeVries, T., (2022). The ocean carbon cycle, *Annual Review of Environment and Resources*, *47*, 317–341. https://doi.org/10.1146/annurev-environ-120920-111307

DeVries, T., & Weber, T. (2017). The export and fate of organic matter in the ocean: New constraints from combining satellite and oceanographic tracer observations. *Global Biogeochemical Cycles*, *31*, 535–555. https://doi.org/10.1002/2016GB005551

DeVries, T., Le Quéré, C., Andrews, O., Berthet, S., Hauck, J., Ilyina, T., et al. (2019). Decadal trends in the ocean carbon sink. *Proceedings of the National Academy of Sciences*, *116*(24), 11646–11651. https://doi.org/10.1073/pnas.1900371116

DeVries, T., Yamamoto, K., Wanninkhof, R., Gruber, N., Hauck, J., Müller, J. D., et al. (2023). Magnitude, trends, and variability of the global ocean carbon sink from 1985-2018, *Global Biogeochemical Cycles*, *37* e2023GB007780. https://doi.org/10.1029/2023GB007780

Dinauer, A., Laufkötter, C., Doney, S. C., & Joos, F. (2022). What controls the large-scale efficiency of carbon transfer through the ocean's mesopelagic zone? Insights from a new, mechanistic model (MSPACMAM). *Global Biogeochemical Cycles*, *36*, e2021GB007131. https://doi.org/10.1029/2021GB007131

Doney, S. C., Lindsay, K., Caldeira, K., Campin, J.-M., Drange, H., Dutay, J. C., et al. (2004). Evaluating global ocean carbon models: The importance of realistic physics. *Global Biogeochemical Cycles*, *18*(3), GB3017. https://doi.org/10.1029/2003GB002150

Doney, S. C., Lindsay, K., Fung, I., J. John, J. (2006). Natural variability in a stable 1000 year coupled climate-carbon cycle simulation. *Journal of Climate*, *19*(13), 3033–3054. https://doi.org/10.1175/JCLI3783.1

Doney, S. C., Yeager, S., Danabasoglu, G., Large, W. G., McWilliams, J. C. (2007). Mechanisms governing interannual variability of upper ocean temperature in a global hindcast simulation. *Journal of Physical Oceanography*, *37*, 1918–1938. https://doi.org/10.1175/JPO3089.1

Doney, S. C., Lima, I., Feely, R. A., Glover, D. M., Lindsay, K., Mahowald, N., Moore, J. K., Wanninkhof, R. (2009): Mechanisms governing interannual variability in upper-ocean inorganic carbon system and air–sea CO_2 fluxes: Physical climate and atmospheric dust. *Deep Sea*

Research Part II: Topical Studies in Oceanography, *56*(8–10) 640–655. https://doi.org/10.1016/j.dsr2.2008.12.006

Döscher, R., Acosta, M., Alessandri, A., Anthoni, P., Arsouze, T., Bergman, T., et al. (2022). The EC-Earth3 Earth system model for the Coupled Model Intercomparison Project 6. *Geoscientific Model Development*, *15*(7), 2973–3020. https://doi.org/10.5194/gmd-15-2973-2022

Ducklow, H. W., & Doney, S. C. (2013). What is the metabolic state of the oligotrophic ocean? A debate. *Annual Review of Marine Science*, *5*, 525–533. https://doi.org/10.1146/annurev-marine-121211-172331

Dunne, J. P., Armstrong, R. A., Gnanadesikan, A., & Sarmiento, J. L. (2005). Empirical and mechanistic models for theparticle export ratio, *Global Biogeochemical Cycles*, *19*, GB4026. https://doi.org/10.1029/2004GB002390.

Dunne, J. P., Sarmiento, J. L., & Gnanadesikan, A. (2007). A synthesis of global particle export from the surface ocean and cycling through the ocean interior and on the seafloor. *Global Biogeochemical Cycles*, *21*, GB4006. https://doi.org/10.1029/2006GB002907

Dutay, J.-C., Bullister, J. L., Doney, S. C., Orr, J. C., Najjar, R., Caldeira, K., et al. (2002). Evaluation of ocean model ventilation with CFC-11: comparison of 13 global ocean models. *Ocean Modelling*, 4, 89–120. https://doi.org/10.1016/S1463-5003(01)00013-0

Falkowski, P. G., Barber, R. T., & Smetacek, V. (1998). Biogeochemical controls and feedbacks on ocean primary production. *Science*, *281*(5374), 200–206. https://doi.org/10.1126/science.281.5374.200

Fay, A. R., & McKinley, G. A. (2014). Global open-ocean biomes: mean and temporal variability. *Earth System Science Data*, *6*, 273–284. https://doi.org/10.5194/essd-6-273-2014.

Fennel, K., Mattern, J. P., Doney, S. C., Bopp, L., Moore, A. M., Wang, B., & Yu, L. (2022). Ocean biogeochemical modelling. *Nature Reviews Methods Primers*, *2*, 76. https://doi.org/10.1038/s43586-022-00154-2

Friedlingstein, P., O'Sullivan, M., Jones, M. W., Andrew, R. M., Gregor, L., Hauck, J., et al. (2022). Global carbon budget 2022. *Earth System Science Data*, *14*, 4811–4900. https://doi.org/10.5194/essd-14-4811-2022

Fu, W., Moore, J. K., Primeau, F., Collier, N., Ogunro, O. O., Hoffman, F. M., & Randerson, J. T. (2022). Evaluation of ocean biogeochemistry and carbon cycling in CMIP earth system models with the International Ocean Model Benchmarking (IOMB) software system. *Journal of Geophysical Research: Oceans*, *127*, e2022JC018965. https://doi.org/10.1029/2022JC018965

Garcia, H. E., Weathers, K., Paver, C. R., Smolyar, I., Boyer, T. P., Locarnini, R. A., et al. (2019). World Ocean Atlas 2018, Volume 3: Dissolved Oxygen, Apparent Oxygen Utilization, and

Oxygen Saturation. A. Mishonov Technical Ed., *NOAA Atlas NESDIS 83*, 38pp. https://www.ncei.noaa.gov/sites/default/files/2020-04/woa18_vol3.pdf

Giering, S., Sanders, R., Lampitt, R., Anderson, T. R., Tamburini, C., Boutrif, M., et al. (2014). Reconciliation of the carbon budget in the ocean's twilight zone. *Nature*, *507*, 480–483. https://doi.org/10.1038/nature13123

Giering, S. L. C., Sanders, R., Martin, A. P., Henson, S. A., Riley, J. S., Marsay, C. M., & Johns, D. G. (2017). Particle flux in the oceans: Challenging the steady state assumption, Global Biogeochemical Cycles, 31, 159–171. https://doi.org/10.1002/2016GB005424

Gloege, L., Yan, M., Zheng, T., & McKinley, G. A. (2022). Improved quantification of ocean carbon uptake by using machine learning to merge global models and pCO_2 data. *Journal of Advances in Modeling Earth Systems, 14*(2), e2021MS002620. https://doi.org/10.1029/2021ms002620

Glover, D. M., Jenkins, W. J., & Doney, S. C. (2011). *Modeling Methods for Marine Science*. Cambridge, United Kingdom: Cambridge University Press. https://doi.org/10.1017/CBO9780511975721

Gregor, L., & Gruber, N. (2021). OceanSODA-ETHZ: A global gridded data set of the surface ocean carbonate system for seasonal to decadal studies of ocean acidification. *Earth System Science Data*, *13*(2), 777–808. https://doi.org/10.5194/essd-13-777-2021

Gruber, N., Bakker, D.C.E., DeVries, T., Gregor, L., Hauck, J., Landschützer, P., McKinley, G. A., & Müller, J. D. (2023). Trends and variability in the ocean carbon sink. *Nature Reviews Earth and Environment*, *4*, 119–134. https://doi.org/10.1038/s43017-022-00381-x

Guidi, L., Legendre, L., Reygondeau, G., Uitz, J., Stemmann, L., & Henson, S. A. (2015). A new look at ocean carbon remineralization for estimating deep water sequestration. *Global Biogeochemical Cycles*, *29*, 1044–1059. https://doi.org/10.1002/2014GB005063

Hauck, J., Zeising, M., Le Quéré, C., Gruber, N., Bakker, D. C. E., Bopp, L., et al. (2020). Consistency and challenges in the ocean carbon sink estimate for the global carbon budget. *Frontiers in Marine Science*, *7*, 571720. https://doi.org/10.3389/fmars.2020.571720

Hauck, J., Gregor, L., Nissen, C., Patara, L., Hague, M., Mongwe, P., et al. (2023). The Southern Ocean carbon cycle 1985–2018: Mean, seasonal cycle, trends, and storage. *Global Biogeochemical Cycles, 37*, e2023GB007848. https://doi.org/10.1029/2023GB007848

Henson, S. A., Sarmiento, J. L., Dunne, J. P., Bopp, L., Lima, I., Doney, S. C., et al. (2010). Detection of anthropogenic climate change in satellite records of ocean chlorophyll and productivity. *Biogeosciences*, *7*, 621–640. https://doi.org/10.5194/bg-7-621-2010

Henson, S. A., Sanders, R., & Madsen, E. (2012). Global patterns in efficiency of particulate organic carbon export and transfer to the deep ocean. *Global Biogeochemical Cycles*, *26*, GB1028. https://doi.org/10.1029/2011GB004099

Henson, S. A., Yool, A., & Sanders, R. (2015). Variability in efficiency of particulate organic carbon export: A model study, *Global Biogeochemical Cycles*, *29*, 33–45. doi:10.1002/2014GB004965

Henson, S. A., Beaulieu, C., & Lampitt, R. (2016). Observing climate change trends in ocean biogeochemistry: When and where. *Global Change Biology*, *22*(4), 1561–1571. https://doi.org/10.1111/gcb.13152

Henson, S. A., Laufkötter, C., Leung, S. Giering, S. L. C., Palevsky, H. I., & Cavan, E. L. (2022). Uncertain response of ocean biological carbon export in a changing world. *Nature Geoscience*, *15*, 248–254. https://doi.org/10.1038/s41561-022-00927-0

Henson, S. A., Briggs, N., Carvalho, F., Manno, C., Mignot, A., Thomalla, S. (2023). A seasonal transition in biological carbon pump efficiency in the northern Scotia Sea, Southern Ocean. *Deep Sea Research Part II*, *208*, 105274. https://doi.org/10.1016/j.dsr2.2023.105274

Henson, S. A., Kelsey Bisson, K., Hammond, M. L., Martin, A., Mouw, C., Yool, A. (2024). Effect of sampling bias on global estimates of ocean carbon export. *Environmental Research Letters*, *19*, 024009. http://dx.doi.org/10.1088/1748-9326/ad1e7f

Ilyina, T., Six, K. D., Segschneider, J., Maier-Reimer, E., Li, H., & Núñez-Riboni, I. (2013). Global ocean biogeochemistry model HAMOCC: Model architecture and performance as component of the MPI-Earth system model in different CMIP5 experimental realizations. *Journal of Advances in Modeling Earth Systems*, *5*(2), 287–315. https://doi.org/10.1029/2012ms000178

Iversen, M. H. (2023). Carbon export in the ocean: a biologist's perspective. *Annual Review of Marine Science*, *15*, 357–381. https://doi.org/10.1146/annurev-marine-032122-035153

Karl, D. M., Church, M. J., Dore, J. E., Letelier, R., & Mahaffey, C. (2012). Predictable and efficient carbon sequestration in the North Pacific Ocean supported by symbiotic nitrogen fixation, *Proceedings of the National Academy of Sciences USA*, *109*, 1842–1849. https://doi.org/10.1073/pnas.1120312109

Khatiwala, S., Tanhua, T., Mikaloff Fletcher, S., Gerber, M., Doney, S. C., Graven, H. D., et al. (2013). Global ocean storage of anthropogenic carbon, *Biogeosciences*, *10*, 2169–2191. https://doi.org/10.5194/bg-10-2169-2013

Kiørboe, T., Grossart, H.-P., Ploug, H., & Tang, K. (2002). Mechanisms and rates of bacterial colonization of sinking aggregates, *Applied and Environmental Microbiology*, *68*, 3996–4006. https://doi.org/10.1128/AEM.68.8.3996-4006.2002

Kiørboe, T., Tang, K., Grossart, H.-P., & Ploug, H. (2003). Dynamics of microbial communities on marine snow aggregates: colonization, growth, detachment, and grazing mortality of attached bacteria, *Applied and Environmental Microbiology*, *69*, 3036–3047. https://doi.org/10.1128/AEM.69.6.3036-3047.2003

Kwon, E., Primeau, F., & Sarmiento, J. (2009). The impact of remineralization depth on the air–sea carbon balance, *Nature Geoscience*, *2*, 630–635. https://doi.org/10.1038/ngeo612

Lam, P. J., Doney, S. C., & Bishop, J. K. B. (2011). The dynamic ocean biological pump: Insights from a global compilation of particulate organic carbon, $CaCO_3$, and opal concentration profiles from the mesopelagic. *Global Biogeochemical Cycles*, *25*, GB3009. https://doi.org/10.1029/2010GB003868.

Lampitt, R. S., Bett, B. J., Kiriakoulakis, K., Popova, E. E., Ragueneau, O., Vangriesheim, A., & Wolff, G. A. (2001). Material supply to the abyssal seafloor in the Northeast Atlantic, *Progress in Oceanography*, *50*, 27–63. https://doi.org/10.1016/S0079-6611(01)00047-7

Landschützer, P., Gruber, N., & Bakker, D. C. (2016). Decadal variations and trends of the global ocean carbon sink. Global Biogeochemical Cycles, *30*(10), 1396–1417. https://doi.org/10.1002/2015gb005359

Landschützer, P., Gruber, N., Bakker, D. C. E., Stemmler, I., Six, K. D. (2018). Strengthening seasonal marine CO_2 variations due to increasing atmospheric CO_2. *Nature Climate Change*, *8*, 146–150. https://doi.org/10.1038/s41558-017-0057-x

Laufkötter, C., Vogt, M., Gruber, N., Aita-Noguchi, M., Aumont, O., Bopp, L., et al. (2015). Drivers and uncertainties of future global marine primary production in marine ecosystem models. *Biogeosciences*, *12*(23), 6955–6984. https://doi.org/10.5194/bg-12-6955-2015

Laufkötter, C., Vogt, M., Gruber, N., Aumont, O., Bopp, L., Doney, S. C., et al. (2016). Projected decreases in future marine export production: The role of the carbon flux through the upper ocean ecosystem. *Biogeosciences*, *13*, 4023–4047. https://doi.org/10.5194/bg-13-4023-2016

Laufkötter, C., John, J. G., Stock, C. A., & Dunne, J. P. (2017). Temperature and oxygen dependence of the remineralization of organic matter. *Global Biogeochemical Cycles*, *31*, 1038–1050. https://doi.org/10.1002/2017GB005643

Laurenceau-Cornec, E. C., Le Moigne, F. A. C., Gallinari, M., Moriceau, B., Toullec, J., Iversen, M. I., Engel, A., & De La Rocha, C. L. (2020). New guidelines for the application of Stokes' models to the sinking velocity of marine aggregates, *Limnology and Oceanography*, *65*, 1264–1285. https://doi.org/10.1002/lno.11388

Laws, E. A., Falkowski, P. G., Smith Jr, W. O., Ducklow, H., & McCarthy, J. J. (2000). Temperature effects on export production in the open ocean. *Global Biogeochemical Cycles*, *14*, 1231–1246. https://doi.org/10.1029/1999GB001229

Laws, E. A., & Maiti, K. (2019). The relationship between primary production and export production in the ocean: Effects of time lags and temporal variability, *Deep Sea Research Part I*, *148*, 100–107. https://doi.org/10.1016/j.dsr.2019.05.006

Laws, E. A., D'sa, E., & Naik, P. (2011). Simple equations to estimate ratios of new or export production to total production from satellite-derived estimates of sea surface temperature and primary production. *Limnology and Oceanography: Methods*, *9*(12), 593–601. https://doi.org/10.4319/lom.2011.9.593

Le Quéré, C., Buitenhuis, E. T., Moriarty, R., Alvain, S., Aumont, O., Bopp, L., et al. (2016). Role of zooplankton dynamics for Southern Ocean phytoplankton biomass and global biogeochemical cycles. *Biogeosciences*, *13*(14), 4111–4133. https://doi.org/10.5194/bg-13-4111-2016

Liao, E., Resplandy, L., Liu, J., & Bowman, K. W. (2020). Amplification of the ocean carbon sink during El Niños: Role of poleward Ekman transport and influence on atmospheric CO_2. *Global Biogeochemical Cycles*, *34*(9), e2020GB006574. https://doi.org/10.1029/2020gb006574

Lima, I. D., Lam, P. J., & Doney, S. C. (2014). Dynamics of particulate organic carbon flux in a global ocean model, *Biogeosciences*, *11*, 1177–1198. https://doi.org/10.5194/bg-11-1177-2014

Lindsay, K., Bonan, G. B., Doney, S. C., Hoffman, F. M., Lawrence, D. M., Long, M. C., et al. (2014). Preindustrial-control and twentieth-century carbon cycle experiments with the Earth System Model CESM1(BGC). *Journal of Climate*, *27*(24), 8981–9005. https://doi.org/10.1175/jcli-d-12-00565.1

Lutz, M. J., Caldeira, K., Dunbar, R. B., & Behrenfeld, M. J. (2007). Seasonal rhythms of net primary production and particulate organic carbon flux to depth describe the efficiency of biological pump in the global ocean. *Journal of Geophysical Research Oceans*, *112*, C10011. https://doi.org/10.1029/2006JC003706

Maier-Reimer, E. (1993). Geochemical cycles in an ocean general circulation model. Preindustrial tracer distributions, *Global Biogeochemical Cycles*, *7*, 645–677. https://doi.org/10.1029/93GB01355

Marinov, I., Gnanadesikan, A., Sarmiento, J. L., Toggweiler, J. R., Follows, M., & Mignone, B. K. (2008). Impact of oceanic circulation on biological carbon storage in the ocean and atmospheric pCO_2, *Global Biogeochemical Cycles*, *22*, GB3007. https://doi.org/10.1029/2007GB002958

Marra, J., Ho, C., & Trees, C. C. (2003). An alternative algorithm for the calculation of primary production from remote sensing data, Rep. LDEO 2003–1, Lamont-Doherty Earth Observatory, Palisades, New York. https://www.ldeo.columbia.edu/~marra/MarraAlgorithm.pdf (Accessed August, 2022).

Marsay, C. M., Sanders, R. J., Henson, S. A., Pabortsava, K., Achterberg, E. P., & Lampitt, R. S. (2015). Attenuation of sinking particulate organic carbon flux through the mesopelagic ocean, *Proceedings of the National Academy of Sciences USA*, *112*(4) 1089–1094. https://doi.org/10.1073/pnas.1415311112

Martin, J. H., Knauer, G. A., Karl, D. M., & Broenkow, W. W. (1987). VERTEX: carbon cycling in the northeast Pacific, *Deep-Sea Research*, *34*, 267–285. https://doi.org/10.1016/0198-0149(87)90086-0

Matsumoto, K., Sarmiento, J. L., Key, R. M., Bullister, J. L., Caldeira, K., Campin, J.-M., et al. (2004). Evaluation of ocean carbon cycle models with data-based metrics, *Geophysical Research Letters*, *31*, L07303. https://doi.org/10.1029/2003GL018970

Mauritsen, T., Bader, J., Becker, T., Behrens, J., Bittner, M., Brokopf, R., et al. (2019). Developments in the MPI-M Earth system model version 1.2 (MPI-ESM1. 2) and its response to increasing CO_2. *Journal of Advances in Modeling Earth Systems*, *11*(4), 998–1038. https://doi.org/10.1029/2018ms001400

Mayor, D. J., Sanders, R., Giering, S. L. C., & Anderson, T. R. (2014). Microbial gardening in the ocean's twilight zone: Detritivorous metazoans benefit from fragmenting, rather than ingesting, sinking detritus, *BioEssays*, *36*, 1132–1137. https://doi.org/10.1002/bies.201400100

Mikaloff Fletcher, S. E., Gruber, N., Jacobson, A. R., Gloor, M., Doney, S. C., Dutkiewicz, S., et al. (2007). Inverse estimates of the oceanic sources and sinks of natural CO_2 and their implied oceanic transport. *Global Biogeochemical Cycles*, *21*, GB1010. https://doi.org/10.1029/2006GB002751

Mouw, C. B., Barnett, A., McKinley, G. A., Gloege, L., & Pilcher, D. (2016a). Global ocean particulate organic carbon flux merged with satellite parameters, *Earth System Science Data*, *8*, 531–541. https://doi.org/10.5194/essd-8-531-2016

Mouw, C. B., Barnett, A., McKinley, G. A., Gloege, L., & Pilcher, D. (2016b). Phytoplankton size impact on export flux in the global ocean, *Global Biogeochemical Cycles*, *30*, 1542–1562. https://doi.org/10.1002/2015GB005355

Müller, Jens Daniel. (2023). RECCAP2-ocean data collection [Data set]. Zenodo. 1631. https://doi.org/10.5281/zenodo.7990823

Najjar, R. G., X. Jin, F. Louanchi, O. Aumont, K. Caldeira, S.C. Doney, et al. (2007). Impact of circulation on export production, dissolved organic matter and dissolved oxygen in the ocean: Results from Phase II of the Ocean Carbon-cycle Model Intercomparison Project (OCMIP-2), *Global Biogeochemical Cycles*, *21*, GB3007. https://doi.org/10.1029/2006GB002857.

Nowicki, M., DeVries, T., & Siegel, D. A. (2022). Quantifying the carbon export and sequestration pathways of the ocean's biological carbon pump. *Global Biogeochemical Cycles*, *36*, e2021GB007083. https://doi.org/10.1029/2021GB007083

Omand, M. M., Govindarajan, R., He, J., & Mahadevan, A. (2020). Sinking flux of particulate organic matter in the oceans: Sensitivity to particle characteristics. *Scientific Reports*, *10*, 5582. https://doi.org/10.1038/s41598-020-60424-5

Orr, J. C., R.G. Najjar, O. Aumount, L. Bopp, J.L. Bullister, G. Danabasoglu, et al. (2017). Biogeochemical protocols and diagnostics for the CMIP6 Ocean Model Intercomparison Project (OMIP). *Geoscientific Model Development*, *10*, 2169–2199. https://doi.org/10.5194/gmd-10-2169-2017

RECCAP2 Ocean Science Team (2022). RECCAP2 Ocean Protocols, accessed August 3rd, 2022. https://reccap2-ocean.github.io/protocols/

Reygondeau, G., Longhurst, A., Martinez, E., Beaugrand, G., Antoine, D., & Maury, O. (2013), Dynamic biogeochemical provinces in the global ocean, *Global Biogeochemical Cycles*, *27*, 1046–1058. https://doi.org/10.1002/gbc.20089

Rödenbeck, C., DeVries, T., Hauck, J., Le Quéré, C., & Keeling, R. F. (2022). Data-based estimates of interannual sea–air CO_2 flux variations 1957–2020 and their relation to environmental drivers. *Biogeosciences*, *19*(10), 2627–2652. https://doi.org/10.5194/bg-19-2627-2022

Rödenbeck, C., Keeling, R. F., Bakker, D. C., Metzl, N., Olsen, A., Sabine, C., & Heimann, M. (2013). Global surface-ocean pCO_2 and sea–air CO_2 flux variability from an observation-driven ocean mixed-layer scheme. *Ocean Science*, *9*(2), 193–216. https://doi.org/10.5194/os-9-193-2013

Rodgers, K. B., Schwinger, J., Fassbender, A. J., Landschützer, P., Yamaguchi, R., Frenzel, H., et al. (2023). Seasonal variability of the surface ocean carbon cycle: A synthesis. *Global Biogeochemical Cycles*, 37, e2023GB007798. https://doi.org/10.1029/2023GB007798

Sarmiento, J. L., & Gruber, N. (2002). Anthropogenic carbon sinks. *Physics Today*, 55(8), 30–36. https://doi.org/10.1063/1.1510279

Sarmiento, J. L., & Gruber, N. (2006). *Ocean Biogeochemical Dynamics*. Princeton University Press. https://doi.org/10.1017/S0016756807003755

Schlitzer, R. (2000). Applying the adjoint method for biogeochemical modeling: Export of particulate organic matter in the World Ocean, *Inverse methods in biogeochemical cycles*, ed. P. Kasibhata, AGU Monograph 114, pp. 107-124.

Schwinger, J., Goris, N., Tjiputra, J. F., Kriest, I., Bentsen, M., Bethke, I., et al. (2016). Evaluation of NorESM-OC (versions 1 and 1.2), the ocean carbon-cycle stand-alone configuration of the Norwegian Earth System Model (NorESM1). *Geoscientific Model Development*, *9*(8), 2589–2622. https://doi.org/10.5194/gmd-9-2589-2016

Séférian, R., Gehlen, M., Bopp, L., Resplandy, L., Orr, J. C., Marti, O., et al. (2016). Inconsistent strategies to spin up models in CMIP5: implications for ocean biogeochemical model performance assessment, *Geoscientific Model Development*, *9*, 1827–1851. https://doi.org/10.5194/gmd-9-1827-2016

Séférian, R., Berthet, S., Yool, A., Palmiéri, J., Bopp, L., Tagliabue, A., et al. (2020). Tracking improvement in simulated marine biogeochemistry between CMIP5 and CMIP6. *Current Climate Change Reports*, 6(3), 95–119. https://doi.org/10.1007/s40641-020-00160-0

Séférian, R., Nabat, P., Michou, M., Saint-Martin, D., Voldoire, A., Colin, J., et al. (2019). Evaluation of CNRM Earth-System model, CNRM-ESM2-1: Role of Earth system processes in present-day and future climate. *Journal of Advances in Modeling Earth Systems*, *11*(12), 4182–4227. https://doi.org/10.1029/2019ms001791

Siegel, D. A., Buesseler, K. O., Doney, S. C., Sailley, S. F., Behrenfeld, M. J., & Boyd, P. W. (2014). Global assessment of ocean carbon export by combining satellite observations and food-web models. *Global Biogeochemical Cycles*, *28*(3), 181–196. https://doi.org/10.1002/2013gb004743

Siegel, D. A., Buesseler, K. O., Behrenfeld, M. J., Benitez-Nelson, C. R., Boss, E., Brzezinski, M. A., et al. (2016). Prediction of the export and fate of global ocean net primary production: the EXPORTS science plan, *Frontiers in Marine Science*, *3*, 22. http://doi.org/10.3389/fmars.2016.00022

Siegel, D. A., DeVries, T., Doney, S. C., & T. Bell, T. (2021). Assessing the sequestration time scales of some ocean-based carbon dioxide reduction strategies, *Environmental Research Letters*, *16*, 104003. https://doi.org/10.1088/1748-9326/ac0be0

Siegel, D. A., DeVries, T., Cetinić, I., & K Bisson, K. M. (2023). Quantifying the ocean's biological pump and Its carbon cycle impacts on global scales, *Annual Review of Marine Science*, *15*, 329–356. https://doi.org/10.1146/annurev-marine-040722-115226

Silsbe, G. M., Behrenfeld, M. J., Halsey, K. H., Milligan, A. J., & Westberry, T. K. (2016). The CAFE model: A net production model for global ocean phytoplankton, *Global Biogeochemical Cycles*, *30*, 1756–1777. doi:10.1002/2016GB005521

Steinberg, D. K., & M.R. Landry, M. R. (2017). Zooplankton and the ocean carbon cycle, *Annual Review of Marine Science*, *9*, 413–444. https://doi.org/10.1146/annurev-marine-010814-015924

Stock, C. A., Dunne, J. P., Fan, S., Ginoux, P., John, J., Krasting, J. P., et al. (2020). Ocean biogeochemistry in GFDL's Earth system model 4.1 and its response to increasing atmospheric CO_2. *Journal of Advances in Modeling Earth Systems*, *12*(10), e2019MS002043. https://doi.org/10.1029/2019ms002043

Stukel, M. R., Ohman, M. D., Kelly, T. B., & Biard, T. (2019). The roles of suspension-feeding and flux-feeding zooplankton as gatekeepers of particle flux into the mesopelagic ocean in the Northeast Pacific. *Frontiers in Marine Science*, *6*, 397. https://doi.org/10.3389/fmars.2019.00397

Takahashi, T., Olafsson, J., Goddard, J. G., Chipman, D. W., & Sutherland, S. C. (1993). Seasonal variation of CO_2 and nutrients in the high-latitude surface oceans: A comparative study, *Global Biogeochemical Cycles*, *7*(4), 843–878. https://doi.org/10.1029/93GB02263

Takahashi, T., Sutherland, S. C., Sweeney, C., Poisson, A., Metzl, N., Tilbrook, B., et al. (2002). Global sea–air CO_2 flux based on climatological surface ocean pCO_2, and seasonal biological and temperature effects. *Deep Sea Research Part II: Topical Studies in Oceanography*, *49*(9–10), 1601–1622. https://doi.org/10.1016/S0967-0645(02)00003-6

Terhaar, T., Goris, N., Müller, J. D., DeVries, T., Gruber, N., Hauck, J., et al. (2023). Assessment of global ocean biogeochemistry models for ocean carbon sink estimates in RECCAP2 and recommendations for future studies. *ESS Open Archive*. https://doi.org/10.22541/essoar.168394734.41886821/v1

Turner, J. T. (2015). Zooplankton fecal pellets, marine snow, phytodetritus and the ocean's biological pump, *Progress in Oceanography*, *130*, 205–248. https://doi.org/10.1016/j.pocean.2014.08.005

Tsujino, H., Nakano, H., Sakamoto, K., Urakawa, S., Hirabara, M., Ishizaki, H., & Yamanaka, G. (2017). Reference manual for the meteorological research institute community ocean model version 4 (MRI. COMv4) (Vol. 80, p. 306). Technical Reports of the Meteorological Research Institute.

Urakawa, L. S., Tsujino, H., Nakano, H., Sakamoto, K., Yamanaka, G., & Toyoda, T. (2020). The sensitivity of a depth-coordinate model to diapycnal mixing induced by practical implementations of the isopycnal tracer diffusion scheme. *Ocean Modelling*, *154*, 101693. https://doi.org/10.1016/j.ocemod.2020.101693

Volk, T., & Hoffert, M. I. (1985). Ocean carbon pumps: Analysis of relative strengths and efficiencies in ocean-driven atmospheric CO_2 changes. In E. Sundquist & W. Broecker (Eds.), *The carbon cycle and atmospheric CO_2: Natural variations archean to present* (Vol. 32, pp. 99–110). American Geophysical Union (AGU). https://doi.org/10.1029/GM032P0099

Wanninkhof, R., Park, G.-H., Takahashi, T., Sweeney, C., Feely, R., Nojiri, Y., et al. (2013). Global ocean carbon uptake: magnitude, variability and trends, *Biogeosciences*, *10*, 1983–2000. https://doi.org/10.5194/bg-10-1983-2013

Watson, A. J., Schuster, U., Shutler, J. D., Holding, T., Ashton, I. G., Landschützer, P., et al. (2020). Revised estimates of ocean-atmosphere CO_2 flux are consistent with ocean carbon inventory. *Nature Communications*, *11*(1), 1–6. https://doi.org/10.1038/s41467-020-18203-3

Weber, T., Cram, J. A., Leung, S. W., DeVries, T., & Deutsch, C. (2016). Deep ocean nutrients imply large latitudinal variation in particle transfer efficiency, *Proceedings of the National Academy of Sciences*, *113*, 8606–8611. https://doi.org/10.1073/pnas.1604414113

Wilson, J. D., Andrews, O., Katavouta, A., de Melo Viríssimo, F., Death, R. M., Adloff, M., et al. (2022). The biological carbon pump in CMIP6 models: 21st century trends and uncertainties. *Proceedings of the National Academy of Sciences USA*, *119*(29), e2204369119. https://doi.org/10.1073/pnas.2204369119

Wright, R. M., Le Quéré, C., Buitenhuis, E., Pitois, S., & Gibbons, M. J. (2021). Role of jellyfish in the plankton ecosystem revealed using a global ocean biogeochemical model. *Biogeosciences*, *18*(4), 1291–1320. https://doi.org/10.5194/bg-18-1291-2021

Yang, S., & Gruber, N. (2016). The anthropogenic perturbation of the marine nitrogen cycle by atmospheric deposition: Nitrogen cycle feedbacks and the ^{15}N Haber-Bosch effect. *Global Biogeochemical Cycles*, *30*(10), 1418–1440. https://doi.org/10.1002/2016gb005421

Zeng, J., Iida, Y., Matsunaga, T., & Shirai, T. (2022). Surface ocean CO_2 concentration and air-sea flux estimate by machine learning with modelled variable trends. *Frontiers in Marine Science*, *9*, 989233. https://doi.org/10.3389/fmars.2022.989233

Supporting Information:
Observational and numerical modeling constraints on the global ocean biological carbon pump

Scott C. Doney[1], Kayla A. Mitchell[1,2], Stephanie A. Henson[3], Emma Cavan[4], Tim DeVries[5], Nicolas Gruber[6], Judith Hauck[7], Colleen B. Mouw[8], Jens D. Müller[6], and Francois W. Primeau[2]

February 4th, 2024

[1] Department of Environmental Sciences, University of Virginia, Charlottesville, VA, USA,

[2] Department of Earth System Science, University of California, Irvine, Irvine, CA, USA,

[3] National Oceanography Centre, Southampton, UK,

[4] Department of Life Sciences, Silwood Park Campus, Imperial College London, Berkshire, UK,

[5] Earth Research Institute and Department of Geography, University of California, Santa Barbara, Santa Barbara, CA, USA,

[6] Environmental Physics, Institute of Biogeochemistry and Pollutant Dynamics, ETH Zurich, Zürich, Switzerland

[7] Alfred-Wegener-Institut, Helmholtz-Zentrum für Polar- und Meeresforschung, Bremerhaven, Germany

[8] Graduate School of Oceanography, University of Rhode Island, Narragansett, RI, USA.

The REgional Carbon Cycle Assessment and Processes (RECCAP) project is a coordinated, international effort to constrain contemporary ocean carbon air-sea fluxes and interior storage trends using a combination of field observations, inverse model products, and ocean biogeochemical hindcast simulations. The second phase, RECCAP2, extends the original synthesis using additional years of ocean observational data and updated numerical results (DeVries et al., 2023) as well as expanding the scope of the observational and model analysis, in this case into the biological carbon pump magnitude and efficiency.

Supplement Figures

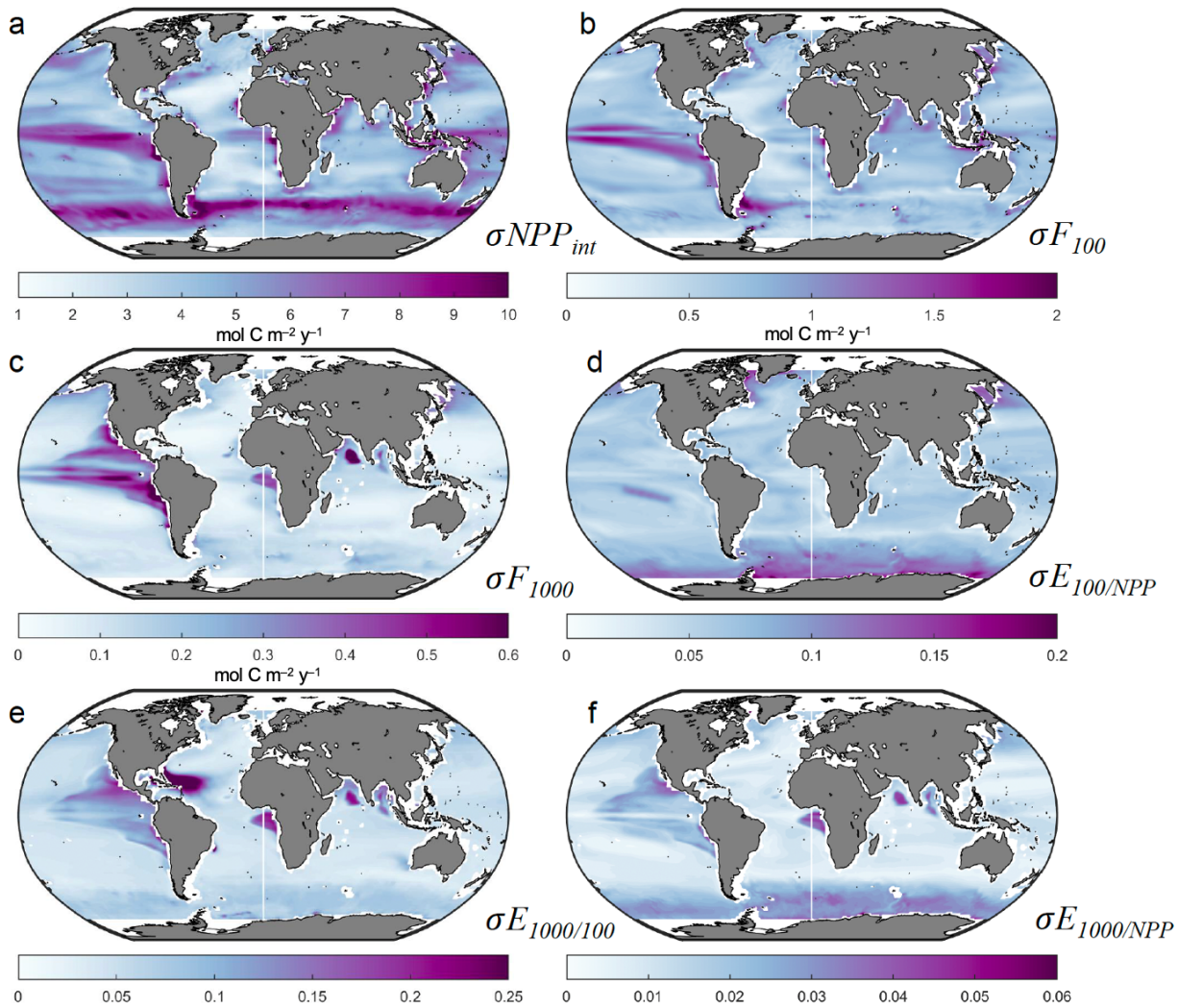

Figure S1. Maps of within-ensemble standard deviation of biological pump parameters. Standard deviations across model ensemble members are computed relative to the average model ensemble presented in Figure 1 for: (a) vertically integrated primary productivity σ_{NPP}, (b) particulate organic carbon export fluxes at 100 m σF_{100}, and (c) 1000 m σF_{1000}, all in moles C m^{-2} y^{-1}, and (d) surface export efficiency ratio $E_{100/NPP} = F_{100}/NPP$, (e) mesopelagic transfer efficiency at 1000 m $E_{1000/100} = F_{1000}/F_{100}$, and (f) export efficiency to the deep ocean $E_{1000/NPP} = F_{1000}/NPP$, all ratios unitless.

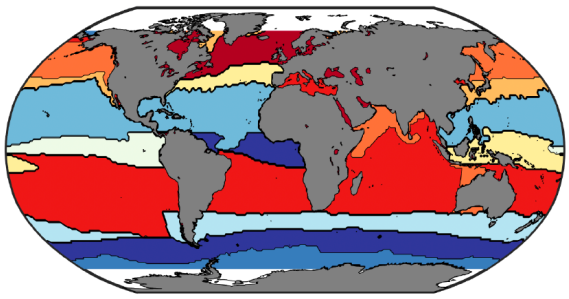

Biome Number	Biome Acronym	Biome Description
18	SOSPSS	Southern Ocean Subpolar Seasonally Stratified
17	NaAEQU	N. Atlantic Equatorial
16	SOICE	Southern Ocean Ice
15	NPICE	North Pacific Ice
14	NPSTPS	N. Pacific Subtropical Permanently Stratified
13	NaSTPS	N. Atlantic Subtropical Seasonally Stratified
12	SOSTSS	Southern Ocean Subtropical Seasonally Stratified
11	BARENTS	Barents Sea
10	PEQUE	Eastern Equatorial Pacific
9	PEQUW	Western Equatorial Pacific
8	NAICE	N. Atlantic Ice
7	NaSTSS	N. Atlantic Subtropical Seasonally Stratified
6	NPSTSS	N. Pacific Subtropical Seasonally Stratified
5	NPSPSS	N. Pacific Subpolar Seasonally Stratified
4	INDSTPS	Indian Ocean Subtropical Permanently Stratified
3	MED	Mediterranean Sea
2	SASTPS	S. Atlantic Subtropical Permanently Stratified
1	NaSPSS	N. Atlantic Subpolar Seasonally Stratified

Figure S2. Map of standard RECCAP2 biomes by ocean basin (Fay and McKinley, 2014). The biomes include polar (ICE), subpolar seasonally-stratified (SPSS), subtropical seasonally stratified (STSS), subtropical permanently stratified (STPS), and equatorial regions (EQU); note the equatorial Pacific is divided into western and eastern sub-basins. The equatorial eastern Pacific and Atlantic, monsoon-influenced Indian, and seasonally-stratified biomes generally exhibited relatively high NPP, F_{100}, and F_{1000}. Polar and sub-polar biomes exhibited relatively high E_{100}.

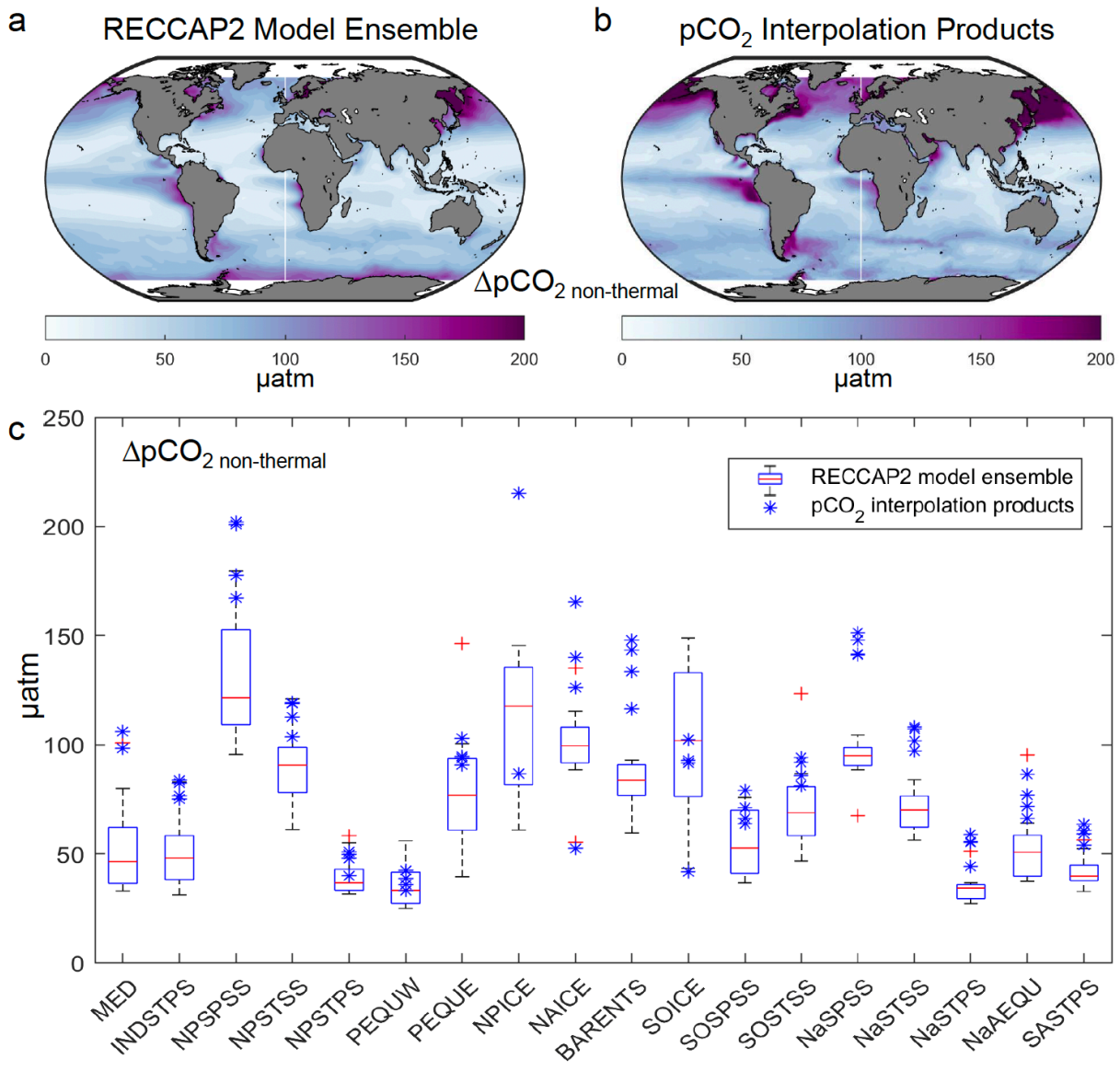

Figure S3. Analysis of the seasonal cycle of non-thermal $\Delta pCO_{2_{non-thermal}}$ (a) spatial map of RECCAP2 multi-model ensemble average, (b) spatial map from pCO_2 observational data products, and (c) box-whisker plot of RECCAP2 multi-model ensemble medians, interquartile ranges, and outliers pooled into Fay and McKinley biomes (Figure S2).

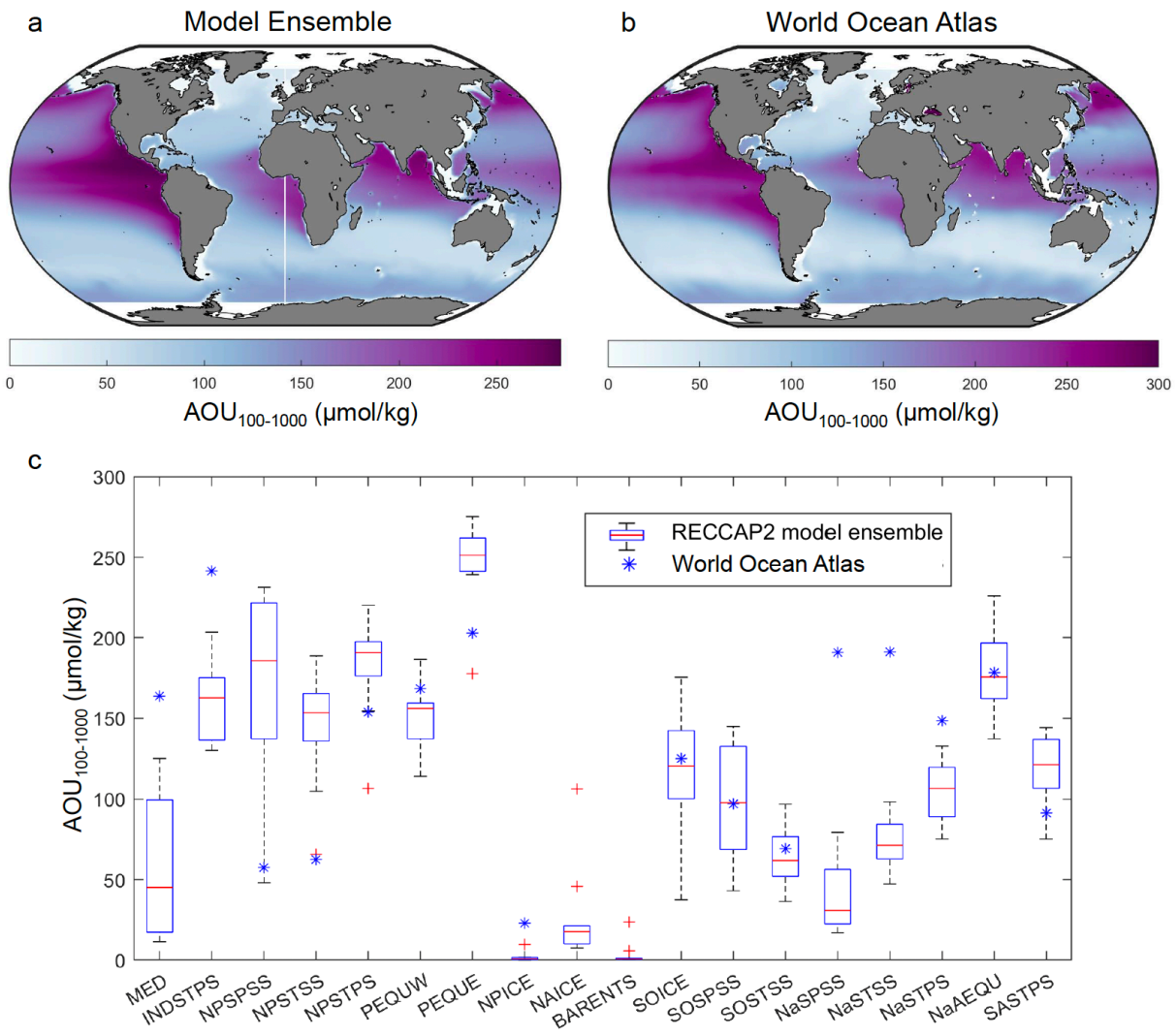

Figure S4. Analysis of apparent oxygen utilization (AOU) vertically averaged over the mesopelagic zone (100-1000 m) (a) spatial map of RECCAP2 multi-model ensemble average, and (b) spatial map from WOA observational data set, and (c) box-whisker plot of RECCAP2 multi-model ensemble medians, interquartile ranges, and outliers pooled into Fay and McKinley biomes (Figure S2).

Supporting Information Tables

Table S1. Interannual variability (1985-2018) for the RECCAP2 simulations (simulation A) for global-integrated, annual-mean variables: vertically integrated net primary productivity NPP and particulate organic carbon export fluxes at 100 m F_{100} and 1000 m depth F_{1000}. Interannual variability (standard deviation) are in Pg C y^{-1}.

	CCSM-WHOI	CESM-ETHZ	CNRM-ESM2	ECCO-Darwin	EC-Earth3	FESOM-REcoM_LR	MOM6-Princeton	MPIOM-HAMOCC	MRI-ESM2-0	Nor_ESM-OC1.2	ORCA1-LIM3-PISCES	PlankTOM12
NPP	0.1914	0.3743	0.2000	0.7272	0.2194	0.3878	0.3204	1.5377	0.4127	0.3518	0.2286	0.3655
F100	0.0352	0.0491	0.0304	0.1966	0.0412	0.1079	0.0383	0.2004	0.0736	0.0717	0.0484	0.1447
F1000	0.0024	0.0140	0.0000	0.1107	0.0000	0.0143	0.0000	0.0419	0.0103	0.0283	0.0000	0.0000

Table S2. Long-term temporal trends (1985-2018) for the RECCAP2 simulations (simulation A) for global-integrated, annual-mean variables: vertically integrated net primary productivity NPP and particulate organic carbon export fluxes at 100 m F_{100} and 1000 m depth F_{1000}. Trends are in Pg C y^{-1}/year,

	CCSM-WHOI	CESM-ETHZ	CNRM-ESM2	ECCO-Darwin	EC-Earth3	FESOM-REcoM_LR	MOM6-Princeton	MPIOM-HAMOCC	MRI-ESM2-0	Nor_ESM-OC1.2	ORCA1-LIM3-PISCES	PlankTOM12
NPP	-0.0140	-0.0172	0.0005	-0.0727	0.0017	-0.0094	0.0102	0.0028	-0.0047	0.0009	0.0190	0.0184
F100	-0.0031	-0.0020	0.0000	-0.0209	0.0000	0.0013	0.0010	0.0001	0.0002	0.0017	0.0029	0.0237
F1000	-0.0002	-0.0002	0.0000	-0.0117	0.0000	0.0004	0.0000	0.0013	0.0000	-0.0001	0.0000	0.0000